

Influence of Carbonitriding Process on Phase Transformation during Case  
Hardening, Retained Austenite and Residual Stresses

Vom Fachbereich Produktionstechnik  
der  
UNIVERSITÄT BREMEN

zur Erlangung des Grades  
Doktor-Ingenieur  
genehmigte

Dissertation

von

Dr.-Ing. Richard J. Katemi

Gutachter: Prof. Dr.-Ing. habil. Franz Hoffmann

Prof. Dr.-Ing. habil. Udo Fritsching

Tag der mündlichen Prüfung: 13.09.2019



## Abstract

The carbonitriding process is a surface hardening technique with an ultimate goal of improving surface hardness, fatigue properties and resistance to wear of highly stressed parts. As opposed to carburizing process which enriches engineering components with carbon atoms only, carbonitriding introduces both carbon and nitrogen atoms in the surface layer. The presence of nitrogen stabilizes austenite and depending on the level of carbon and nitrogen content reached, as high as 70 mass-% of austenite can be retained. The thermal and mechanical stability of such high amount of retained austenite is vital as retained austenite should remain stable to avoid shape and dimensional changes especially in close fittings. Moreover, such high amount of retained austenite affects the nature, magnitudes and distribution of residual stresses which can influence the service properties.

In the present work, the influence of carbonitriding process on the phase transformation during case hardening, retained austenite and residual stresses were investigated. In particular, the following points were taken into consideration: (1) characterization of the state after carbonitriding, (2) analysis of the state during and after tempering, (3) investigation of the state after tempering coupled with cryogenic treatment, (4) investigation of the state after thermal stabilization, and (5) investigation of the mechanical stability of carbonitrided samples.

Five carbonitriding variants with different carbon and nitrogen contents were considered. The phase compositions and residual stress analysis was carried out using X-ray diffraction. For each variant, the amount of retained austenite was dependent on the level of carbon and nitrogen reached which in turn depends on the carbon and nitrogen potential in the carbonitriding atmosphere. Besides the misfit between the case and the core, the amount and distribution of retained austenite in the case affects the nature, magnitudes and distribution of residual stresses in both retained austenite and martensite phase.

The thermal stability of retained austenite and residual stress relaxation during the process of tempering was captured in situ, using a diffractometer equipped with a position sensitive detector with high resolution and a heating system. This study establishes the range of thermal stability of retained austenite and its kinetics of decomposition during continuous heating and isothermal holding. Further, it helped to quantify the magnitudes and kinetics of

residual stress relaxation. Analysis of state after cryogenic treatment revealed that indeed tempering prior cryogenic treatment does stabilize retained austenite which then becomes difficult to transform to martensite during cryogenic treatment. The new martensite formed during the cryogenic treatment enhances significantly the compressive residual stresses in the martensite phase. Via shot-peening treatment it could be revealed that retained austenite was mechanically unstable and readily transforms; consequently high compressive residual stresses in both retained austenite and martensite phase are resulting.

## Zusammenfassung

Carbonitrieren ist ein Randschichthärteverfahren mit dem Ziel der Verbesserung der Verschleißfestigkeit und der Dauerfestigkeitseigenschaften von hochbeanspruchte Teile. Im Gegensatz zu Aufkohlen, bei dem nur Kohlenstoff eindiffundiert; diffundieren beim Carbonitrieren zusätzlich Stickstoffatome ein. Die Präsenz von Stickstoff stabilisiert Austenit in Abhängigkeit von der Höhe des Kohlenstoff- und Stickstoffgehalts von bis zu 70 Gew.-%. Die thermische und mechanische Stabilität eines so hohen Restaustenitgehalts ist wichtig, da Restaustenit stabil bleiben muss, um Form und Dimensionsänderungen zu vermeiden. Außerdem beeinflussen so hohe Restaustenitanteile Natur, Größe und Verteilung von Eigenspannungen, die die Betriebseigenschaften beeinflussen können.

In der vorliegenden Arbeit werden der Einfluss des Carbonitrierprozesses auf die Phasenumwandlung während des Härtens, den Restaustenitgehalt und den Eigenspannungszustand untersucht, insbesondere aber die folgenden Arbeiten:

- (1) Charakterisierung des Zustandes nach dem Carbonitrieren,
- (2) Analyse des Zustands während und nach dem Anlassen,
- (3) Untersuchung des Anlasszustands in Verbindung mit einer Tiefkühlbehandlung,
- (4) Untersuchung des Zustands nach der thermischen Stabilisierung,
- (5) Untersuchung der mechanischen Stabilität von carbonitrierte Proben.

Fünf Carbonitriervarianten mit unterschiedlichen Kohlenstoff- und Stickstoffgehalt wurden berücksichtigt. Es wurden Phasenzusammensetzungen und Restspannungsanalysen mit Röntgenbeugung durchgeführt. Für jede Variante war der Restaustenitgehalt vom Kohlenstoff- und Stickstoffgehalt abhängig, der über die Carbonitrierparameter eingestellt wurde. Außer der Fehlanpassung zwischen der Oberfläche und dem Kern beeinflussen die Menge und Verteilung des Restaustenits in der Oberfläche den Eigenspannungszustand sowohl im Restaustenit als auch im Martensit. Die thermische Stabilität von Restaustenit und die Restspannungsrelaxation während des Anlassens wurde in situ unter Verwendung eines Diffraktometers, das mit einem positionsempfindlichen Detektor mit hoher Auflösung und einem Heizsystem ausgestattet war erfasst. Damit konnte der Bereich der thermischen Stabilität von Restaustenit und seine Zerfallskinetik während kontinuierlicher Erwärmung und nachfolgendem isothermischem Halten untersucht werden. Weiterhin wurde die Kinetik der Eigenspannungsrelaxation quantifiziert. Die Analyse des Zustands nach der kryogenen Behandlung ergab, dass Anlassen vor einer kryogenen Behandlung Restaustenit stabilisiert, sodass kein oder nur wenig Martensit während der kryogenen Behandlung gebildet wird.

Der neue, bei einer Tiefkühlbehandlung gebildete Martensit erhöht signifikant die Druckeigenspannungen in der Martensitphase. Durch Kugelstrahlen konnte nachgewiesen werden, dass der Restaustenit mechanisch instabil war und leicht umgewandelt werden konnte, was zu hohen Druckeigenspannungen in Restaustenit und Martensit

## **Acknowledgement**

The completion of this thesis owes to assistance of individuals and organisations. In a special way I would like to express my sincere gratitude to my supervisor Professor Franz Hoffmann and co-supervisors Dr. Matthias Steinbacher and Dr. J  r  my Epp for their helpful guidance, encouragement and dedication throughout the duration of research and writing of this thesis. I could not have imagined having a better supervisor and mentor for my PhD study.

My sincere thanks go to the Leibniz-Institut f  r Werkstofforientierte Technologien - IWT Bremen for offering me a chance to carry out my research, provision of experimental material and equipment. Special thanks to all members of the Physikalische Analytik and W  rmebehandlung research groups for their assistance, constructive advice, friendship and the good study environment they provided.

I would like to thank the Ministry of Education and Vocational Training of Tanzania (MoEVT) and the Deutscher Akademischer Austauschdienst (DAAD) for sponsorship.

Last but not the least I would like to give my special thanks to my children Jackson, Japhiter, Joanne, and Jasson. This thesis would certainly not have existed without them. Also, I would like to thank my parents and other friends for their help and encouragement



# Table of Content

Abstract .....	iii
Zusammenfassung .....	v
Acknowledgement .....	vii
Table of Content .....	ix
List of Figures .....	xiii
List of Tables .....	xvi
<b>1 Introduction .....</b>	<b>1</b>
1.1 Research objectives .....	2
<b>2 Literature Review .....</b>	<b>5</b>
2.1 Carbonitriding process .....	6
2.1.1 The Carbonitriding Atmosphere .....	7
2.1.2 Control of Carbonitriding Atmosphere .....	10
2.1.3 Carbon and nitrogen diffusion into steel .....	11
2.2 Retained austenite .....	13
2.2.1 Origins of retained austenite .....	13
2.2.2 Factors that influence the amount of retained austenite .....	15
2.2.3 Influence of retained austenite on material properties .....	18
2.3 Stabilization of retained austenite .....	20
2.3.1 Chemical stabilization of retained austenite .....	20
2.3.2 Thermal stabilization of retained austenite .....	20
2.3.3 Mechanical stability of retained austenite .....	22
2.4 Tempering of case-hardened parts .....	23
2.4.1 Structural changes during tempering .....	23
2.5 Residual Stresses .....	30
2.5.1 Definition and Origins of Residual Stresses .....	30
2.5.2 Thermal residual stresses .....	33
2.5.3 Transformation residual stresses .....	35
2.5.4 Hardening residual stresses .....	37
2.6 X-ray diffraction .....	42

2.6.1	Principles of quantitative phase analysis by X-ray diffraction.....	43
2.6.2	Principles of residual stress measurement by X-ray diffraction .....	46
2.6.3	Line broadening analysis .....	49
<b>3</b>	<b>Material and Experimental Procedures .....</b>	<b>51</b>
3.1	Material and Sample Preparations .....	51
3.2	Carbonitriding Treatments .....	52
3.3	Tempering treatment .....	54
3.3.1	Ex-situ/conventional Tempering .....	54
3.3.2	In-situ Tempering Experiments.....	55
3.4	Tempering and cryogenic treatment.....	60
3.5	Thermal stability investigation.....	61
3.6	Mechanical stability investigation.....	62
3.7	X-ray Diffraction measurements.....	63
3.7.1	Quantitative phase analysis .....	63
3.7.2	Residual stress analysis.....	65
3.7.3	Line broadening analysis .....	67
3.8	Complementary investigations.....	70
3.8.1	Chemical composition analysis .....	70
3.8.2	Metallography and microhardness analysis .....	70
<b>4</b>	<b>Results .....</b>	<b>73</b>
4.1	State after carbonitriding.....	73
4.1.1	Carbon and nitrogen depth profiles .....	73
4.1.2	Retained austenite distributions .....	76
4.1.3	Residual Stress Distributions .....	79
4.1.4	Line broadening analysis .....	82
4.1.5	Discussion on state after carbonitriding .....	85
4.2	State during and after tempering.....	89
4.2.1	State during tempering.....	89
4.2.2	State after tempering.....	101
4.2.3	Line broadening during tempering.....	105
4.2.4	Discussion on state during and after tempering.....	109

4.3	State after cryogenic treatment.....	112
4.3.1	Carbon and nitrogen depth profiles .....	112
4.3.2	Metallography and microhardness distributions .....	112
4.3.3	Retained austenite distribution .....	115
4.3.4	Martensite tetragonality ratio.....	118
4.3.5	Residual stress distributions in martensite .....	119
4.3.6	Discussion on state after cryogenic treatment .....	122
4.4	Thermal stability investigation.....	126
4.4.1	Carbon and nitrogen depth profiles .....	126
4.4.2	Metallography and microhardness distributions .....	126
4.4.3	Retained austenite distributions .....	129
4.4.4	Residual stress distributions.....	132
4.4.5	Discussion on thermal stability of retained austenite .....	134
4.5	Mechanical stability.....	136
4.5.1	Retained austenite distribution .....	136
4.5.2	Residual stress distributions.....	137
4.5.3	Discussion on mechanical stability of retained austenite .....	139
<b>5</b>	<b>General Discussion of Results .....</b>	<b>141</b>
<b>6</b>	<b>Research Conclusion and Future Perspective.....</b>	<b>147</b>
<b>7</b>	<b>Bibliography.....</b>	<b>153</b>



## List of Figures

Figure 2.1 Sketch of a 2-steps carbonitriding process.....	7
Figure 2.2 Main reactions occurring in the carbonitriding atmosphere.....	9
Figure 2.3 Schematic presentation of carbon transport for carburizing part .....	12
Figure 2.4 Carbonitrided case microstructures.....	14
Figure 2.5 Martensitic transformation.....	15
Figure 2.6 Experimentally determined martensite transformation and modelled kinetics .....	17
Figure 2.7 Influence of alloying elements on retained austenite.....	17
Figure 2.8 Influence of RA on surface hardness of carburized alloy steels .....	18
Figure 2.9 Retained austenite and residual stress distribution in case-hardened steel.....	19
Figure 2.10 Influence of stabilizing temperature and time on retained austenite .....	22
Figure 2.11 Structural changes of martensitic steel resulting from tempering.....	24
Figure 2.12 Dependence of structural changes on temperature and time .....	25
Figure 2.13 Evolution of lattice parameters of martensite during tempering .....	27
Figure 2.14 Thermally induced-volumetric transformation strain .....	29
Figure 2.15 Kinds of residual stresses in a two-phase material after quenching .....	33
Figure 2.16 Evolution of thermal residual stresses during quenching .....	35
Figure 2.17 Transformation residual stresses during and after quenching.....	37
Figure 2.18 Residual stress distributions when transformation starts at the core.....	39
Figure 2.19 Residual stress distributions transformation starts at the surface .....	40
Figure 2.20 Temperature distribution and progress of martensitic transformation .....	41
Figure 2.21 Influence of retained austenite on residual stress distributions.....	42
Figure 2.22 Example of X-Ray Diffraction Full Pattern Refinement.....	45
Figure 2.23 Rotation axes used to measure stresses with diffraction.....	47
Figure 2.24 Types of “d” vs $\sin^2\psi$ plots in residual stress analysis.....	48
Figure 3.1 Sample dimensions: .....	52
Figure 3.2 Carbonitriding treatment set-up.....	53
Figure 3.3 Variation of carbonitriding parameters during carbonitriding.....	54

Figure 3.4 Time-temperature cycles for in-situ experiments:.....	56
Figure 3.5 Experimental set-up for in-situ X-ray diffraction investigation .....	59
Figure 3.6 Temperature dependence of elastic constants.....	59
Figure 3.7 Refined X-ray diffraction pattern.....	64
Figure 3.8 Electro-polishing set-up .....	65
Figure 3.9 Experimental set-up for residual stress measurement.....	66
Figure 3.10 Standard residual stress analysis.....	67
Figure 3.11 Separation of line reflections pertaining to each phase .....	68
Figure 3.12 Typical example of W-H plot of the X-ray diffraction line profiles .....	69
Figure 3.13 Sample sectioning for metallographic examination and hardness testing.....	71
Figure 4.1 Carbon and nitrogen depth profiles after carbonitriding treatment.....	75
Figure 4.2 Depletion of alloying elements after carbonitriding treatment.....	76
Figure 4.3 Variation of X-ray diffraction patterns as function of depth.....	77
Figure 4.4 Retained austenite depth profiles .....	78
Figure 4.5 Residual stress distributions for untempered carbonitrided samples .....	81
Figure 4.6 Residual stresses in martensite as function of maximum retained austenite.....	81
Figure 4.7 Residual stresses in martensite as a function of C+N content.....	82
Figure 4.8 Change in crystallite as a function of retained austenite content:.....	84
Figure 4.9 Change in r.m.s strain as a function of retained austenite content: .....	84
Figure 4.10 Change in dislocation density as a function of retained austenite content:.....	85
Figure 4.11 Oxygen distribution after carbonitriding in an endothermic atmosphere .....	86
Figure 4.12 Residual stress and microstructure distributions.....	88
Figure 4.13 Variation of microstructure, carbon+nitrogen content and Ms with depth.....	88
Figure 4.14 Carbon and nitrogen depth profiles for in-situ investigations .....	90
Figure 4.15 Evolution of X-ray diffraction patterns during continuous heating .....	92
Figure 4.16 Evolution of retained austenite and martensite during continuous heating.....	92
Figure 4.17 Variation of lattice parameters and C+N content during heating .....	94
Figure 4.18 Evolution of retained austenite during tempering cycles .....	96
Figure 4.19 Evolution of lattice parameter of austenite during tempering cycles .....	97
Figure 4.20 Evolution of residual stresses during heating.....	99

Figure 4.21 Effect of tempering cycles on the evolution of residual stresses.....	100
Figure 4.22 Comparison CN2 carbon and nitrogen profiles before and after tempering .....	101
Figure 4.23 X-ray diffraction patterns before and after tempering.....	102
Figure 4.24 Typical example of case microstructures for carbonitrided samples.....	103
Figure 4.25 Microhardness depth profiles .....	104
Figure 4.26 Residual stresses before and after tempering in RA phase: .....	105
Figure 4.27 Residual stresses before and after tempering in martensite phase .....	105
Figure 4.28 Evolution of crystallite size during heating .....	108
Figure 4.29 Evolution of r.m.s strain during heating.....	108
Figure 4.30 Evolution of dislocation density during heating .....	108
Figure 4.31 Percentage of retained austenite decomposed during tempering.....	110
Figure 4.32 Typical case microstructures after cold treatment.....	114
Figure 4.33 Variation of microhardness and case microstructures .....	115
Figure 4.34 Retained austenite profiles for as-quenched and cold treated samples.....	116
Figure 4.35 Retained austenite distributions after cold treatment.....	117
Figure 4.36 Martensite tetragonality ratio for initial conditions.....	118
Figure 4.37 Martensite tetragonality ratio (c/a) depth profiles after cold treatment .....	119
Figure 4.38 Residual stress distributions for initial conditions.....	120
Figure 4.39 Residual stress distributions after cryogenic treatment .....	122
Figure 4.40 Carbon and nitrogen depth profiles in quench + tempered condition.....	126
Figure 4.41 Unetched case microstructures after thermal cycles.....	127
Figure 4.42 Etched case microstructure after thermal cycles .....	128
Figure 4.43 Microhardness distributions after thermal treatment.....	129
Figure 4.44 X-ray diffraction patterns after thermal cycles .....	130
Figure 4.45 Retained austenite distributions after thermal cycles.....	131
Figure 4.46 Residual stress distributions after thermal cycle treatment at -30 °C .....	133
Figure 4.47 Residual stress distributions after thermal cycle at RT after Q + T .....	133
Figure 4.48 Residual stress distributions after thermal cycle at 90 °C after Q+T .....	134
Figure 4.49 Residual stress distributions after thermal cycle at 150 °C after Q + T .....	134
Figure 4.50 Retained austenite after shot peening treatment.....	136

Figure 4.51 Residual stresses in retained austenite after shot peening .....	138
Figure 4.52 Residual stress in martensite after shot peening .....	138
Figure 4.53 Volume of retained austenite transformed after shot peening treatment.....	140
Figure 5.1 Variation of retained austenite as a function of C+N content.....	142

## List of Tables

Table 2.1 Reaction rate coefficients for carburizing reactions .....	11
Table 3.1 Chemical composition of 18CrNiMo7-6 (DN 1.6587) steel grade .....	51
Table 3.2 The different carbonitriding treatments and parameters .....	53
Table 3.3 Theta and corresponding Psi angles for austenite and martensite.....	58
Table 3.4 Tempering and cryogenic conditions .....	61
Table 3.5 Thermal stabilization conditions.....	62
Table 3.6 Thermal stabilization conditions for shot peening treatment.....	63
Table 3.7 Shot peening conditions.....	63
Table 4.1 Carbon and nitrogen contents at a depth of 50 $\mu\text{m}$ .....	75
Table 4.2 Peak compressive residual stresses for untempered carbonitrided samples .....	82
Table 4.3 Lattice parameter coefficients .....	94

# 1 Introduction

The application, performance and reliability of power transmission components depend on surface mechanical properties. For power transmission components such as gear, bearing and shafts, a hard surface is needed to resist wear while the core of such components remains soft and tough to resist breakage due to impact that may occur while in service. In the engineering field, it is rare to have a steel grade with the standard properties required for different applications. High carbon/alloy steels by nature are not only hard but also brittle. The brittleness of such steels limits some of the parts from being directly used as machine parts because when such parts are in service are subjected to bending and tensile stresses. In contrast, low alloy steels are characterized by high toughness and ductility; hence they cannot be directly applied as machine parts due to low hardness and poor resistance to wear. As a result, thermochemical treatment, which is one of the surface hardening techniques, is used to impart a hard and wear resistant layer on low alloy steels while the core remaining soft and tough. The common thermochemical techniques include carburizing, nitriding and carbonitriding. For decades, carburizing and quenching has been used as a conventional technique to enhance the surface mechanical properties and endurance limit of gears components. In the last decade, the carbonitriding treatment has been extensively investigated to reach improved mechanical properties [OKH 06, WIN 11]. In particular, within the actual context of CO<sub>2</sub> emission reduction, the tendency of downsizing automotive power train components like gears and shafts is an important strategic issue for industries. In order to do so, strength and endurance limit of materials always need to be improved by enhanced treatments.

Carbonitriding process, which is considered to be the modified form of the carburizing process, involves a simultaneous diffusion of carbon and nitrogen atoms in the interstitial sites of austenite at high temperature. The advantages of carbonitriding over carburizing process arise from the presence of nitrogen which leads to improved hardenability, resistance to wear and softening at elevated service temperature, higher fatigue limits and low operating cost because of lower temperatures and shorter time cycle involved [HER 11]. After carbonitriding, treated parts get high-carbon/nitrogen content and can retain as high as 70% austenite [STE

15]. Several researchers [DEB 75, FRA 60] have pointed out that, such high amount of retained austenite might be disadvantageous for fatigue strength of the hardened structural parts due to decrease in elastic limit and diminishing of the compressive residual stresses in the hardened surface zone. However, it has been also demonstrated that retained austenite under certain circumstances, influences positively the fatigue limit of engineering materials, in particular for gear bending fatigue. One reason for this phenomenon is the increase in plasticity of the case-hardened zone [BRA 83]

Substantial work has, in the past, been carried out to investigate the effect of gaseous composition and control of the carbonitriding atmosphere [DAV 78, SLY 81a, WIN 11]. However, this is not the case when it comes to the impact of varying level of carbon and nitrogen reached after carbonitriding on the phase composition and residual stress distributions. The content, distribution, thermal and mechanical stability of such high amount of retained austenite are a key to guarantee geometrical stability especially in close fittings and pre-mature fatigue failure of the components. Moreover, it is evident that such varying amounts of retained austenite would significantly influence the magnitudes and distribution of residual stresses. However, only limited information is available about the influence of varying the amount of retained austenite on the nature, magnitudes and distribution of residual stresses in both retained austenite and martensite as well as about the thermal and mechanical stability of retained austenite. Above all, nearly all the available information on residual stresses belongs to martensite/bainite phase neglecting the role of RA on macroscopic RS in a multiphase material [CHO 82].

## **1.1 Research objectives**

The aim of this project was to investigate the influence of the carbonitriding process on phase transformation, retained austenite and resulting residual stresses which was carried out using 18CrNiMo7-6 low alloy steel. The specific objectives of this work were to:

- Characterize the state after carbonitriding,
- Analyse the state during and after tempering,
- Investigate the state after tempering coupled with cryogenic treatment,

- Investigate the thermal stability of carbonitrided and tempered samples,
- Investigate the mechanical stability of carbonitrided and tempered samples.

This research was based on both experimental and theoretical work. Five carbonitriding treatments with different carbon and nitrogen contents were carried out. After carbonitriding, the case hardening was done by quenching into oil held at 60 °C. Analysis of the samples in their state after carbonitriding and post-carbonitriding treatments were done using X-ray diffraction. Moreover, other characteristics such as micro-hardness, microstructures, and chemical compositions were also investigated.



## 2 Literature Review

In engineering field, it is rare to have a steel grade with the standard properties required for different applications. For example, high carbon/alloy steels throughout the component are not only hard but also brittle. The brittleness of such steels limits their applicability as machine parts that necessitate high toughness at the core and poses a serious problem during machining. In contrast, low carbon/alloy steel grades consist of low hardness, low resistance to wear, and high ductility, which again limit their applicability as power transmission parts which require hard surface. As a result, a combination of these properties in automotive industry is necessary. For power transmission components like gears and shafts, a hard surface is needed to resist wear while the core of such components remaining soft and tough to resist breakage due to impact that may occur while in service [DOS 13].

To achieve a combination of a hard surface and soft core, one possibility is to subject low carbon/alloy steel grades such as 18CrNiMo7-6 to a case hardening process to improve the wear resistance of the parts without affecting the soft and tough core of the component. Depending on the modification introduced in the case-hardened layer, case hardening processes are divided into two groups [DAV 02]:

- i) Processes which do not change the chemical composition of the component being treated. These processes include induction, flame, electron beam, and laser hardening and
- ii) Processes which do change the chemical composition of the surface/subsurface layer of the component being treated. These processes are also known as thermochemical diffusion processes and include carburizing, nitriding, and carbonitriding etc.

Carbonitriding is a thermochemical process which has been increasingly applied to improve the surface properties of low alloy steel components while the core of such parts remaining relatively soft and tough. Moreover, although the process has proven advantages [PRA 88] competes with other thermochemical processes including carburizing and to a less extent nitriding process.

Theories and principles of the carbonitriding process are primarily the focus in section 2.1. Section 2.2 presents and discusses the various post-carbonitriding treatments, which include tempering, aging, cryogenic and shot-peening treatments.

## 2.1 Carbonitriding process

The carbonitriding process is one of the common case hardening processes during which carbon and nitrogen atoms diffuse simultaneously into the surface of the component at a predetermined temperature above  $A_1$  followed by quenching. The process can be carried out with solid (pack carbonitriding), liquid (cyaniding), and gaseous state (gas carbonitriding) as well as plasma carbonitriding [EL-H 01]. Among these carbonitriding techniques, the gaseous carbonitriding process has found wide industrial application.

The gaseous carbonitriding process is considered to be the modified form of the carburizing process rather than nitriding [DAV 02]. The modification consists of introducing ammonia gas ( $\text{NH}_3$ ) into the gaseous-carburizing atmosphere. In normal industrial practice, the addition of ammonia accounts for about 2 to 10 %  $\text{NH}_3$  Vol.-% of the furnace atmosphere [DAV 78]. On entering the furnace atmosphere, as high as 98% of ammonia dissociates into hydrogen and nitrogen gas ( $\text{NH}_3 \rightarrow \text{H}_2 + \text{N}_2$ ). This reaction does not cause any nitriding effect. Only less about 2 %  $\text{NH}_3$ , known as residual  $\text{NH}_3$ , which can be as high as 3500 ppm in the exhaust gas [PRE 66], realises nascent nitrogen as well as hydrogen gas ( $\text{NH}_3 \rightarrow 3/2\text{H}_2 + \underline{\text{N}}$ ) and causes the nitriding effect. The nascent nitrogen together with carbon diffuses into interstitial sites of the austenite. The presence of nitrogen in solid solution considerably enhances the hardenability of carbonitrided components by reducing the diffusion controlled transformation of austenite to ferrite and pearlite and allows low alloy steel to be oil quenched. Moreover, it stabilizes austenite and lowers the martensite start temperature.

In comparison to the carburizing process, the carbonitriding process is carried out at relatively low temperatures between 800°C and 900 °C as opposed to the carburizing process which is normally carried out between 870 to 1065 °C. The low temperature employed during carbonitriding offers added advantage as it reduces operating cost and the risk of grain coarsening. The specific carbonitriding temperature and time, however, depends

on a number of factors such as composition of material, dimensional tolerances, wear resistance, fatigue limit and hardness level required [PRA 88].

In order to reduce the carbonitriding time operating cost, a two-stage gaseous carbonitriding process consisting of boost and diffusion stage is increasingly applied. At IWT - Bremen, the boost stage is commonly carried out at 940 °C coupled with high carbon potential ( $\approx 1.1\%$ ) and ammonia enrichment gas of about 10% that enables rapid saturation of surface with carbon and nitrogen [STE 16]. In contrast, the diffusion stage is carried out at relatively low temperatures in the range of 815 °C to 900 °C, in particular at 850 °C. This in turn enhances nitrogen diffusion into the steel and minimizes distortion of components during quenching.

Figure 2.1 illustrates a typical sketch of a 2-step carbonitriding process indicating the carbon potential and ammonia enrichment rate during boost and diffusion stage. Other carbonitriding parameters used depend on the target of carbon and nitrogen content at the surface and the case depth required.

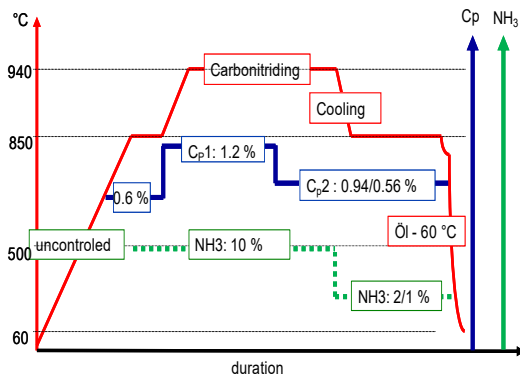


Figure 2.1 Sketch of a 2-steps carbonitriding process consisting of boost and diffusion stage

### 2.1.1 The Carbonitriding Atmosphere

The carbonitriding atmosphere consists of a mixture of carrier gas, enrichment gas and ammonia gas.

- **Carrier gas (Endothermic gas)**, which is a mixture of carbon monoxide (CO), hydrogen (H<sub>2</sub>) and nitrogen (N<sub>2</sub>). In addition, the endothermic atmosphere contains

small amounts of carbon dioxide (CO<sub>2</sub>), water vapour (H<sub>2</sub>O) and methane (CH<sub>4</sub>). Such a carrier gas may have carburizing or decarburizing effect depending on gases composition. Generally, a typical endothermic composition. Generally, a typical endothermic composition would be 0.4–0.5% CO<sub>2</sub>; 20–25% CO; 35–40% H<sub>2</sub>; 1% H<sub>2</sub>O; 40–45% N<sub>2</sub> and 0.1–0.2% CH<sub>4</sub>.

- **Enrichment gas**, a gas that supplies the necessary carbon for the process. Usually methane (CH<sub>4</sub>) or propane (C<sub>3</sub>H<sub>6</sub>) is used.
- **Ammonia gas (NH<sub>3</sub>)**, a gas supplying the necessary nitrogen to the process. The ammonia gas dissociates to liberate nascent nitrogen.

The primary function of the carbonitriding atmosphere is to supply the needed carbon and nitrogen containing species to the surface of the steel part (s) being treated. The transfer and absorption of carbon and nitrogen to the atmosphere/steel interface is a rather complex process involving several reactions [KRA 89] and interactions of CO, N<sub>2</sub>, CO<sub>2</sub>, H<sub>2</sub>O, CH<sub>4</sub>, C<sub>3</sub>H<sub>6</sub>, and residual NH<sub>3</sub>. A successful carbonitriding process is assured by homogeneous gaseous compositions in the furnace atmosphere. The interactions among gases in the furnace atmosphere as well as the interaction between the atmosphere and the steel being carbonitrided never establish equilibriums [BOY 87] mainly due to addition of enrichment gas (CH<sub>4</sub> or C<sub>3</sub>H<sub>6</sub>) which counteract the effect of decarburization. Harris reports that as many as 180 reactions may occur simultaneously in the carbonitriding atmosphere [HAR 43]. Recently, Bischoff [BIS 10] presented a graph showing the main carburizing and nitriding reactions occurring during carbonitriding process which gives distinct carburizing and nitriding processes as indicated in Figure 2.2.

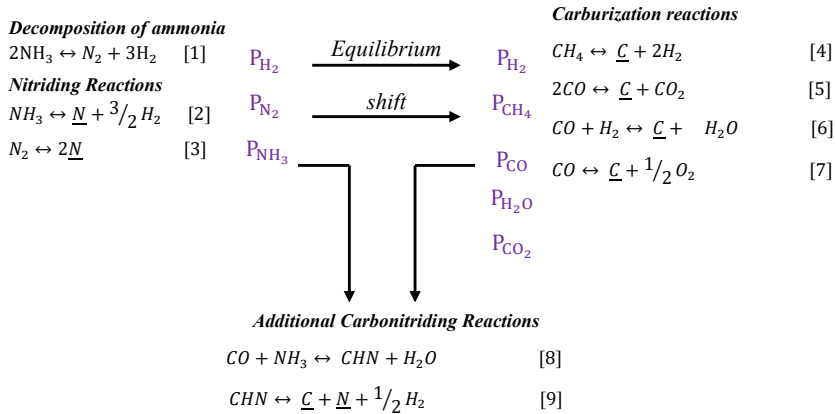


Figure 2.2 Main reactions occurring in the carbonitriding atmosphere[BIS 10]. NB:  $\underline{\text{C}}$  and  $\underline{\text{N}}$  denote the carbon and nitrogen in solid solution austenite

**The carburizing process** - only reactions 4 to 6 are considered important and transfer carbon atoms to the surface of the steel component. Among these three reactions, reaction 5 is by far the fastest and is considered to be the rate determining step in carburizing process with CO and H<sub>2</sub> being the major gas components [KAR 07]. Due to the fact that reaction 4 to 6 are reversible reactions and that CO<sub>2</sub> and H<sub>2</sub>O are strong decarburizers, excessive amounts of these gases can cause reactions 5 and 6 to proceed to the left in order to establish equilibrium constant (K). The side effect is that these reactions will lead to decarburization of the steel component which necessitates the introduction of methane (CH<sub>4</sub>) or propane (C<sub>3</sub>H<sub>6</sub>) to counteract the decarburization effect according to:



If reactions 10 and 11 proceed to the right, CO and H<sub>2</sub> insure that reaction 5 and 6 proceed to the right and that carburization continues. As a result, the process becomes self-sustaining as long as the CH<sub>4</sub> or C<sub>3</sub>H<sub>8</sub> enrichment gas is added to the endothermic carrier gas.

**The nitriding process** - in normal industrial practice, the addition ammonia accounts from about 2 to 10 % NH<sub>3</sub> Vol.-% of the furnace atmosphere [DAV 78]. Upon addition into the

furnace atmosphere, a large proportion (about 98%) of ammonia dissociates according to reaction 1 of which the partial pressure of nitrogen does not significantly affect the diffusion of nitrogen penetration in the steel. Only a small portion of ammonia less than 2 % (residual NH<sub>3</sub>), which can be as high as 3500 ppm in the exhaust gas [PRE 66] releases nascent nitrogen and hydrogen gas according to reaction 2 in Figure 2.2 and causes the nitriding effect. One of the common effects for addition of ammonia to the carburizing atmosphere is that it dilutes the atmosphere by adding nitrogen and hydrogen gas further affecting the carbon potential.

### 2.1.2 Control of Carbonitriding Atmosphere

The carbon potential (C<sub>p</sub>) in the furnace atmosphere at a specified temperature is defined as the carbon content of pure iron (*unalloyed steel*) that is in thermodynamic equilibrium with the atmosphere. Similarly, nitrogen potential (N<sub>p</sub>) is the nitrogen content of pure iron that is thermodynamic equilibrium with the furnace atmosphere. In the carbonitriding furnace, the carbon potential (C<sub>p</sub>) can be estimated using reaction 12 to 14. On the other hand, the nitriding potential (K<sub>N</sub>) can be determined using reaction 2. However, the important parameters during carbonitriding is the carbon activity (a<sub>c</sub>) and reaction rate coefficient (k) which can be determined according to equation 12 to 14 [KAR 07].

$$a_{C_4} = \frac{P_{CH_4}}{P_{H_2}^2} \cdot \exp\left(\frac{10949.68}{T} - 13.31\right), \quad k_4 = 1.96 \cdot 10^{-2} \cdot P_{H_2}^{1.5} \cdot \exp\left(\frac{-17600}{T}\right) \quad [12]$$

$$a_{C_5} = \frac{P_{CO}^2}{P_{CO_2}} \cdot \exp\left(\frac{20530.65}{T} - 20.98\right), \quad k_6 = 184 \cdot \left(\frac{P_{CO_2}}{P_{CO}}\right)^{-0.3} \cdot P_{CO_2} \cdot \exp\left(\frac{-22400}{T}\right) \quad [13]$$

$$a_{C_6} = \frac{P_{CO} \cdot P_{H_2}}{P_{H_2O}} \cdot \exp\left(\frac{16333.11}{T} - 17.26\right), \quad k_5 = \frac{4.75 \cdot 10^5 \cdot \exp\left(\frac{-27150}{T}\right) \cdot \frac{P_{H_2O}}{\sqrt{P_{H_2}}}}{1 + 5.6 \cdot 10^6 \cdot \exp\left(\frac{-12900}{T}\right) \cdot \frac{P_{H_2O}}{\sqrt{P_{H_2}}}} \quad [14]$$

As an example, Table 2.1 presents the calculated reaction rate coefficients (k<sub>s</sub>) for the carburizing reactions 4 to 6 for a typical endothermic atmosphere composition of 18.3% CO, 0.23% CO<sub>2</sub>, 46.6% H<sub>2</sub>, 0.3% H<sub>2</sub>O, and 10% NH<sub>3</sub> at 940 °C. From this table, the reaction rate

coefficient reaction 6 ( $k_5$ ) is the fastest among the three reactions and determines the transfer and adsorption of carbon at the steel.

Table 2.1 Reaction rate coefficients for carburizing reactions 12 to 14 at 940 °C

	Reaction 12	Reaction 13	Reaction 14
Reaction rate (k, cm/s)	$3.12 \cdot 10^{-9}$	$1.51 \cdot 10^{-8}$	$2.50 \cdot 10^{-7}$
Normalized rate coefficient	0.01	0.03	1

Recently, however, Winter [WIN 11] considered re-defining the  $C_p$  and  $N_p$  taking into account the influence of carbon on nitrogen and vice versa. In this context, nitrogen acts as alloying element for carbon. Similarly, carbon acts as alloying element for nitrogen. He re-defines  $C_p$  as the equilibrium surface carbon weight percentage in iron found in addition to nitrogen. In the same manner, he re-defines nitrogen potential as the nitrogen weight percentage in iron found in addition to carbon. Under this consideration, one can determine  $C_p$  and  $N_p$  according to expression 15 and 16 respectively [WIN 11]:

$$C_p = 10^{-0.081 \cdot \%N} \cdot C_{p_{atm}} \quad [15]$$

$$N_p = 10^{-0.187 \cdot \%C} \cdot N_{p_{atm}} \quad [16]$$

where  $C_{p_{atm}}$  and  $N_{p_{atm}}$  are carbon and nitrogen potentials in the furnace atmosphere respectively. In this case, the carbon and nitrogen potentials in the furnace atmosphere can be determined according to equation 17 and 18.

$$\log(a_{catm}) = \frac{2300}{T} - 2.21 + 0.15 \cdot C_{p_{atm}} + \log(C_{p_{atm}}) \quad [17]$$

$$\log(N_{p_{atm}}) = \log\left(\frac{P_{NH_3}}{(P_{H_2})^{1.5}}\right) - \frac{2210}{T} + 3.91 \quad [18]$$

### 2.1.3 Carbon and nitrogen diffusion into steel

The transport of carbon and nitrogen from the furnace atmosphere into the interior part of the component being carbonitrided involves three steps as illustrated in Figure 2.3. The first step involves the diffusion of carbon and nitrogen gas carriers ( $CO$ ,  $NH_3$ ) from the atmosphere to the component surface, which is controlled by mass transfer coefficient. In the second step,

carbon and nitrogen carrier species adsorb on the metal surface and immediately reactions occur at the metal surface realising nascent carbon and nitrogen. Lastly, both carbon and nitrogen atoms simultaneously diffuse into the interior of the component, controlled by Fick's diffusion laws. Several researchers have investigated the effect of different parameters governing the mass transfer and diffusion of carbon and nitrogen [KAR 06, WIN 11]. The mass transfer coefficient has been reported to be a complex function dependent on the atmosphere composition, carbon/nitrogen potential, temperature and surface carbon/nitrogen content [WEI 13]. In addition, the carbon/nitrogen diffusion coefficient determines the rate of carbon/nitrogen transfer and is strongly dependent on temperature and the initial carbon/nitrogen concentration of the steel [SLY 81b, OHK 06].

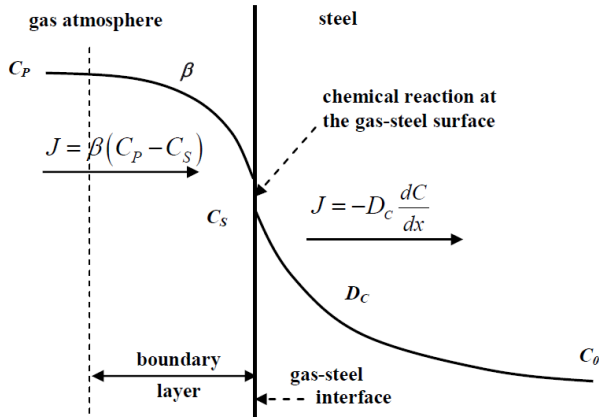


Figure 2.3 Schematic presentation of carbon transport for carburizing part [KAR 07]

From Figure 2.3,  $J$  is the flux representing the amount of carbon or nitrogen atoms that pass through unit area of plane per unit time. In gaseous carbonitriding, it is assumed that the amount of carbon or nitrogen atoms transferred from the atmosphere to the surface of steel component equals to the amount of same species diffusing from the surface to the interior of the steel component. This can be represented using equation 19 and 20 for carbon and nitrogen respectively.

$$\beta(C_p - C_s) = -D_c \frac{dC}{dx} \quad [19]$$

$$\beta(N_p - N_s) = -D_N \frac{dN}{dx} \quad [20]$$

Where  $\beta$  is the mass transfer coefficient,  $C_p/N_p$  is the carbon/nitrogen potential in the atmosphere,  $C_s/N_s$  is the surface carbon/nitrogen concentration,  $D_c/D_N$  is the carbon/nitrogen diffusion coefficient,  $C/N$  is the carbon/nitrogen concentration at a distance  $x$  from the surface of the component.

If nitrogen is present in the austenite during diffusion of carbon, it is reasonable to assume that it will affect the diffusion coefficient for carbon in a similar manner as carbon does itself. An approximate value of the diffusion coefficient of carbon and nitrogen in Fe-C-N austenite considering the effect on each other is thus obtained by using equation 21 and 22 respectively [SLY 81b]. The detailed information on the mass transfer and diffusion coefficients for carbon and nitrogen are presented in [OHK 06, SYL 81b].

$$D_C^Y = 4.84 \cdot 10^{-5} \cdot \exp\left(-\frac{155,000}{RT}\right) \cdot \exp\left[\frac{570,000-320 \cdot T}{RT} \cdot (x_C + 0.72 \cdot x_N)\right] \cdot \frac{1-5x_N}{1-5(x_C+x_N)} \text{ m}^2/\text{s} \quad [21]$$

$$D_N^Y = 9.1 \cdot 10^{-5} \cdot \exp\left(-\frac{168,600}{RT}\right) \cdot \exp\left[\frac{570,000-320 \cdot T}{RT} \cdot (x_C + 0.72 \cdot x_N)\right] \cdot \frac{1-5x_C}{1-5(x_C+x_N)} \text{ m}^2/\text{s} \quad [22]$$

## 2.2 Retained austenite

### 2.2.1 Origins of retained austenite

Austenite which is a stable phase at high temperatures is essential to manufacturing of carbonitrided/carburized steels. The austenite phase has high solubility for carbon/nitrogen that can be induced by exposure to a carburizing or carbonitriding atmosphere. On rapid cooling/quenching to room or quenchant temperature ( $T_q$ ), austenite transforms by displative shear mechanism to martensite, a hard body centered tetragonal phase [LAR 80]. The austenite to martensite transformation reaction starts at a characteristic temperature known as martensite start temperature ( $M_s$ ) and continues with decreasing temperature until the austenite to martensite reaction ceases at martensite finish temperature ( $M_f$ ).

In most hardenable steels, however, the range of martensite transformation ( $M_s \rightarrow M_f$ ) lies below the quenchant temperature ( $T_q$ ) implying that the transformation of austenite to

martensite will remain incomplete; consequently some amount of austenite will be retained (Figure 2.4). The untransformed austenite is known as retained austenite and depends on different factors including chemical composition, cooling rate and quenchant temperature. Furthermore, the quenchant temperature influences considerably the fraction of retained austenite and it increases with increasing quenchant temperature. Figure 2.5 presents a sketch of the range of martensitic transformation ( $M_s \rightarrow M_f$ ) in which when the composition of the treated part lies beyond 0.7 % wt carbon the  $M_f$  lies well below 0 °C. If the treated part is quenched to 60 °C it retains appreciable fraction of austenite.

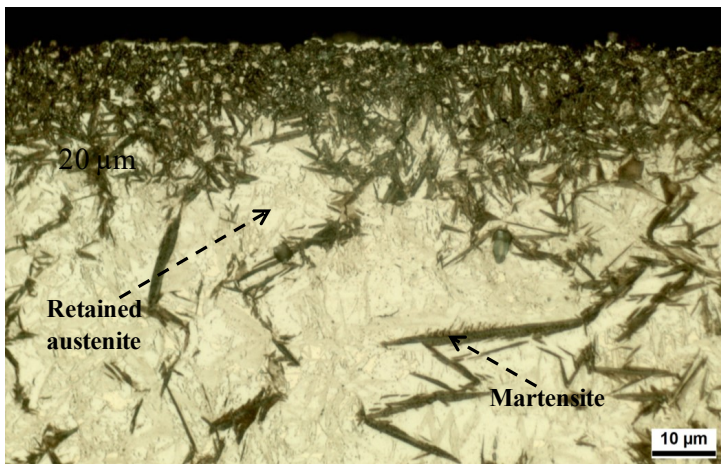


Figure 2.4 Carbonitrided case microstructures (20MnCr5: RA~70%)

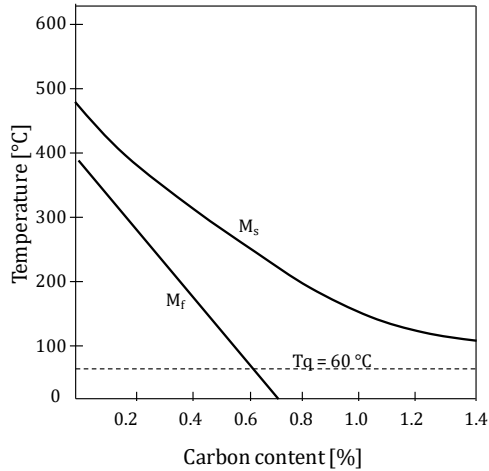


Figure 2.5 Typical example of the range of martensitic transformation

### 2.2.2 Factors that influence the amount of retained austenite

The main factors that influence the amount of retained austenite in the carbonitrided components after quenching are the same ones that affect the formation of martensite. These include: 1) austenite chemical composition prior to quenching, 2) the lowest temperature to which the steel part is quenched and, and 3) the rate of cooling from the hardening temperature [LAR 80]. The specific influence of the first two factors is well established by the Koistinen-Marburger model [KOI 59], equation [23]. For decades, this equation has been applied to estimate the volume fraction of untransformed austenite  $R_A$  as a function of volume of austenite present just above the martensite start  $A$  (100% austenite), the temperature of quenchant medium  $T_q$  below  $M_s$  and the parameter  $b$ , which is commonly kept constant for most steels at a value of 0.011[KOI 59].

$$R_A = A \cdot \exp[-b(M_s - T_q)] \quad [23]$$

To model the kinetics of transformation precisely, Wildau [WIL 86] introduced a modification to the Koistinen-Marburger model according to equation 24. Furthermore, recent

investigations [EPP 12] have found a significant disparity between experimentally determined phase fractions and that determined using Koistinen-Marburger model (Figure 2.6).

$$R_A = A \cdot \exp[-b(M_s - T_q)^n] \quad [24]$$

The temperature at which austenite starts to transform to martensite ( $M_s$ ) is a function of chemical composition and can be estimated using one of the empirical equations published by Steven and Haynes [STE 56]. Among the different equations, equation 25 is regarded to be the most accurate among the several empirical equations [KUN 82].

$$M_s(^{\circ}\text{C}) = 561 - 474(\text{C} + \text{N}) - 33\text{Mn} - 17\text{Ni} - 17\text{Cr} - 21\text{Mo} \quad [25]$$

This equation demonstrates that  $M_s$  is very strongly dependent on carbon and nitrogen content. Carbon is more potent in promoting the retention of austenite due to its ability to change the relative thermodynamic stability of  $\gamma$ - and  $\alpha$ -phases of iron [TOT 98]. Similarly, the presence of nitrogen in carbonitrided components enhances the stability of austenite and lowers further the martensite start temperature; consequently after quenching it is possible to retain over 50 mass.-percent austenite. Such high amount of retained austenite influences not only the mechanical properties but also the magnitude and distribution of residual stresses in the case-hardened layer [KAT 14, PAR 99]. More importantly, such high amount of retained austenite must remain stable in service, because transformation of retained austenite to martensite can lead to dimensional and shape changes, fracture and unpredictable wear and corrosion behaviour of material.

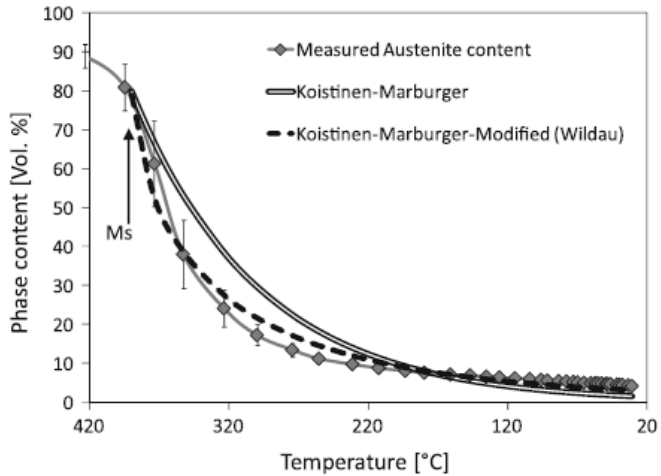


Figure 2.6 Experimentally determined martensite transformation and modelled kinetics by Koistinen-Marburger and by a modification of this equation [EPP 12]

The majority of alloying elements such as manganese, chromium, and nickel decrease the  $M_s$ ; consequently increase the fraction of retained austenite in carburized/carbonitrided parts (Figure 2.7). On the contrary, cobalt and aluminium increase the  $M_s$  as a result decrease the amount of retained austenite and other alloying elements such as silicon have no influence on  $M_s$ .

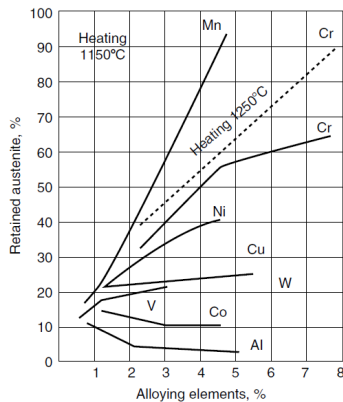


Figure 2.7 Influence of alloying elements on retained austenite [TOT 06]

### 2.2.3 Influence of retained austenite on material properties

- **Influence on hardness**

Although retained austenite is supersaturated with carbon atoms, it is relatively soft in comparison to martensite. The coexistence of retained austenite and martensite microstructure in the case layer lowers the overall hardness of a structure to below that of a structure containing only martensite as illustrated in Figure 2.8.

On the other hand the hardness is considerably improved when a carburized part is subjected to rolling. For example, Razim [RAZ 68] reported an increase in hardness after rolling a component with a case layer containing  $\approx 50\%$  of retained austenite hardness increases due to rolling, whereas the surface containing no austenite are hardly affected.

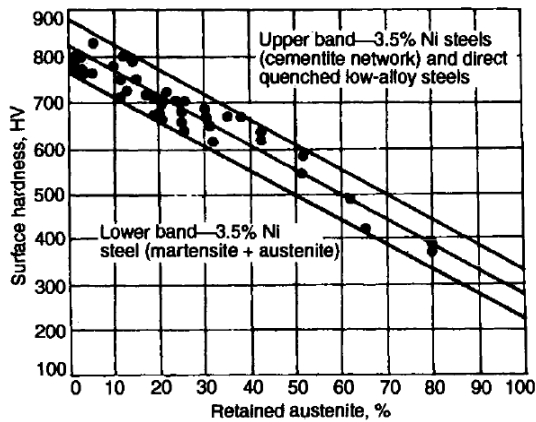


Figure 2.8 Influence of RA on surface hardness of carburized alloy steels [PAR 99].

- **Influence on residual stresses**

In case-hardened steels, the magnitude and distribution of residual stresses is highly dependent on degree and sequence of the martensite transformation reaction [KOI 58]. The co-existence of retained austenite with martensite lowers the compressive residual stresses and in some cases may lead to tensile residual stresses in case-hardened layer (Figure 2.9). The maximum compressive RS occur at some distances from the surface

where the ratio of martensite to retained austenite is about 80%. Recent researches have indicated that the location at which the maximum (peak) compressive occurs has a carbon/nitrogen content of about 0.5 %wt [KAT 14].

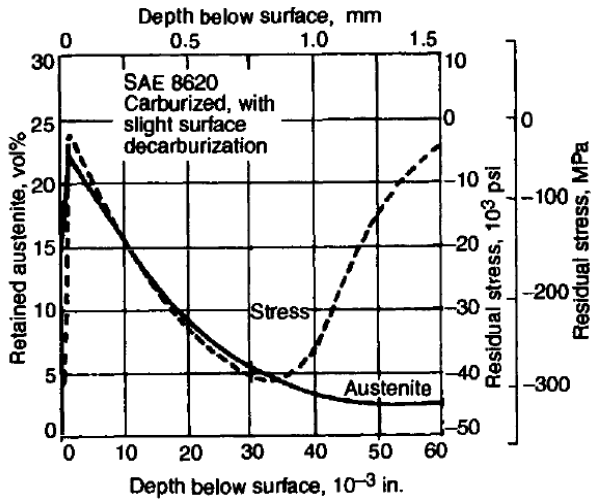


Figure 2.9 Retained austenite and residual stress distribution in case-hardened steel [KOI 58]

- **Influence on fatigue**

Fatigue crack initiation and propagation in the case-hardened layer are strongly dependent on the strength and the nature and magnitude of the residual stresses. The presence of retained austenite in the case layer reduces not only the strength but also the magnitude of compressive residual stresses. Many researchers [WIE 67, BRU 73] reported that fatigue limit decreases with increasing in retained austenite and generally, it would be acceptable that retained austenite is detrimental to the bending fatigue limit. On the other hand, it is possible that retained austenite is beneficial when it slows down the crack growth rate of crack when crack tip in austenite grain triggers the austenite to martensite transformation reaction, thereby raising the strength as well as improving the compressive residual stresses [ZAC 89].

In case of bending fatigue limit, retained austenite is beneficial only if it triggers the retained austenite to martensite reaction. In rolling operation, however, retained austenite is more important due to its ability to undergo plastic deformation. In the work of Razim [RAZ 67] the surface fatigue resistance was reported to increase with increasing amount of retained austenite (up to about 55%).

### **2.3 Stabilization of retained austenite**

Stabilization of retained austenite essentially refers to an impediment to further martensitic transformation. The stabilization of retained austenite may result due to the change in chemical composition, internal compression stress and the possibility to create Cottrell's atmosphere [WAN 01]. In contrast, any process favouring transformation of retained austenite to martensite or high transformation temperature such as bainite as known to destabilize austenite. Such processes include generation of internal tension and shear stresses, and nucleation sites [NIS 78].

According to the nature and mechanisms involved, the stabilization of retained austenite has been divided into three types, mainly: chemical stabilization (due to change in chemical composition), thermal stabilization (due to thermal treatment), and mechanical stabilization (plastic deformation) [KOK 05].

#### **2.3.1 Chemical stabilization of retained austenite**

Chemical stabilization of retained austenite refers to the impediment of transformation of retained austenite to martensite due to change in chemical composition. In this case, the change in chemical composition simply leads lowering of the  $M_s$ . In carbonitrided and/or carburized components, stabilization retained austenite occurs due to diffusion of C (N) atoms from martensite phase that is already transformed into retained austenite.

#### **2.3.2 Thermal stabilization of retained austenite**

Thermal stabilization of retained austenite occurs when a steel component is kept at room temperature for sufficient time or subjected to a temperature range corresponding to the first stage of tempering [THE 74]. The stabilization requires the presence of interstitial atoms

mainly carbon and nitrogen atoms and sufficient time for the atoms to segregate toward the area of high dislocations and austenite/martensite interface, thereby pinning them [STR 09]. The pinning mechanism inhibits further martensitic transformation and hinders the growth of martensite nuclei through loss of mobility of austenite-martensite interface and strengthening of retained austenite matrix [EPP 12, NIS 78]. Some alloying elements, such as nickel if present in the component promote stabilization [ABU 06]. As a result, retained austenite in alloys containing nickel such as 18CrNiMo7-6 and carbonitrided cases will have a greater tendency to stabilize.

One of the common methods to study the degree of thermal stabilization of retained austenite after quenching is by cryogenic treatment. If after quenching, the carbonitrided or carburized parts are immediately subjected to cryogenic treatment, virtually significant amount of retained austenite present at room temperature can further be transformed into martensite. In this case, little or no auto-tempering effect is considered to occur [STR 09]. On the other hand, holding these parts at room temperature or at elevated temperatures for some time can lead to stabilization of retained austenite and becomes more difficult to transform into martensite during cryogenic treatment. As a result, lesser retained austenite would be expected to transform to martensite when subjected to a cryogenic (subzero) treatment in comparison to specimens directly cryogenically treated after quenching. Liebmann [LIE 66] using a ball-bearing steel AISI52100 conducted a series of experiments to investigate the transformation of austenite at -180 °C after stabilizing at various temperatures and times. Figure 2.10 presents one of the results indicating the stabilization effect of retained austenite increases with increasing temperature and time. In addition, the formation of new martensite during cryogenic treatment raises the hardness and compressive residual stresses on the surface while the austenite remaining after cryogenic treatment is susceptible to be set in tensile state [PAR 99].

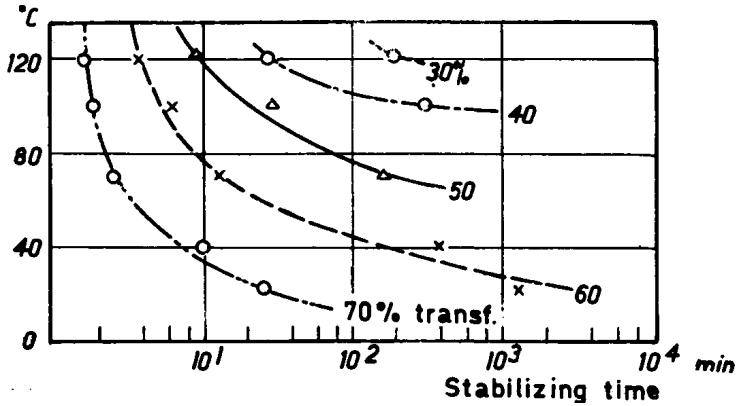


Figure 2.10 Influence of stabilizing temperature and time on retained austenite that transforms on being subzero treated at  $-180\text{ }^{\circ}\text{C}$  [THE 74]. Ball-bearing steel AISI52100 quenched from  $900\text{ }^{\circ}\text{C}$  with 27% retained austenite.

### 2.3.3 Mechanical stability of retained austenite

The mechanical stability of retained austenite is defined as its resistance to undergo transformation under the influence of applied stresses. However, in the literature there is plenty of evidence that retained austenite, particularly blocky austenite, can be stimulated to decompose to martensite under stresses [HOR 78]. Under these circumstances, retained austenite can remain mechanically stable or undergoes decomposition depending on the degree of mechanical stability and the magnitude of applied stresses. To put it another way, retained austenite exhibiting high mechanical stability is strengthened without transformation whereas retained austenite exhibiting low mechanical stability undergo martensitic transformation [KOK 10].

The low mechanical stability of retained austenite is a favourite property in TRIP steel. In TRIP steel, retained austenite is mechanically unstable and can easily transform into martensite under the influence of plastic deformation [SAK 91]. The morphology of retained austenite is described as coarser/blocky or film. According to Yi and co-workers [YI 11], the blocky or coarser austenite transforms during the early stage of deformation but film austenite which is mechanically stabilized remains untransformed until the point of fracture.

In view of degree of stability, several researchers have suggested that there is an optimum stability for retained austenite [SUG 92, GAR 05].

## **2.4 Tempering of case-hardened parts**

The martensite phase which is formed by virtue of diffusion-less and shears nature of austenite transformation is highly unstable during aging and tempering process. Such instability of the as-quenched martensite has been attributed to the high dislocation density in the martensite crystals [SPE 69], supersaturation of carbon and /or nitrogen atoms in the interstitial sites and presence of retained austenite [KRA 12]. The first two features render martensite phase brittle, as a result case-hardened parts are rarely put into service without tempering. Tempering is often applied to improve toughness, ductility and makes carbonitrided parts more amenable to subsequent manufacturing operations, more structurally and dimensionally stable and more durable in service than they would have been remained in their as-quenched state [PAR 99]. Depending on temperature and time employed, as-quenched martensite undergoes a variety of structural changes during tempering.

### **2.4.1 Structural changes during tempering**

After quenching, case-hardened parts (such carbonitrided and carburized parts) are tempered to improve material properties as a result of structural changes occurring during tempering. An extensive work to classify the stages of tempering, driven by the need to understand the practical effects structural changes occurring during tempering, was carried out in the 1950s [WER 57, LEM 54, JAC 51]. The mechanisms associated with the structural changes occurring tempering are best grouped into stages, which in most cases overlap and may be occur concurrently. Most researchers [PAR 99, DAV 02] have established, at least loosely defined, three distinct stages of tempering:

- stage I (80 to 200 °C), is characterized by formation of transition carbides and lowering of carbon content (loss of tetragonality) in martensite phase,
- stage II (150 to 300 °C) during which retained austenite transforms,
- stage III (above 200 °C) , is characterized by replacement of transition carbides and low temperature martensite by cementite and ferrite.

Figure 2.12 presents the structural changes in martensitic steel that can occur at various stages of tempering. However, it is well established that the formation of various precipitates and decomposition of retained austenite during tempering is both temperature and time dependence [NAG 83, THE 74]. This indicates that temperature and time can be traded one another to yield the expected results. Such structural change dependence on both temperature and time is illustrated in Figure 2.14.

Besides classical stages of tempering, other structural changes that may occur prior to the first stage of tempering or after the third stage of tempering have been recognized. In the latter, steel grades containing strong carbide forming elements (such as Cr, Mo, W, V etc.,) can precipitate alloy carbides which are responsible for secondary hardening. Precipitation of alloy carbides is sometime referred to a fourth (IV) stage of tempering [TOT 06].

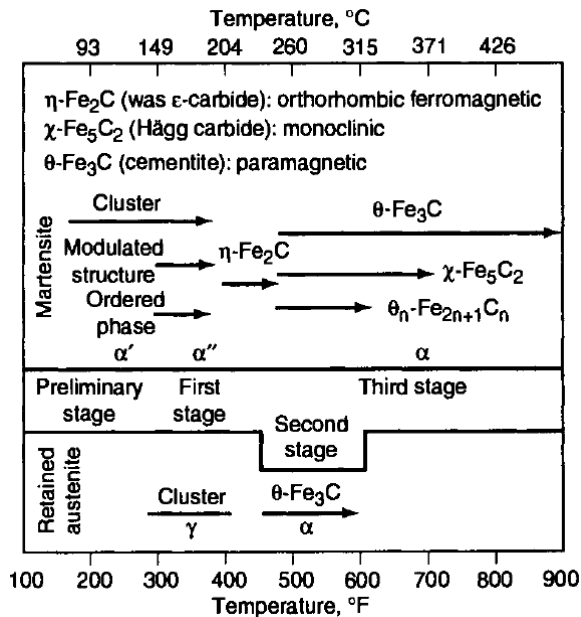


Figure 2.11 Structural changes of martensitic steel resulting from tempering [PAR 99]

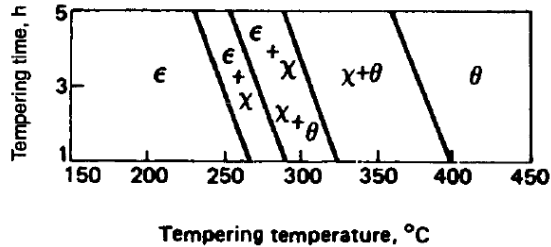


Figure 2.12 Dependence of structural changes on temperature and time for 1.34% C steel [PAR 99]

- **Segregation and clustering of interstitial atoms (0 to 80 °C)**

It is well established that prior to the first stage of tempering, carbon atoms segregation to dislocations and various boundaries may occur during quenching and aging at room temperature [SPE 69, 72]. Atom clustering in as-quenched martensite may precede precipitation of transition carbides/nitrides [GEN 68] that occur in the first stage of tempering. Recent study by Morra et. al., on the decomposition of iron-based martensite using DSC indicated that segregation to dislocations and clustering do not show a distinct length but are characterized by a significant heat release [MOR 01]. Both segregation and clustering occur simultaneously and are governed by diffusion of carbon atoms. It was further observed from their study that the activation energy values for segregation and clustering of carbon atoms are in the range of 81-91 kJmol<sup>-1</sup>. Such observations are in line with the results from the work of Mittemeijer et. al [MIT 88].

Unlike to the significant heat release observed during segregation and clustering of carbon atoms in pure iron-carbon martensite, no such pronounced heat release is observed for pure iron-nitrogen martensite [MIT 88]. Based on investigations using Transmission Electron Microscopy (TEM) and X-ray diffraction, no evidence of clustering of nitrogen atoms was observed [GEN 85]. It is suggested that the high diffusion rate of nitrogen atoms (probably more rapid than that of carbon atoms) can cause a more pronounced auto-tempering for iron-nitrogen martensite than for iron-carbon martensite, which might lead to absence of significant clustering of nitrogen atoms and it appears that nitrogen atoms directly form

regions in the iron matrix with an ordered arrangement of nitrogen atoms identical to that of  $\alpha''$ -nitrides ( $\alpha''$ -Fe<sub>16</sub>N<sub>2</sub>) [MIT 88].

Given the observed differences for segregation and clustering of interstitial atoms in iron-carbon martensite and iron-nitrogen martensite, the need to understand the structural changes in iron-carbon-nitrogen martensite (Fe-C-N) attracted much attention. Ferguson and Jack [FER 84] conducted the first study of tempering Fe-C-N and it was concluded that initially clusters containing both carbon and nitrogen atoms develop, which subsequently evolve into  $\alpha''$ -Fe<sub>16</sub>(C,N)<sub>2</sub> carbonitrides. However, the work of Cheng et. al [CHE 92] and Mittemeijer et. al [MIT 88] on tempering of Fe-C-N martensite, clustering of both carbon and nitrogen atoms as carbonitrides was not observed.

- **Formation of transition precipitates**

This stage is characterized by the formation of transition precipitates whereas the retained austenite remaining relatively stable. It was first reported that the first stage of tempering of Fe-C-N martensite with relatively high concentration of nitrogen atoms is characterized by the formation of  $\alpha''$ -Fe<sub>16</sub>(C, N)<sub>2</sub> carbonitrides [FER 84]. However, such claim was incompatible with the work of Mittemeijer and his colleagues who conducted experiments with the need to understand the structural changes occurring during tempering of FeCN martensite [MIT 88, GEN 92, CHE 92, and BÖT 99]. From their results it was concluded that both carbon and nitrogen follow a different path of precipitation whereas carbon atoms precipitate mainly as  $\epsilon/\eta$  carbide ( $\epsilon$ -Fe<sub>2.4</sub>C with hexagonal crystal structure)/ $\eta$ -Fe<sub>2</sub>C with orthorhombic crystal structure), the nitrogen atoms precipitate mainly as  $\alpha''$ -Fe<sub>16</sub>N<sub>2</sub>. In the work of Genderen [GEN 92] using high energy intensity synchrotron radiations was able to detect the very weak  $\alpha''$  superstructure reflections ( $\{110\}_{\alpha''}$ ,  $\{002\}_{\alpha''}$ , and  $\{211\}_{\alpha''}$ ) in the nitrogen-rich FeCN alloy and a weak  $\epsilon/\eta$  reflection ( $\{100\}_{\epsilon}/\{101\}_{\eta}$ ) in the carbon-rich FeCN alloys. This confirmed the formation of interstitial-rich  $\alpha''$  and  $\epsilon/\eta$  precipitates develop simultaneously in FeCN martensite during first stage of tempering with activation energy of 110 to 125 kJmol<sup>-1</sup> and is ascribed to volume diffusion of interstitials.

The formation of transition carbide and nitride is accompanied by evolution of heat as well as volume misfit between the precipitate and the matrix of which a volume misfit of about 17%

and 6% for FeC and FeN alloy, respectively, can occur [MIT 88]. Such volume misfit can be accommodated by dislocations which are expected to occur during precipitation. In addition, this stage is accompanied by loss of martensite tetragonality and the tetragonal martensite transforms to a cubic tempered martensite form. The work of Wießener et. al [WIE 05] reports that during tempering high speed steel the loss of martensite tetragonality starts at about 100 °C and continues to decrease until 180 °C where it remains relatively stable as illustrated in Figure 2.13. Such decrease is ascribed to the formation of transition precipitates.

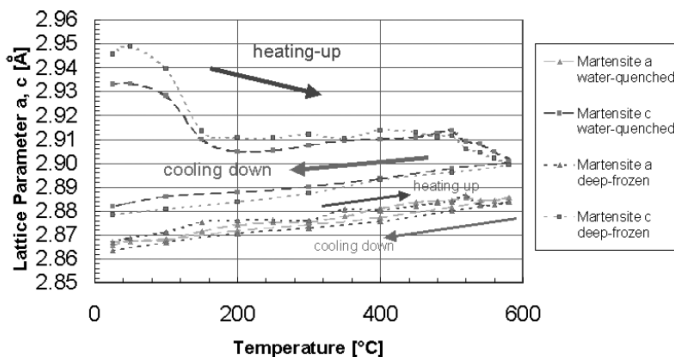


Figure 2.13 Evolution of lattice parameters of martensite during tempering for water-quenched and liquid-nitrogen quenched [WIE 05]

- **Decomposition of retained austenite during tempering**

The second stage of tempering is characterized by transformation of retained austenite which occurs by heating at temperatures and times well above those at which transition carbide and nitride precipitates. Besides the influence of thermal, retained austenite may transform to martensite mechanically under various conditions stress and strain at temperatures lower than those at which thermal decomposition occurs [KRA 15]. The retained austenite substructure differs from that of initial austenite by higher density of imperfections occurring under local plastic deformation and dislocations pileups and stacking faults may be observed in austenite around martensite crystals [TOT 06].

For decades, the need to establish the decomposition range of retained austenite for different steel grades has constantly attracted more researches [SKR 72, NAZ 59, CHE 92]. In the study of Gulyaev [GUL 53] on tempering of plain carbon steels concluded that retained austenite decomposes between 200 °C - 300 °C. This is in good agreement with study of Cheng et. al [CHE 92] on tempering of FeCN in which it was concluded that retained austenite decomposes above 267 °C (540 K). In addition, Cheng et. al suggest that retained austenite decomposes in FeCN at relatively higher temperature as compared to that in FeC and FeN. By contrast, Nazarenko reports decomposition of retained austenite in carbon steel to be in the range of 100 °C - 275 °C with maximum decomposition rate occurring at 200 °C [NAZ 59]. The results of Nazarenko find support from the work of Neu and Sehitoglu [NEU 93] for carburized 4320 steel as illustrated in Figure 2.14. It can be noted from this figure that retained austenite may decompose at lower temperatures if the holding time is extended. Furthermore, the work of Wießner on in-situ investigation during tempering by X-ray diffraction indeed indicates that retained austenite decomposes at about 100 °C [WIE 06]. This research notes significant differences in the temperature range for decomposition of retained austenite. Such differences, however, can be ascribed to the differences in alloying elements. Some of alloying elements such as chromium, nickel and silicon inhibit decomposition, shifting it to higher temperatures and longer tempering time [TOT 02].

The decomposition of retained austenite is accompanied by evolution of heat and volume change [MOR 01]. The activation energy of retained austenite decomposition is about 115 kJmol<sup>-1</sup> [ROB 53, KRA 12], which is consistent with the activation energy for the diffusion of carbon atoms in austenite [WEL 70]. This suggests interstitial atom diffusion in austenite as the rate determining step for the transformation. In this case, interstitial atoms in the supersaturated martensite migrate to the martensite-austenite interface creating local high concentrations of these atoms which later dissolve in austenite [KOG 68]. On the other hand, decomposition retained austenite by interstitial diffusion of carbon/nitrogen atoms is accompanied by volume changes. As the carbonitrided/carburized and hardened parts are typically tempered at 180 °C which is high in temperature range of stage I and low in the temperature of stage II, the contraction due to stage I reactions far outweighs the expansion due to any retained austenite transformation likely to occur [PAR 99]. Besides, Zabil'skii et al.

pointed out that the overall volume change accompanying tempering cannot be fully accounted for by the transformation and precipitation processes [ZAB 79]. They suggest the difference is due to healing of defects in the martensite structure.

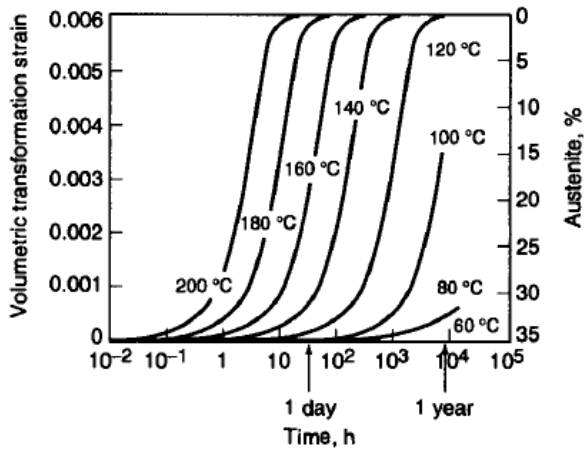


Figure 2.14 Thermally induced-volumetric transformation strain as a function of temperature. (Carburized 4320 steel with 35% initial retained austenite) [NEU 93]

- **Precipitation of equilibrium carbide/nitride**

Tempering in stage III is characterized by conversion of transition precipitates to form equilibrium precipitates during which  $\epsilon/\eta$ -carbides and  $\alpha''$ -Fe<sub>16</sub>N<sub>2</sub> nitrides are converted into more stable  $\theta$ -Fe<sub>3</sub>C and  $\gamma'$ -Fe<sub>4</sub>N nitride respectively. This stage overlap with stage II of tempering and it occurs above 200 °C. As it has been pointed out that no indication of significant joined precipitation of carbon and nitrogen in the form of nitrocarbides or carbonitrides [CHEN 92], it can be speculated that conversion of these transition precipitates into equilibrium precipitates equally follows different routes.

In the literature, it is reported that the conversion reaction of  $\epsilon/\eta$  carbide commences as low as 100 °C and is fully developed at about 300 °C with precipitates up to 200 nm long and 15 nm in diameter [HON 81]. During tempering, the possible nucleation sites for  $\theta$ -Fe<sub>3</sub>C are the  $\epsilon/\eta$ -

carbide interface with the ferrite matrix and grow at the expense of the transition carbides. The activation energy for the process is reported to be between 163 and 212 kJmol<sup>-1</sup> [MOR 01] which is within the range of 152 kJmol<sup>-1</sup> [COH 70] for pipe diffusion of iron and 251 kJmol<sup>-1</sup> [BUF 61] for volume diffusion of iron. This suggests that formation of cementite is a combination of the two mechanisms. In some cases, the steel grade contains substitutional elements such as chromium, manganese and molybdenum which are carbide forming elements. If given mobility at high temperatures, these elements can diffuse into cementite leading to the formation of alloy carbides [TOT 06].

Cheng and his colleagues [CHE 90, MIT 88, GEN 92, BÖT 99] conducted extensive study of the structural changes occurring on tempering FeCN martensite. They reported that conversion of transition  $\alpha''$ -Fe<sub>16</sub>N<sub>2</sub> into equilibrium  $\gamma'$ -Fe<sub>4</sub>N occurs between 200 °C and 350 °C and is accompanied by significant decrease in specific volume and consumption of heat. A specific volume difference of up to 16% between  $\gamma'$ -nitride and the matrix can be observed. As a result pipe diffusion along dislocations to accommodate the volume misfit can occur. The work of Cheng report that for martensite containing 4.6 at.-%N, about 0.32 kJmol<sup>-1</sup> martensite is consumed on the conversion of  $\alpha''$  to  $\gamma'$ -nitride [CHE 90]. The activation energy observed for conversion of  $\alpha''$  to  $\gamma'$ -nitride are in the same range (163 and 212 kJmol<sup>-1</sup>), suggesting a combination of both pipe and volume diffusion mechanisms. In contrast with the formation of cementite on tempering of FeC martensite, the formation of  $\gamma'$ -nitride on tempering FeN martensite can occur before the decomposition of retained austenite [MIT 88], hence it is likely to occur at relatively low temperatures.

## 2.5 Residual Stresses

### 2.5.1 Definition and Origins of Residual Stresses

Residual stresses can be defined as self-equilibrating internal stresses existing in a free body when no external load is applied on a component with homogeneous temperature and remain constant overtime. It is well established that principally no materials and no components or structures of technical importance exist free of residual stresses [MAC 86]. These stresses exist if a component is inhomogeneously deformed.

Within the material, the stresses can be of different nature and balance depending on the level of analysis. Macherauch and Kloss [MAC 86] established the well-known classification of residual stresses. Depending on the scale of observation, he classified residual stresses into three types or kinds which include:

- Residual stresses of type I (*1<sup>st</sup> Kind*) are nearly homogeneous across large areas of a material (i.e. across several grains or different phases) and are in equilibrium over the bulk of the material.
- Residual stresses of type II (*2<sup>nd</sup> Kind*) are nearly homogeneous across microscopic areas (one grain or parts of a grain) of a material and are equilibrated across sufficient number of grains.
- Residual stresses of type III (*3<sup>rd</sup> Kind*) are inhomogeneous across submicroscopic areas of a material, say some atomic distances within a grain and are equilibrated across small parts of a grain.

Figure 2.15 schematically presents three kinds of residual stresses and their superposition across various grains in a two-phase material. Residual stresses of type I (*1<sup>st</sup> kind*) are called macrostresses while that of type II and III (*2<sup>nd</sup> and 3<sup>rd</sup> kinds*) are collectively known as microstresses. Considering macro- and microstresses group, the origin of residual stresses in a component depends on the scale of observation.

The origin of residual stresses can be traced through the different manufacturing and processing route of a component. These are classified as mechanical (*machining, shot-peening*), thermal (*heat treatment, laser treatment*), thermo-mechanical (*forging, welding*), and thermochemical (*carburizing, carbonitriding*) [FIT 03]. During these operations, the residual stresses in a component arise mainly due to inhomogeneous deformations and misfit in different zones [NOY 87].

In the view of Mittemeijer [MIT 83], the inhomogeneous deformation and misfit during thermochemical treatment occur because of:

- **Compositional variations:** Thermochemical heat treatments such carbonitriding and carburizing evoke carbon and nitrogen concentration profile which in turn lead to macro-stress profile. Similarly, micro-stresses are likely to be introduced by carbon and nitrogen atoms dissolved interstitially in the octahedral interstices of the iron matrix.

- **Thermal effect:** Steels possess a relatively low thermal conductivity and relatively strong temperature dependence of yield strength. During quenching, the surface of a specimen cools faster than its core, creating temperature gradient; consequently stresses develop. If such stresses cannot be accommodated fully elastically, residual stresses will be present after cooling. In the latter case, compressive residual stresses occur in the case layer and the tensile stresses in the core are evoked. In the above case it has been considered that the work piece is an isotropic monophase system, where in reality multiphase materials are generally used. This should especially be realized in the view of residual microstresses which are generated as a result of the difference between thermal expansion coefficients of a dispersed (carbides, nitrides) phase and the steel matrix.
- **Phase Transformation.** Thermochemical and induction treatment are case-hardening methods where the austenite to martensite phase transformation plays a central role. The formation of martensite in the case leads to formation of compressive residue stresses in the subsurface whereas formation of bainite microstructure in the core leads generation of tensile residue stresses in the core.
- **Lattice defects.** The lattice defects such as misfit due to precipitates dissolved alloying atoms, and dislocations can evolve during case-hardening and contribute to residual microstresses. However, the contribution of these defects on the average microstrain is difficult to assess.

In thermochemical treatments such as carbonitriding, residual stresses after quenching are mainly considered to be due to temperature differences between the case and the core and volume change due to austenite to martensite transformation [TOT 06]. In order to understand the evolution and the formation of residual stresses during and after quenching of carbonitrided parts, one needs to be acquainted with the basic mechanisms of how the temporal and local differences in cooling and transformation processes yield thermal stresses, transformation stresses and the change in microstructural state. The basic mechanisms of how thermal, transformational and hardening stresses occur are presented in the subsequent sections.

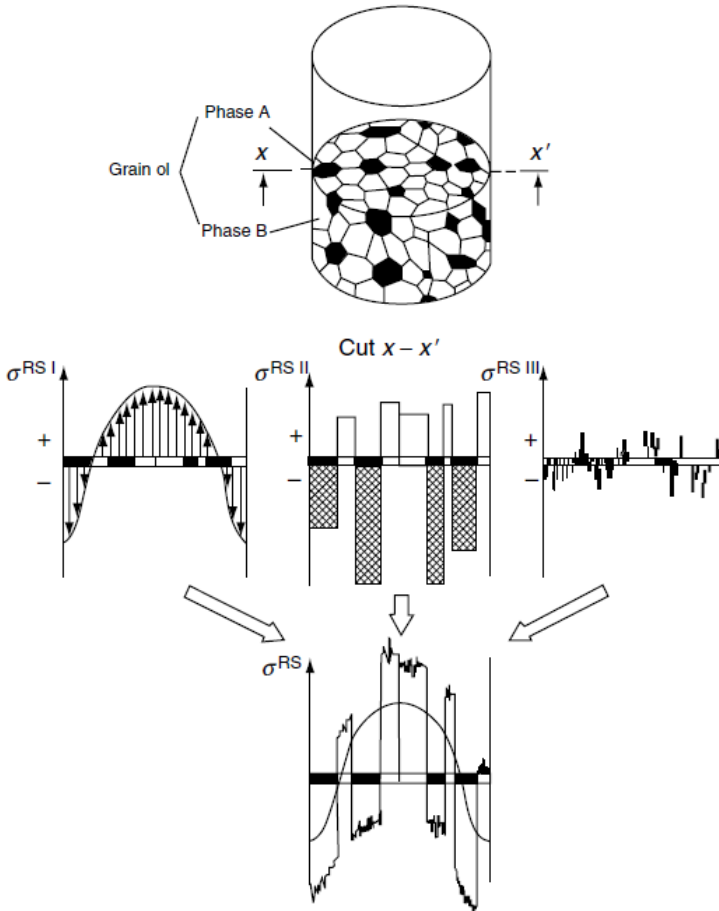


Figure 2.15 Kinds of residual stresses in a two-phase material after quenching and their superposition [LIS 06]

### 2.5.2 Thermal residual stresses

The basic principles for the development of thermal (*transformation-free*) stresses are described in many textbooks [TOT 98, THE 74]. When a component is heated up and then quenched, a temperature difference between the surface and the core is established leading to

the generation of thermal stresses. At start of quenching the surface temperature decreases faster than the core temperature (Figure 2.16a). As a result, tensile stresses develop at the surface and compressive stresses develop in the core. If during quenching the stresses were elastically accommodated, their development during and after quenching would appear as shown in Figure 2.16b. However, in real case the yield strengths ( $R_y$ ) of the surface and the core are temperature dependent and neither the surface nor the core can withstand the thermal stresses without plastic deformation. After time  $t = t_{\max}$ , the temperature gradient between surface and core starts to decrease. As a result, the magnitude of stresses at the surface and the core decrease continuously reaching zero value at different instants. On further cooling, the extension and compressive lead to development of compressive and tensile stresses, respectively, compensating stresses due to temperature difference that are still exist between the surface and the core. At the end of quenching, the thermal residual stresses remaining are compressive at the surface and tensile at the core as depicted in Figure 2.16c.

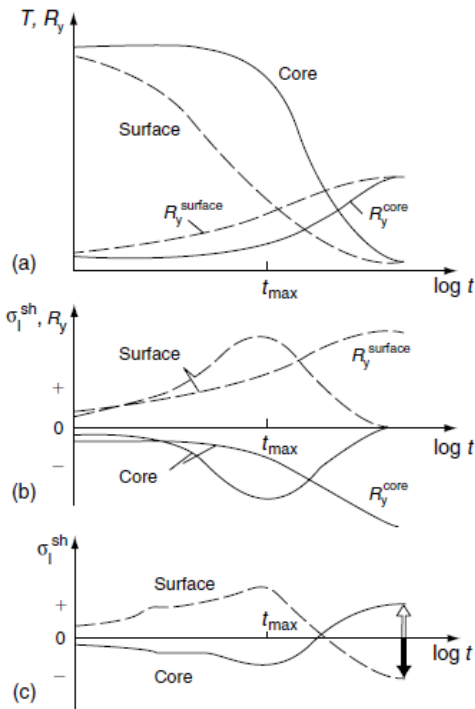


Figure 2.16 Evolution of thermal residual stresses during quenching [Lišćić 92]

### 2.5.3 Transformation residual stresses

Depending on the cooling rate, austenite which is a stable phase at high temperature, can transform to various microstructural constituents including martensite, bainite, pearlite or ferrite. Rapid cooling (quenching) of components with sufficient amount of interstitial carbon or nitrogen always leads to the formation of martensite phase leading to residual stresses of second kind. The nature and magnitudes of these stresses highly depend on the initial position and time of transformation.

A typical example transformation residual stresses during cooling is illustrated in Figure 2.17 as explained by Lišćić [Lišćić 92]. In addition, the figure contains the yield strengths ( $R_y$ ) of the

surface and core, showing their strong increase with the onset of martensitic transformation. For simplicity, it is assumed that no thermal stresses occur. In this case, the surface transforms at time  $t_1$  (Figure 2.17a) prior to core transformation leading to the development of compressive stresses in the surface and balancing tensile stresses in the core. The compressive residual stresses in the case increases with the increasing degree of transformation in the surface which finishes at time  $t_2$ . Similarly, at this time  $t_2$  the core starts to transform and reduces both the magnitudes of compressive residual stresses in the surface and the tensile residual stresses in the core.

If during quenching the stresses were elastically accommodated, their development during and after quenching would appear as shown in Figure 2.17b. However, in real case the yield strengths of the surface and the core are temperature dependent and neither the surface nor the core can withstand the transformational stresses without plastic deformation. As a result, at the end of quenching the transformational residual stresses are compressive at the core and tensile in the surface as illustrated in Figure 2.17c. In contrary to the nature of the transformational residual stresses shown in Figure 2.17c, if the core transforms prior to the surface transformation then the transformational residual stresses would have been compressive in the surface and tensile in the core.

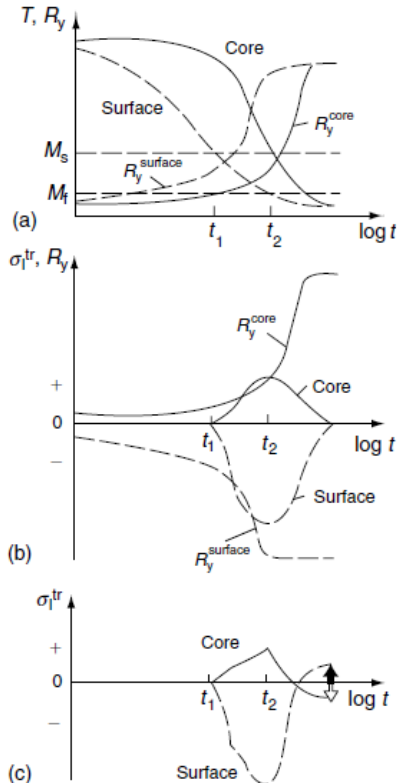


Figure 2.17 Transformation residual stresses during and after quenching [LIŠ 92]

### 2.5.4 Hardening residual stresses

When carbonitrided steel components are quenched to room temperature, both thermal stresses and transformational stresses develop, leading to hardening residual stresses. Macherauch and Vöhringer [MAC 92] pointed out that the hardening residual stresses resulting after quenching cannot be accounted for by a simple superposition of thermal stresses and transformation stresses. This is mainly due to the fact that during quenching, any local martensitic transformation is accompanied with volume increase and always shifts the existing stress values (*both tensile and compressive stresses*) to more negative magnitudes. In

view of this, transformations occurring in the tensile stressed-zones are therefore inevitable to reduce the magnitudes of stresses, whereas transformations taking place in the compressive stressed-zones enhance the magnitudes of stresses. Given the thermal stresses in the case and core evolved during quenching, the relative positions of the initiation time of time transformation in the case and in the core are of fundamental importance for the stresses remaining after quenching [MAC 92a].

The relative position and time at which martensitic transformation begins is dependent on martensite start temperature ( $M_s$ ). The  $M_s$  is further dependent on composition of alloying elements of the steel component in addition to the carbon and nitrogen gradients developed during thermochemical treatment. With regard to the relative position and time at which transformation at the surface and the core could begin, several researchers [RÉT 02, MAC 92] proposed different possibilities for generation and development of hardening stresses, in particular surface compressive residual stresses. In a more detailed way, Macherauch and Vöhringer pointed three cases for the initiation position and time of transformation that are likely to occur during quenching. In the first case, the core transformation occurs prior to surface transformation. Consequently, after quenching compressive residual stresses are developed in the surface and tensile residual stresses at the core (Figure 2.18). The second considers that the surface transformation occurs prior to core transformation which leads to the formation of tensile stresses in the surface and compressive residual stresses at the core (Figure 2.19). The last case is when there is no preference concerning the sequence of transformation in the case and the core. In this case there exist several intermediate residual stress distributions between the above-mentioned extremes. In the same way, Liščić [LIŠ 92] has emphasized that in order to develop surface compressive stress austenite transformation during quenching should proceed progressively from the case/core interface outward toward the surface component. This view is also sustained by the work of Dawes and Tranter [DAW 74] on application of carburizing theory to practice. They have shown that austenite to martensite or bainite transformation begins at the case/core interface and progresses outward as indicated in Figure 2.20.

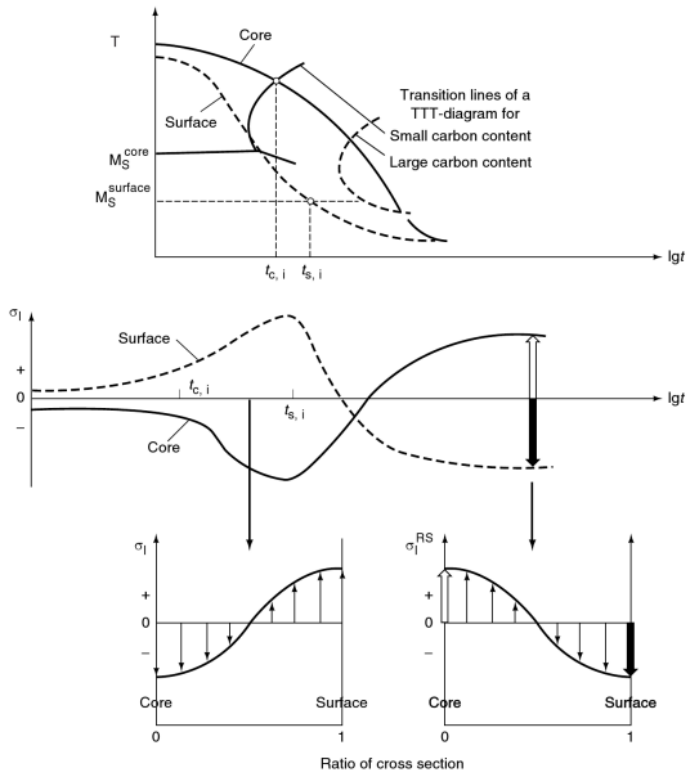


Figure 2.18 Residual stress distributions when transformation starts at the core [MAC 92]

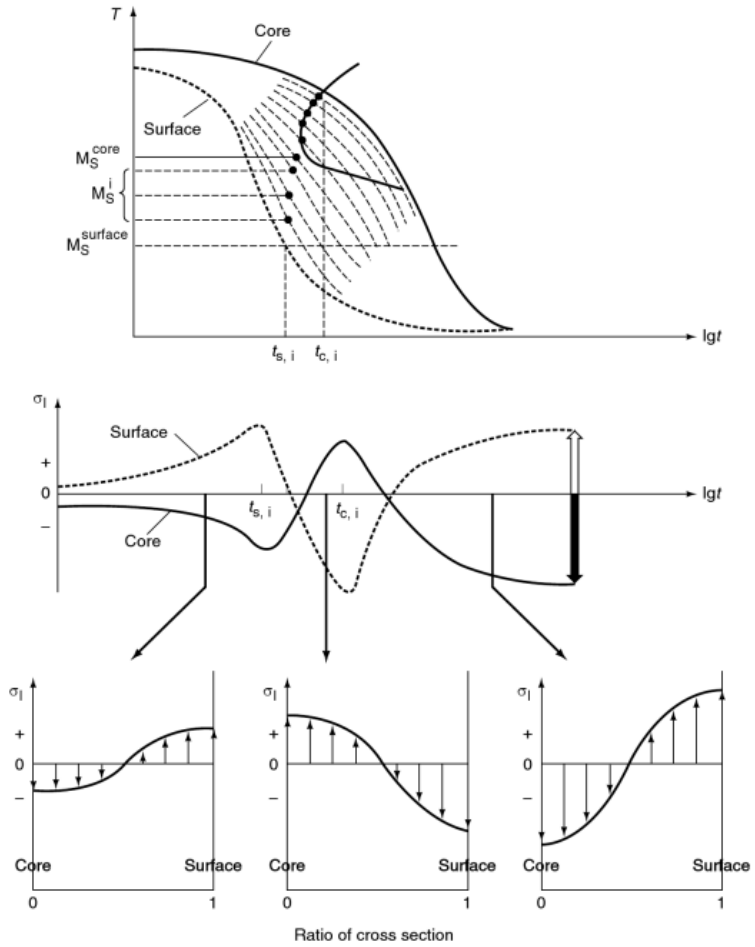


Figure 2.19 Residual stress distributions transformation starts at the surface [MAC 92]

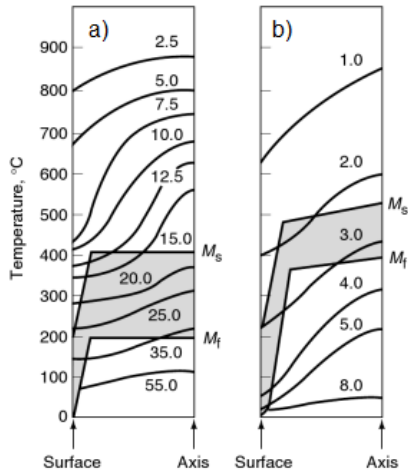


Figure 2.20 Temperature distribution and progress of martensitic transformation during quenching of carburized components. Figures in curves indicate time in seconds: a) oil quenched steel, b) water quenched steel [DAW 74].

The three cases presented for the development of hardening residual stresses during quenching and the nature of residual stresses after quenching assume that after quenching the surface/subsurface contains 100% martensite. However, the case microstructures are characterized by not only martensite and finely disseminated precipitates but also with retained austenite depending on the local carbon content in solution. The latter tends to increase with increasing amount of carbon and nitrogen content and alters significantly the nature and distribution of hardening residual stresses after quenching. Maximum compressive residue stress occurs at some distance from the surface where the proportion of martensite to retained austenite is high, but lower compressive residue stresses occur at the surface/subsurface where the proportion of martensite to retained austenite is low [PAR 99]. Figure 2-21 is a typical sketch illustrating the low compressive residue stresses the region of high retained austenite content whereas the peak compressive residue stresses occurring at the region where retained austenite content is about 20%.

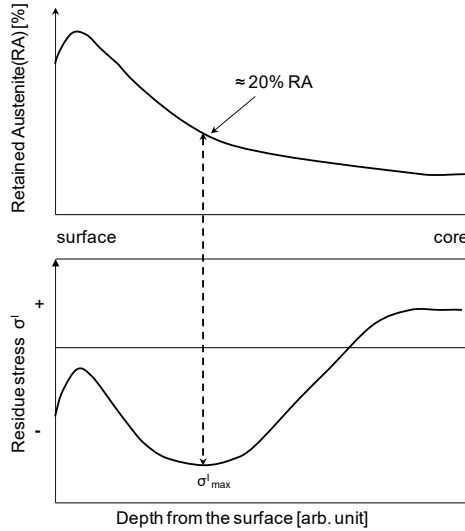


Figure 2.21 Influence of retained austenite on residual stress distributions

## 2.6 X-ray diffraction

X-rays are electromagnetic radiations with a wavelength of about  $1\text{ \AA}$  which is about the same size as lattice parameters. Although Röntgen discovered X-rays on 8th November 1895, it was until in November 1912 when W. L. Bragg, the son of W. H. Bragg, established a fundamental relationship describing the diffraction of X-rays by crystalline structure [GUI 07] of which became to be known as Bragg's law. The Bragg's law (equation 26) describes the interaction between x-rays and atoms in a crystalline material [ELT 66]:

$$n\lambda = 2d\sin\theta \quad [26]$$

where,  $\lambda$  is the wavelength of the radiation used,  $\theta$  is the Bragg angle, and  $d$  is the average interplanar spacing for the given reflection in a crystalline material.

## 2.6.1 Principles of quantitative phase analysis by X-ray diffraction

- **Introduction**

Quantitative phase analysis (QPA) of diffraction patterns by X-ray diffraction (XRD) refers to the determination of the amount of different phases in multi-phase specimens. Also, QPA can signify the determination of particular characteristics of a phase such as crystal structure, diffracting crystallite size and shape.

In the use of quantitative analysis, its success does not only depend on the initial inputs mainly standard diffraction pattern and structural data but also the modelling of the diffraction pattern such that the calculated pattern duplicates the experimental one. The analysis requires precise and accurate determination of both peak positions and intensities of diffraction patterns for a sample. The peak positions are indicative of the crystal structure and symmetry of the contributing phase whereas the peak intensities reflect the total scattering from each in the phase's crystal structure, and are directly dependent on the distribution of particular atoms in the structure [CON 12]. The diffracted intensity is related to both the structure and composition of the phase according to equation 27:

$$I_{(hkl)\alpha} = \frac{I_0 \lambda^3}{64\pi r} \left[ \frac{e^2}{m_e c^2} \right]^2 \frac{M_{(hkl)}}{V_\alpha^2} |F_{(hkl)\alpha}|^2 \left[ \frac{1 + \cos^2(2\theta) \cos^2(2\theta_m)}{\sin^2 \theta \cos \theta} \right]_{hkl} \frac{\vartheta_\alpha}{\mu_s} \quad [27]$$

where:

- $I_{(hkl)\alpha}$  = Intensity of reflection of  $hkl$  in phase  $\alpha$
- $I_0$  = incident beam intensity
- $r$  = distance from specimen to detector
- $\lambda$  = X-ray wavelength
- $\left[ \frac{e^2}{m_e c^2} \right]^2$  = square of classical electron radius
- $\mu_s$  = linear absorption coefficient of the specimen
- $\vartheta_\alpha$  = volume fraction of phase  $\alpha$
- $V_\alpha^2$  = volume of the unit cell of phase  $\alpha$
- 0 = Lorentz-polarization (and monochromator) correction
- $2\theta_m$  = diffraction angle of the monochromator

$F_{(hkl)\alpha}$  = structure factor for reflection hkl of phase  $\alpha$

Most of these terms are consistent for a particular experimental setup and can be defined using an experimental constant  $K_e$ . For a particular phase, another constant ( $K_{(hkl)\alpha}$ ) describing the structure factor term for phase- $\alpha$  is given. The intensity of peak hkl in phase after substituting the weight fraction ( $X_\alpha$ ) for the volume fraction, the density for the volume and the mass absorption coefficient is given by equation 28:

$$I_{(hkl)\alpha} = \frac{K_e K_{(hkl)\alpha} X_\alpha}{\rho_\alpha (\mu/\rho)_s} \quad [28]$$

Traditionally, quantitative phase analysis had been based on a single or small part of the total peaks in the diffraction patterns. In the 1960s, the growth of powerful pattern decomposition techniques provided the analyst with the most of the tools for working with the full diffraction patterns [RIE 69]. The full pattern diffraction method involves fitting the entire diffraction pattern with a synthetic diffraction pattern. The synthetic diffraction can either be calculated and fitted dynamically from crystal structure data [BIS 88] or can be produced from a combination of observed or calculated diffraction patterns [SMI 87]. One of the most useful techniques in working with full diffraction pattern is the Rietveld Method initially conceived as the method of refining crystal structure using neutron powder diffraction data.

- **The Rietveld Method**

Quantitative phase analysis using calculated full pattern is a natural outgrowth of the Rietveld method originally conceived as a method of refining crystal structure using neutron powder diffraction data [RIE 67]. The initial input data requires the knowledge of the approximate crystal structure of all phases of interest including the space group symmetry, atomic positions, site occupancy, and lattice parameters. Furthermore, refining to match the calculated and observed profile patterns requires parameters defining the profile shape, a background function and scale factor for each phase.

The least-square refinement using the Rietveld Method minimizes the sum of the weighted, square differences between observed and calculated intensities at every step in a digital x-ray profile. The refinement process is carried out until the best fit is obtained between the observed and the calculated diffraction pattern based on the simultaneously refined models for the crystal structure(s), diffraction optics effects, instrumental factors and other specimen characteristics. The quantity minimized during least-squares refinement is the conventional least square residual (R):

$$R = \sum_j w_j |I_{j(o)} - I_{j(c)}|^2 \quad [29]$$

where  $I_{j(o)}$  and  $I_{j(c)}$  are the observed and calculated intensities, respectively at the  $j^{\text{th}}$  step in the data and  $w_j$  is the weight. A typical of the observed and calculated diffraction patterns is presented in Figure

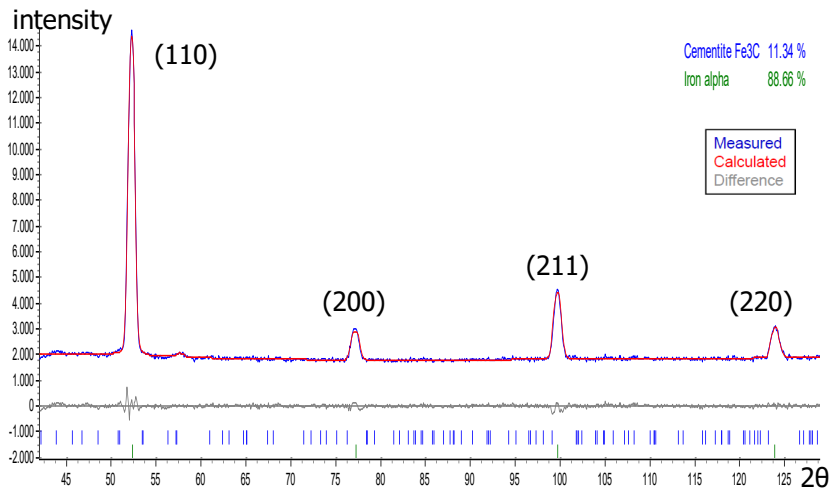


Figure 2.22 Example of X-Ray Diffraction Full Pattern Refinement using TOPAS for 20MnCr5 steel grade

## 2.6.2 Principles of residual stress measurement by X-ray diffraction

- **Introduction**

The application of X-ray diffraction on the determination of stresses is based on the fact that when the part/crystalline material is subjected to applied or residual stresses, the resulting elastic strains cause the plane interplanar spacings to change. The change in planar spacings can be determined using X-ray diffraction which the magnitude and nature of stresses can be determined.

Suppose that  $d$  and  $\theta$  are the stressed lattice spacing and corresponding Bragg's angle and  $d_0$  and  $\theta_0$  are stress free lattice spacing and corresponding Bragg's angle, then the elastic strain can be calculated as:

$$\varepsilon = \frac{d-d_0}{d} = \frac{\sin\theta_0}{\sin\theta} - 1 \quad [30]$$

The state of strain in a material can thus be determined using X-ray diffraction by measuring the strain ( $\varepsilon_{\phi\psi}$ ) in a number of directions considering the rules on how the components of a second-order tensor transform with direction. The quantities  $d_{\phi\psi}$  and  $d_0$  are related to the strain tensor components ( $\varepsilon_{ij}$ ) in the material according to equation 30. This equation is regarded as the fundamental X-ray equation for the determination of strain and it contains six unknown strain components. In order to find the solution for the strain components, measurements are conducted at six or more angles mainly between  $-45^\circ$  and  $+45^\circ$  of  $\psi$ . In practice, however, more points are measured in order to improve accuracy. A sketch showing the different rotation axes for stress measurement is illustrated in Figure 2.23.

$$\varepsilon_{\phi\psi} = \frac{d_{\phi\psi}-d_0}{d_0} = \varepsilon_{11}\cos^2\phi\sin^2\psi + \varepsilon_{22}\sin^2\phi\sin^2\psi + \varepsilon_{33}\cos^2\psi + \varepsilon_{12}\sin 2\phi\sin^2\psi + \varepsilon_{13}\cos\phi\sin 2\psi + \varepsilon_{23}\sin\phi\sin 2\psi \quad [31]$$

The strain tensor components are related to stress components using Hooke's law:

$$\sigma_{ij} = \frac{1}{1/2s_2} \left[ \varepsilon_{ij} - \delta_{ij} \frac{s_1}{1/2s_2 + 3s_1} \varepsilon_{ii} \right] \quad [32]$$

where  $s_1$  and  $1/2s_2$  are the diffraction elastic constants [NOY 87, HAU 97].

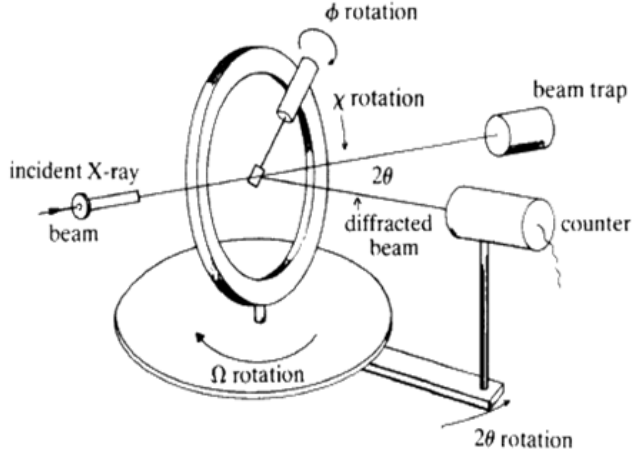


Figure 2.23 Rotation axes used to measure stresses with diffraction

- **Biaxial stress analysis – The  $\text{Sin}^2\psi$  Method**

The  $\text{Sin}^2\psi$  Method is the standard method for measuring near surface stresses with X-rays [NOY 87, HAU 97]. The analysis of residual stress measurements using the standard  $\text{sin}^2\psi$  method is based on the assumption that a plane stress state with the normal component equal to zero ( $\sigma_{33}=0$ ) mainly due to low penetration depth of Cr-K $\alpha$  radiation ( $\approx 5 \mu\text{m}$ ).

If Hooke's law, equation 31, is substituted into the fundamental X-ray diffraction strain equation 30 and considering  $\cos^2\psi=1-\text{sin}^2\psi$ , yield:

$$\varepsilon_{\phi\psi} = \frac{d_{\phi\psi} - d_0}{d_0} = \frac{1}{2} s_2 (\sigma_{11} \cos^2\phi + \sigma_{12} \sin 2\phi + \sigma_{22} \sin^2\phi - \sigma_{33}) \sin^2\psi + \frac{1}{2} s_2 \sigma_{33} + s_1 (\sigma_{11} + \sigma_{22} + \sigma_{33}) + \frac{1}{2} s_2 (\sigma_{13} \cos\phi + \sigma_{23} \sin\phi) \sin 2\psi \quad [33]$$

Since in the near-surface region, the  $\sigma_{i3}$  cannot exist as macrostresses [NOY 87] their components vanish and equation 34 reduces to:

$$\varepsilon_{\phi\psi} = \frac{d_{\phi\psi} - d_0}{d_0} = \frac{1}{2} s_2 (\sigma_{11} \cos^2\phi + \sigma_{12} \sin 2\phi + \sigma_{22} \sin^2\phi) \sin^2\psi + s_1 (\sigma_{11} + \sigma_{22}) \quad [34]$$

Defining further  $\sigma_\phi$  as the stress along the  $\phi$  direction as:

$$\sigma_\phi = 1/2 s_2 (\sigma_{11} \cos^2 \phi + \sigma_{12} \sin 2\phi + \sigma_{22} \sin^2 \phi) \sin^2 \psi \quad [35]$$

Then equation 33 becomes:

$$\varepsilon_{\phi\psi} = \frac{d_{\phi\psi} - d_0}{d_0} = 1/2 s_2 \sigma_\phi \sin^2 \psi + s_1 (\sigma_{11} + \sigma_{22}) \quad [36]$$

The equation 34 is the traditional x-ray residual stress equation and has been in use for over 60 years [NOY 87]. On plotting  $\varepsilon_{\phi\psi}$  or  $d_{\phi\psi}$  on y-axis against  $\sin^2 \psi$  at constant  $\sigma_\phi$ , three basic types of " $d_{\phi\psi}$  vs  $\sin^2 \psi$ " behaviours are observed as shown in Figure 2.24.

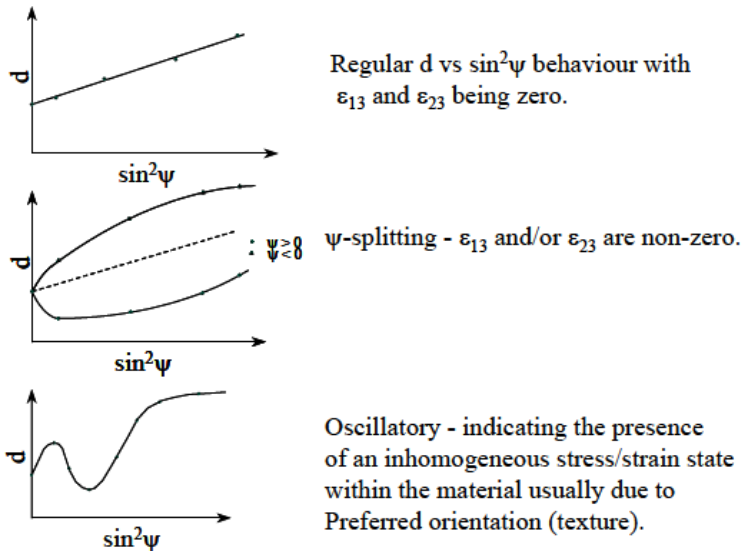


Figure 2.24 Types of "d" vs  $\sin^2 \psi$  plots in residual stress analysis from polycrystalline materials [FIT 05]

### 2.6.3 Line broadening analysis

In principle, line broadening analysis of X-ray diffraction profiles can be used to provide quantitative description of the metallurgical imperfections (defects) in the crystalline structured materials. In engineering materials, the crystalline imperfections leading to line broadening include stress gradient, dislocations, stacking faults, coherently diffracting crystallite size and micro-strain within the crystallite [DEL 88]. Analysis of these imperfections is of great importance because such imperfections highly affect the material properties like mechanical, thermal, optical, magnetic and chemical composition.

After introduction of Bragg's law in 1912, Scherrer conducted initial attempts to quantify the observed line broadening due to metallurgical imperfections [SCH 18]. He suggested that the observed line broadening of X-ray diffraction patterns was due to coherently diffracting crystallite (domain) size and proposed the relationship:

$$\beta_L = \frac{K\lambda}{D_v \cos \theta} \quad [37]$$

where  $D_v$  is the volume weighted crystal size,  $K$  is the Scherrer constant which ranges between 0.87 and 1.0,  $\lambda$  is the wavelength of the radiation and  $\beta_L$  is the integral breath of Lorentzian component of the reflection in radians  $2\theta$  located at  $2\theta$ . Three decades later, Stokes and Wilson [STO 44] suggested that microstrain contributes to line broadening according to:

$$\beta_G = 4\varepsilon_{max} \tan \theta \quad [38]$$

where  $\varepsilon_{max}$  is the weighted average strain (upper limit),  $\beta_G$  is the integral breath of the Gaussian component of the reflection in radians  $2\theta$  located at  $2\theta$ . In short time, Hall [HAL 49] proposed a method for separating the crystallite size and microstrain contributions to the line broadening. It was further developed to form the basis of what is nowadays known as “the Williamson-Hall plot method” [WIL 53] according to the relation:

$$\frac{\beta \cos \theta}{\lambda} = \varepsilon_{max} \left( \frac{4 \sin \theta}{\lambda} \right) + \frac{1}{D_v} \quad [39]$$

A linear least-square regression for Williamson-Hall plot of  $\frac{\beta \cos \theta}{\lambda}$  on the y-axis against  $\left( \frac{4 \sin \theta}{\lambda} \right)$  on the x-axis yields the upper limit micro-strain ( $\varepsilon_{max}$ ) as the slope and the crystallite size ( $D_v$ )

as the inverse of the y-intercept. Moreover, the use of *root-mean square strain*  $\langle \epsilon_0^2 \rangle^{1/2}$  instead of the upper limit strain is highly preferable and may be determined using expression:

$$\langle \epsilon_0^2 \rangle^{1/2} = (2/\pi)^{1/2} \epsilon_{max} \quad [40]$$

Apart from diffracting crystalline size and microstrain being the main sources of line broadening, instrument contributes significantly to the observed line broadening. The instrumental line broadening contribution may arise due to non-ideal optics, wavelength dispersion, and detector resolution. For accurate analysis of the crystalline size and microstrain contribution to line broadening, one must first correct the instrumental line broadening contribution. According to Radoi et al [RAD 04], the correction of instrumental contribution depends on the peak shape and may be corrected according to:

- For lorentzian:

$$\{\beta_{observed} - \beta_{instrument}\} = \beta_{size} + \beta_{strain} \quad [41]$$

- For Gaussian:

$$\beta_{observed}^2 - \beta_{instrument}^2 = \beta_{size}^2 + \beta_{strain}^2 \quad [42]$$

- For Voigt, Pseudo-Voigt peak shape requires deconvolution into Gaussian and Lorentzian before instrumental broadening correction.

### 3 Material and Experimental Procedures

This section presents the material used in this work. Further, it provides the experimental procedures for the different experiments conducted to attain the specific and finally the main objective of this research. The experiments conducted include: carbonitriding, tempering, cryogenic and lastly thermal and mechanical stability treatments. In addition, this section provides information about analysis techniques for chemical composition, metallography, micro-hardness and phase composition and residual stresses using X-ray diffraction.

#### 3.1 Material and Sample Preparations

The material used in this investigation was 18CrNiMo7-6 (*DIN - 1.6587 German standards*) low alloy steel with the initial chemical composition is shown in Table 3.1. This steel is essentially used for heavy and high performance gear parts with the high demand of core toughness. The initial microstructures of the as-received material consisted of ferrite + pearlite.

Disc samples were machined from steel rods with the diameter of 35 mm. Figure 3.1 presents the shape and dimensions of the samples used in this study. For standard investigation (ex-situ analysis), the samples' diameter was 34 mm and 8 mm thick. For in-situ investigations, the dimensions were  $\varnothing 22$  mm and thickness of 4 mm thickness. These reduced dimensions are essential for rapid and homogenous heat distribution during rapid heating and cooling stages.

Table 3.1 Chemical composition of 18CrNiMo7-6 (DN 1.6587) steel grade determined using OES

Element [Mass.-%]	C	Cr	Ni	Mn	Mo	Si	Al	S	Fe
<b>18CrNiMo7-6</b>	0.15 –	1.50–	1.40–	0.50–	0.25–	<0.40	-	<0.035	Bal
<b>(DIN 1.6587)</b>	0.21	1.80	1.70	0.90	0.35				
<b>OES</b>	0.157	1.65	1.57	0.517	0.259	0.269	0.022	0.028	Bal

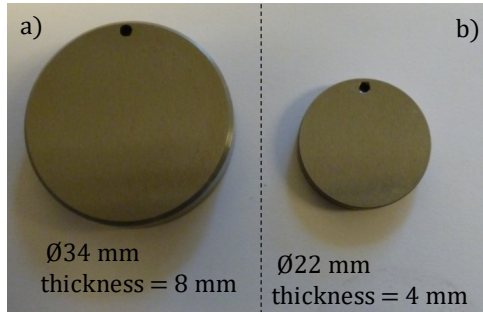


Figure 3.1 Sample dimensions: a) for ex-situ investigations; b) for in-situ investigations

### 3.2 Carbonitriding Treatments

The carbonitriding treatments of the samples were carried out using a SOLO furnace (Figure 3.2). The samples were subjected to a gaseous carbonitriding process. Five different carbonitriding treatments designated as CN1, CN2, CN3, CN4, and CN5 were conducted. The gaseous carbonitriding processes consisted of a boost and diffusion-stage. In each carbonitriding condition, the boost-stage was carried out at 940 °C with carbon potential ( $C_p$ ) of 1.2 %-C and  $\text{NH}_3$  flow rate 0.05 l/h. The high temperature, carbon potential, and ammonia flow are necessary in order to reduce the carbonitriding time. On the other hand, the diffusion-stage was carried out at 850 °C. In this stage, different values of the carbon potential and  $\text{NH}_3$  flow rates were set to achieve the target surface carbon and nitrogen content while maintaining a constant total case depth of about 1 mm. The carbon potential in the carbonitriding atmosphere was controlled by measuring the voltage output of a Zirconia oxygen sensor, the nitrogen potential was controlled by using the  $\text{NH}_3$ -enrichment flow rate. The carbon potentials and  $\text{NH}_3$  enrichment rates used during for the different carbonitriding treatment are given in Table 3.2. Figure 3.3 presents a typical example of the variation of different gaseous components during the carbonitriding process for carbonitriding treatment CN2. After carbonitriding, specimens were quenched into oil held at 60 °C followed by tempering at 170 °C for 2 hours. Several specimens were not tempered and analysed in as-quenched state.

Table 3.2 The different carbonitriding treatments and parameters

S/No.	Temperature [°C]	Carbon potential [%C]	NH <sub>3</sub> addition [%NH <sub>3</sub> ]
	Boost/diffusion stage	Boost/diffusion stage	Boost/diffusion stage
CN1	940/850	1.2/0.60	10/1
CN2	940/850	1.2/0.94	10/2
CN3	940/850	1.2/0.80	10/2
CN4	940/850	1.2/0.94	10/2
CN5	940/850	1.2/0.60	10/1

▪ Carbonitriding furnace



▪ Sample fixture



▪ After carbonitriding



Figure 3.2 Carbonitriding treatment set-up

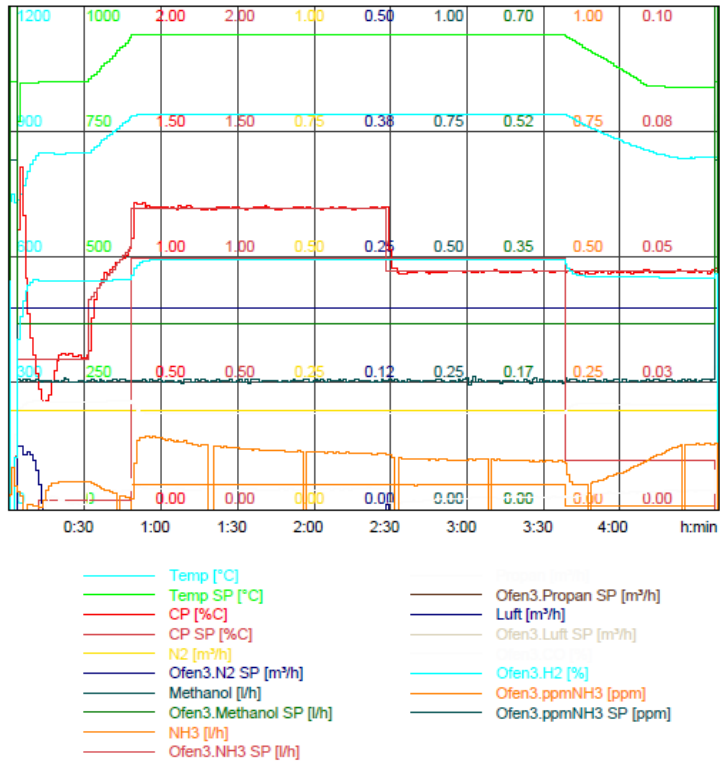


Figure 3.3 Variation of carbonitriding parameters during carbonitriding CN2

### 3.3 Tempering treatment

#### 3.3.1 Ex-situ/conventional Tempering

To improve the microstructure characteristics of the as-quenched specimens, which is a common practice for case-hardened components, specimens were subjected to a tempering treatment. In all experiments, conventional tempering process was carried out at 170 °C for 2 h.

### **3.3.2 In-situ Tempering Experiments**

The in-situ tempering process was conducted to investigate in real time both retained austenite and residual stress evolutions, using X-ray diffraction.

- **Material and Carbonitriding Treatments**

The same material described in section 3.1 was used for in-situ investigation. In this case, the sample dimensions were diameter 22 mm and thickness 4 mm. These dimensions were smaller in comparison to the ones used for ex-situ investigations as the success of this of investigation relied on the capacity of heating element as well as the installation configuration. For this reason, samples with small dimensions have to be used to enable temperature homogeneity during rapid heating or cooling.

Two carbonitriding treatments CN1 and CN2 were investigated. After carbonitriding, the surface carbon and nitrogen content were 0.6 and 0.4 mass.-percent for CN1 and 0.87 and 0.34 mass.-percent for CN2 respectively. The details of the carbonitriding treatments are presented in section 3.2. Case-hardening was carried out by quenching into oil held at 60 °C and finally rinsing in water.

In order to avoid self-tempering/aging at room temperature, specimens were immediately subjected to in-situ X-ray diffraction investigation carried out after electro-polishing. The oxidized and alloy depleted layer was removed by electro-polishing of 50 µm; consequently, all the in-situ X-ray diffraction analysis were carried out at a depth of 50 µm from the initial surface. The importance of analysing at this depth is that it contains the maximum amount of retained austenite, which enables following residual stress evolution in both retained austenite and martensite.

- **In-situ tempering Cycles**

In the first place, in situ investigation was carried out to establish the temperature range of thermal stability of retained austenite. For this, a continuous heating from room temperature (RT) to 650 °C at a slow heating rate of 10 °C/min was used (Figure 3.4a). After the determination of the range of stability of retained austenite, isothermal in-situ tempering experiments were carried out at different temperatures. In each case, the complete tempering

cycle comprised of heating at a heating rate of 10 °C/min from RT to the holding temperature, isothermally holding at this temperature for 2 hours then cooling at a cooling rate of 10 °C/min to RT. The holding temperatures used were 170, 240, and 300 °C (Figure 3.4b). A type-K thermocouple was used to control the temperature using a Eurotherm™ temperature controller (Figure 3.5). For each tempering cycle, two experiments were conducted, and the results were averaged; the results were reproducible.

In order to avoid surface oxidation of the samples, purging process using nitrogen gas was employed. In all cases, prior to the start of the heating cycle, a 30 minutes' purging process was conducted. After purging for 30 minutes, primary and secondary pumps were used to create a vacuum in the furnace chamber down to about 10<sup>-3</sup> mbar. Finally, during the acquisition of the X-ray diffraction patterns, a purging rate of 0.5 liter/min was maintained throughout the heating cycle.

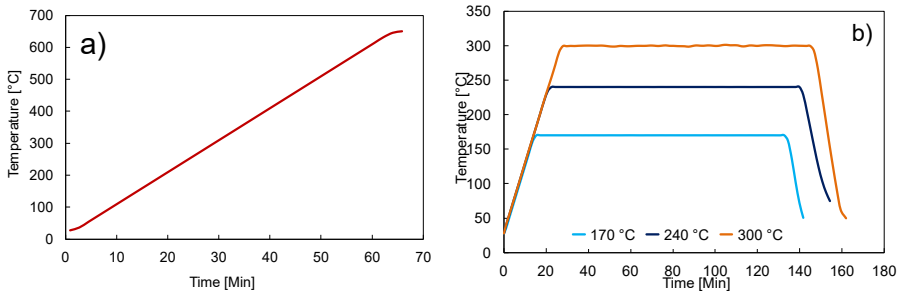


Figure 3.4 Time-temperature cycles for in-situ experiments: a) during continuous heating; b) during isothermal holding

- **Estimation of Carbon + Nitrogen Content in Retained Austenite and Martensite**

The concentration of carbon and nitrogen content in retained austenite were determined using eqn1 [ONI 93], which takes into account the effect of temperature and carbon content on the lattice parameter of austenite. A modification of this equation was done to take into account the effect of both carbon and nitrogen as described in Cheng's work [CHE 92].

$$a_{(T, X_{C+N})} = a_{\gamma}^{25} [1 + \alpha(T - 25)] \quad [43]$$

where  $a_{(T, X_{C+N})}$  is the lattice parameter of retained austenite determined experimentally from analysis of diffraction patterns at each temperature,

$$a_{\gamma}^{25} = 0.3573 + 0.000775 * x_{C+N} \quad [44]$$

is the lattice parameter at room temperature of which the value 0.3575 contains the effect of alloying elements such as chromium and nickel with the coefficient of 0.000158 and 0.000092 respectively [LEE 11], and

$$\alpha [^{\circ}C^{-1}] = (24.9 - 0.5 * x_{C+N}) * 10^{-6} \quad [45]$$

is the thermal expansion coefficient as a function of C+N content. Upon re-arrangement, the value of  $X_{C+N}$  (at.-%) can be determined.

The C+N content in solution for martensite was determined considering the lattice parameter of martensite “a” and “c” [EPP 12].

$$X_{C+N} [wt.-%] = \frac{\left(\frac{c}{a} - 1\right)}{0.0443} \quad [46]$$

- **Analysis of Retained Austenite and Residual Stresses using X-ray Diffraction**

The in-situ X-ray diffraction measurements were performed using a Bruker AXS D8 diffractometer (Figure 3.5) equipped with a Position Sensitive Detector (PSD) with high resolution and a chromium rotating anode ( $\lambda_{\alpha 1} = 2.28975 \text{ \AA}$ ). The operating conditions were selected to enable rapid acquisition of data with high signal-to-noise ratio. In this case, a current of 300 mA and a voltage of 33 kV were used.

For phase analysis, the scanning range was from 62 to 132° 2 $\theta$  with a step size of 0.114° 2 $\theta$ , scan rate of 0.100°/s and scanning time of 79.95 seconds. The measurements were performed after a layer removal of about 50  $\mu\text{m}$  by electro-polishing. Electro-polishing was necessary to remove inter/intra granular oxidized and alloy depleted layer of about 50  $\mu\text{m}$ , which is common under endothermic carbonitriding atmosphere. The X-ray diffraction patterns collected were analysed using the Rietveld Method (software Topas 4.2, Bruker Axs) [YOU 93] using a fundamental parameter refinement approach. A NIST LaB<sub>6</sub> reference powder was measured to determine the instrumental contribution on the diffraction patterns. The analysis of these diffraction patterns yielded the phase fraction of retained austenite and martensite/ferrite and their respective lattice parameters.

For residual stresses in retained austenite phase {220}, the scanning range was from 122° to 132° 2θ with a scan step of 0.073° 2θ. For martensite phase {211}, the scan range was from 148 to 158° 2θ with a scan step of 0.12226° 2θ. The theta angles and their corresponding Psi (ψ) angles used for retained austenite and martensite phase are given in Table 3.3. In this case the value of θ corresponding to ψ=0 was determined after correcting the influence of temperature on the interplanar spacing d. The corrected interplanar spacing (d<sub>corr</sub>) for both retained austenite and martensite phase was determined using the expression:

$$d_{corr} = (1 + 0.000012 * (T_{target} - T_{measured})) * d \quad [47]$$

T<sub>target</sub> and T<sub>measured</sub> is the target and measured temperature, respectively.

The collected diffraction patterns for both {220} and {211} lines were analyzed using a DIFFRAC<sup>plus</sup> STRESS considering the sliding gravity method. The sliding gravity thresholds used were 30, 40, 50, 60 and 70% of the maximum intensity. In this case, only the background correction was done.

Table 3.3 Theta and corresponding Psi angles for austenite and martensite

Retained austenite {220}		Martensite {211}	
2θ°	Corresponding Psi (ψ)	2θ°	Corresponding Psi (ψ)
21.5	-42.0	34.5	-43.5
35.5	-28.0	48.7	-29.4
49.9	-13.7	62.8	-15.2
63.5	0.0	76.5	-1.22
78.2	14.7	91.2	13.1
92.4	28.8	105.3	27.3
106.5	43	119.5	41.5

The dependence of X-ray elastic constants on temperature for both retained austenite and martensite phases were calculated as described by Richter [RIC 83]. For martensite phase, the coefficient of Poisson and Young's modulus dependence on temperature was corrected as:

$$\nu^{(211)} = 0.283 + 4 \times 10^{-5} T \quad [48]$$

$$E^{\{211\}} = [214 - 5.2 \times 10^{-2} \times T - 4.7 \times 10^{-5} T^2] * 1000 \text{ [MPa]} \quad [49]$$

On the other hand, the X-ray constants for retained austenite were collected as:

$$\nu^{\{220\}} = 0.292 + 5.4 * 10^{-5} * T \quad [50]$$

$$E^{\{220\}} = [200 - 8.3 * 10^{-2} * T] * 1000 \text{ [MPa]} \quad [51]$$

Such dependence of elastic constants on temperature is illustrated in Figure 3.6.

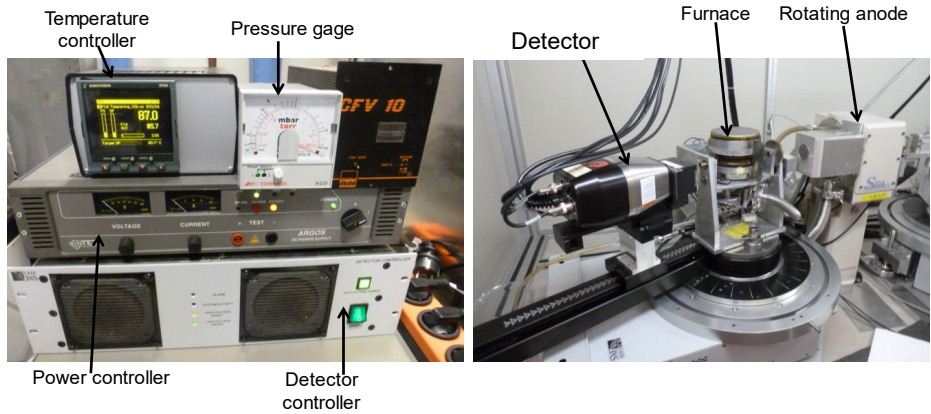


Figure 3.5 Experimental set-up for in-situ X-ray diffraction investigation

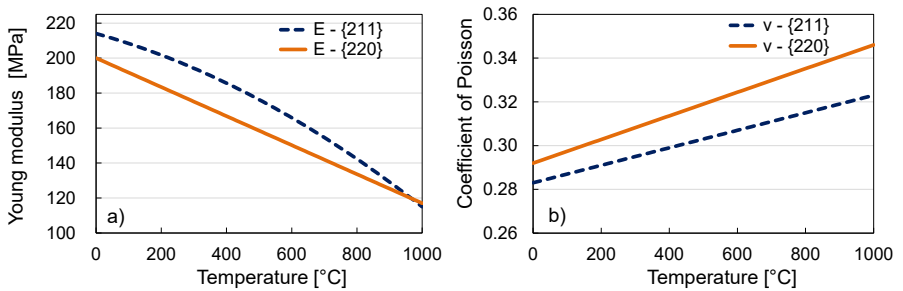


Figure 3.6 Temperature dependence of elastic constants : a) Young's modulus, E; b) Poisson coefficient,  $\nu$

### **3.4 Tempering and cryogenic treatment**

The effect of combined tempering and cryogenic treatment on retained austenite and residual stresses were investigated. The purpose of these investigations is to study the stability of retained austenite as carbonitrided components containing high proportion should stay dimensionally stable to avoid failures on service. Moreover, the combined treatment of tempering and cryogenic treatment enables determining the effect of martensite formed during cryogenic treatment on residual stresses.

- **Material and Carbonitriding Treatment**

The same material described in section 3.1 was used in this investigation. The sample dimensions were diameter 34 mm and thickness 8 mm.

As the success of this investigation depends highly on the initial amount of retained austenite in the sample, the carbonitriding conditions were set to enable as high as 50 mass.-percent of austenite to be retained after quenching. In this case, samples were carbonitrided according to the CN2 conditions to attain surface carbon content of 0.87% C, nitrogen content of 0.34% N, and retain austenite about 50 mass.-percent of austenite after quenching. The details of the carbonitriding process for CN2 are provided in section 3.1.

- **Tempering and cryogenic conditions**

After carbonitriding and quenching, samples contain high proportion of retained austenite ( $\approx$  50 mass.-percent). It is established in the literature [STR 09] that if samples with high proportion of retained austenite are immediately subjected to a cryogenic treatment, little or no autotempering effect is considered to occur; hence more austenite can be expected to transform into martensite. However, during holding the carbonitrided samples at room temperature or at elevated temperature, retained austenite stabilizes and becomes difficult to transform into martensite during cryogenic treatment. To investigate this effect on carbonitrided samples, different set of tempering and cryogenic conditions were used. Table 3.2 presents the tempering and cryogenic temperatures and times. Three tempering temperatures 120, 170, and 240 °C were considered. At each temperature, three sets of samples were isothermally held; the first for 1 h, the second for 2 h, and the third for 14 h.

Moreover, a stage tempering at 80 °C for 14 h followed by tempering at 120 °C for 2 h, 170 °C for 2 h, and 240 °C for 2 h was carried out. After tempering at each condition, samples were cryogenically treated at -120 °C for 2 h using nitrogen gas. Additionally, one set of samples was analyzed in its as-quenched state whereas another set was directly cold treated at -120°C for 2 hours. In addition, one set of the sample was analyzed in its as-quenched state, one set was directly cryogenically treated after quenching and another set was only tempered at 170 °C for 2 hours without subjecting it to cryogenic treatment.

Table 3.4 Tempering and cryogenic conditions

S/No	Tempering		Cryogenic treatment (CT)		Samples
	Temperature [°C]	Time [h]	Temperature [°C]	Time [h]	
1	-	-	-120	2	3
2	170	2	-	-	3
3	120	1/2/14	-120	2	12
4	170	1/2/14	-120	2	12
5	240	1/2/14	-120	2	12
6	120/170/240	14/2	-120	2	12

- **Retained austenite and residual stress analysis**

After tempering coupled with cryogenic treatment at -120 °C for 2 h, the retained austenite and residual stress analyses were performed using X-ray diffraction. The details of the analysis are described in section 3.3. Due to the small amount of austenite remaining after cryogenic treatment, the residual stress analysis was only conducted in martensite phase.

### 3.5 Thermal stability investigation

In this section, the main objective was to investigate the effect of thermal loading on microstructural changes and evolution of residual stresses that can occur while component is on service. Components subjected under static or dynamic thermal and /or mechanical loading can undergo volumetric-induced transformation leading to changes in shape and dimensions of the component. These changes are not always welcome particularly in close fittings.

- **Material and Carbonitriding Treatment**

The dimensions of the samples used in this investigation were 34 mm in diameter and thickness 8 mm. Similarly, only carbonitriding treatment CN2 with the target of retaining high amount of austenite of about 50 Mass.-percent after quenching was used. The details of carbonitriding treatment CN2 have been described in section 3.2. After quenching into oil held at 60 °C, specimens were subjected to conventional tempering at 170 °C for 2 hours.

- **Thermal stabilization conditions**

After carbonitriding and tempering, specimens consisted of tempered martensite and potentially thermally stabilized retained austenite prior to aging investigations. Then, specimens were subjected to different aging conditions (*temperature and time*) to study the microstructure changes such as decomposition of retained austenite and precipitates formations which are likely to occur due to thermal loading in service. Table 3.5 presents the aging conditions employed. It has to be mentioned here that the term aging as used in this work refers to isothermally holding specimens at room temperature (*RT*) whereas holding specimens at temperature different from RT is referred as *accelerated aging*.

Following the aging process at different conditions, some samples were then subjected to shot-peening process to investigate mechanical stability of retained austenite and residual stress changes.

Table 3.5 Thermal stabilization conditions

No.	Temperature [°C]	Time [h]				# samples
1	-30	14	96	360	720	12
2	RT	14	-	-	720	6
3	90	14	96	360	720	12
4	150	14	96	360	720	12

### 3.6 Mechanical stability investigation

In order to investigate the mechanical stability of retained austenite in carbonitrided which contain appreciably high amount of retained austenite of about 50 mass.-percent, carbonitrided samples were subjected to a shot peening treatment. Samples used in this

investigation were thermally stabilized (aged) at different temperatures and times prior to shot peening process. The thermal stabilizations conditions used in this investigation are given in Table 3.6 whereas Table 3.7 provides the shot-peening conditions.

Table 3.6 Thermal stabilization conditions for shot peening treatment

Aging temperature [°C]	Aging time [h]	
-30	96	720
RT	-	720
90	96	720
150	96	720

Table 3.7 Shot peening conditions

Blasting	StD – G3 -0.6 mm VDFI 8001
Intensity	0.25 – 0.3 mmA
Coverage	1.00 – 1.24 x t 98%

### 3.7 X-ray Diffraction measurements

#### 3.7.1 Quantitative phase analysis

The phase composition of the carbonitrided samples was determined using two diffractometers interchangeably. The first is an MZ VI E (*GE Inspection Technology*) diffractometer with a Position Sensitive Detector (Figure 3.9a). For the measurements, Cr-K $\alpha$  radiations ( $\lambda_{\alpha 1}=2.28975 \text{ \AA}$ ) produced by a standard sealed X-Ray tube operated at 33 kV and 40 mA was used. The primary beam was defined by a collimator with 2 mm in diameter and vanadium was used as a filter for Cr-K $\beta$  radiations. In this case, the scan range was from 60° to 164° 2 $\theta$  with a scan step size of 0.050° 2 $\theta$  and scan speed of 0.658 steps per second. The measurements were performed at the centre of the disc samples after a successive layer removal by electro-polishing. The electro-polishing was carried out using an electrolyte solution containing 80%  $H_3PO_4$  and 20%  $H_2SO_4$  as indicated in Figure 3.8. The low current setting was used to enable a smooth surface and avoid heating of the solution and of the sample which in turn could lead to microstructural changes and residual stress relaxation.

The second is a D8-Diffractometer equipped with a Vantec-1 Bruker-AXS Position Sensitive Detector (Figure 3.7). In this case, Co-K $\alpha$  radiations produced by a rotating anode set at a voltage of 35 kV and a current of 40 mA was used. The use of rotating anode enables high signal intensity which is a prerequisite for rapid acquisition of X-ray diffraction patterns during in-situ experiment. In this case, the scanned range was from 42° to 145° 2 $\theta$ , step size of 0.057°, scan rate of 0.1°/s and scanning time of 3084.54 seconds.

In both cases, analysis of collected diffraction patterns was performed using the Rietveld Method (*Topas 4.2, Bruker Axs*) [YOU 93] under the fundamental parameter refinement approach (FPA). A NIST LaB<sub>6</sub> reference powder was measured to determine the instrumental contribution on the diffraction patterns. LaB<sub>6</sub> is a standard material, with no microstrain and domain size broadening effects in the XRD patterns and no preferred orientation.

Besides the reference standard sample profile, the refinement by the Rietveld method requires knowledge of the approximate crystal structure of all the phases of interest in the pattern. The refinement is based on the minimization of the difference between the observed (experimental) profile and the calculated profile in which the discrepancy index, the R-weighted pattern (equation 28) is used as a measure of quality of fit. Typical example of X-ray diffraction analysis of untempered sample is illustrated in Figure 3.7 with an experimental profile in *red* and theoretical profile in *blue*. The quality of fitting is good characterized with a low value of  $R_{wp} \leq 2$ .

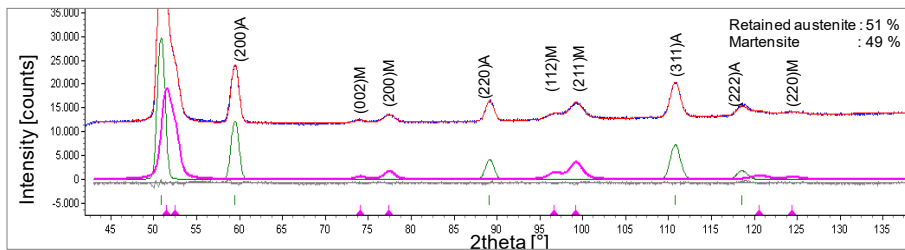


Figure 3.7 Refined X-ray diffraction pattern for untempered CN2 sample collected at room temperature using D8-diffractometer

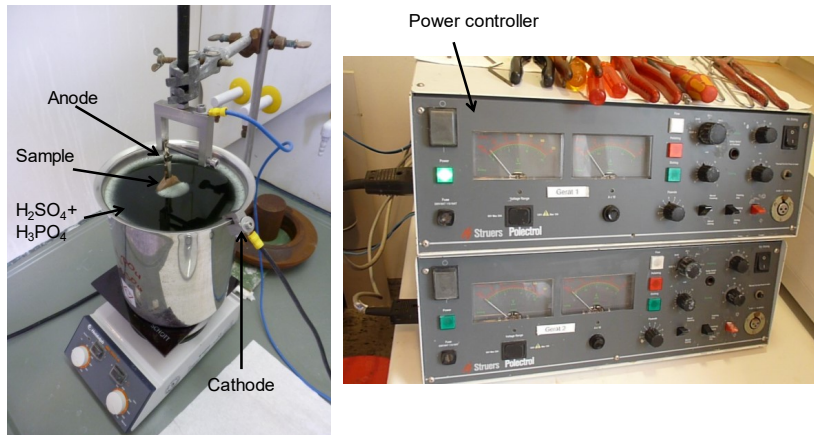


Figure 3.8 Electro-polishing set-up using 20% H<sub>2</sub>SO<sub>4</sub> and 80% H<sub>3</sub>PO<sub>4</sub>

### 3.7.2 Residual stress analysis

- **Residual Stress Analysis - The Standard  $\sin^2\psi$  Method**

The ex-situ investigation of residual stresses was carried out using a diffractometer MZ VI E (*GE Inspection Technology*) equipped with a Position Sensitive Detector (PSD) (Figure 3.9a). The **standard  $\sin^2\psi$  method** which assumes no macroscopic stress ( $\sigma_{33\text{macro}} = 0$ ) perpendicular to the plane surface was used for analysis. Due to the high amount of retained austenite (>20%) in the carbonitrided samples, the measurements were performed in both martensite and austenite {220} phase using Cr-K $\alpha$  radiations and vanadium K $\beta$  filter. The Cr-radiation was produced using a sealed tube operated at 33 kV and 40 mA. A collimator with a 2 mm diameter was used to limit the incident X-ray beam. The measurements were performed in a Chi-mode with tilt angles between -45° to +45° in 17 steps. Figure 3.9b and c present a typical example of residual stress diffraction patterns for austenite {220} and martensite {211} respectively. For {211}, the scan range was from 140° to 164° 2 $\theta$  with a step size of 0.15° 2 $\theta$  and measurement time of 25 seconds. For austenite {220} of which its residual stress diffraction patterns is illustrated in Figure 3.9b, the scan range was from 125° to 133° 2 $\theta$  with a step size of 0.10° 2 $\theta$  and measurement time of 35 seconds per step. The peak position

(Figure 3.10a) was determined by the average gravity method after smoothing and linear background correction. The Young's modulus and Poisson coefficient were 220 GPa and 0.28 for  $\alpha\{211\}$  and 207 GPa and 0.28 for  $\gamma\{220\}$  [EIG 96]. Figure 10b gives a typical residual stress evaluation for  $\{211\}$  at a depth of 911  $\mu\text{m}$  from the surface. At this depth the residual stress determined was -343 MPa. Correction of residual stresses due to layer removal was performed according to Moore and Evans [TOT 02].

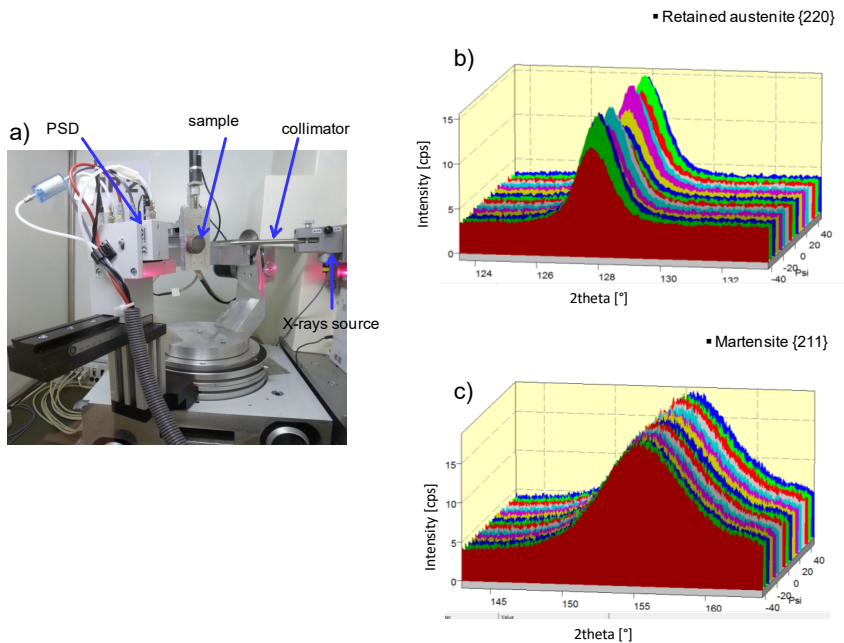


Figure 3.9 Experimental set-up and residual stress measurement: a) Diffractometer MZ VI E (GE Inspection Technology); b)  $\gamma\{220\}$  - 17 diffraction patterns; c)  $\alpha'\{211\}$  - 17 diffraction patterns

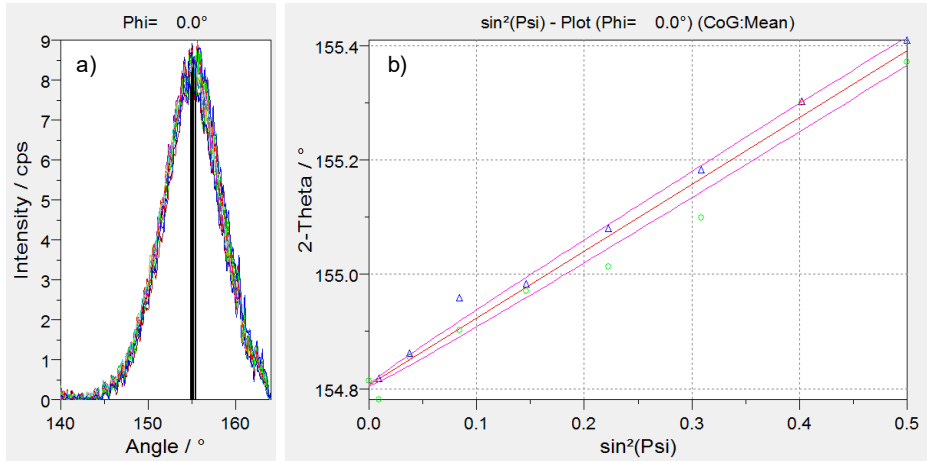


Figure 3.10 Standard residual stress analysis:a) Peak graphic, b) Evaluation graphic

### 3.7.3 Line broadening analysis

Line broadening analysis of the experimental X-ray diffraction line profiles was carried out to provide quantitative information of the crystalline imperfections of the carbonitrided samples in various states. These include: as-quenched state, after tempering (ex-situ and in-situ), cryogenic treatment, and aging as well as shot-peening treatments. It is well established that, line broadening observed on the experimental X-ray diffraction profiles is a convolution of broadening due to metallurgical imperfections in the sample and broadening due to instrumental contribution. In this context, correction is done to remove instrumental broadening in order to obtain line broadening exclusively related to the sample. After correction, then metallurgical imperfections, which among other include, crystallite (domain) size, micro-strain and resulting dislocation density can be determined.

In this work, line-broadening analysis was carried out using software TOPAS 4.2 [YOU 93]. The NIST LaB<sub>6</sub> reference powder was measured to correct for instrumental broadening contribution on the X-ray diffraction profiles. Fundamental parameter (FP) approach was used to refine and decompose the overlapping reflections pertaining to retained austenite and martensite phase. The decomposition of overlapping line reflections is essential to obtaining reliable estimates of line profile parameters, particularly the Bragg's angles and the full width

at half maximum (FWHM) used in subsequent crystallite size and micro-strain analysis. A typical example of decomposed retained austenite and martensite reflections are given in Figure 3.11. These line reflections were then subjected to a second peak refinement.

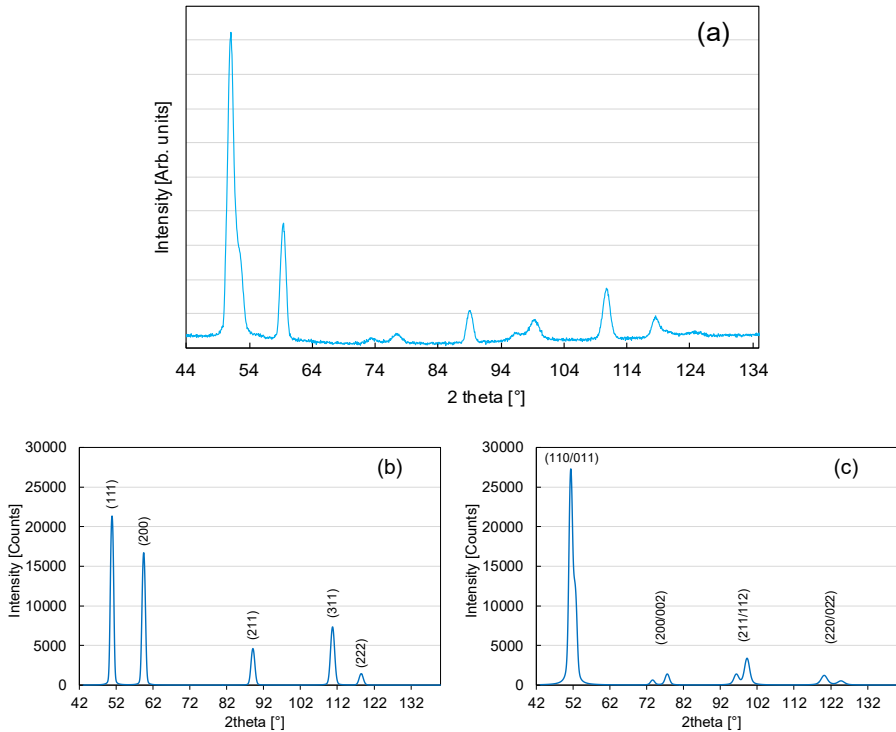


Figure 3.11 Separation of line reflections pertaining to each phase after Rietveld refinement using fundamental parameter approach: a) Full X-ray diffraction profile; b) retained austenite; c) Martensite

In the second refinement, the split pseudo-Voigt peak function which has allowance for asymmetry of the experimental profile was carried out to obtain the FWHM ( $\Gamma$ ) and  $2\theta$  for each peak. These were then used to determine Lorentzian and Gaussian Integral Breadth (IB Lorentz and IB Gauss respectively) which were then used to estimate the average integral breadth ( $\beta$ ). This value was employed in plotting the W-H plots. From these plots, the mean

micro-strain, crystallite size and resulting dislocation density were estimated using regression analysis. In this case, the crystallite size was estimated by satisfying a boundary condition  $D_v < 1000$  nm, where  $D_v$  is the crystallite size. Typical W-H plot for retained austenite and martensite phase are given in Figure 3.12.

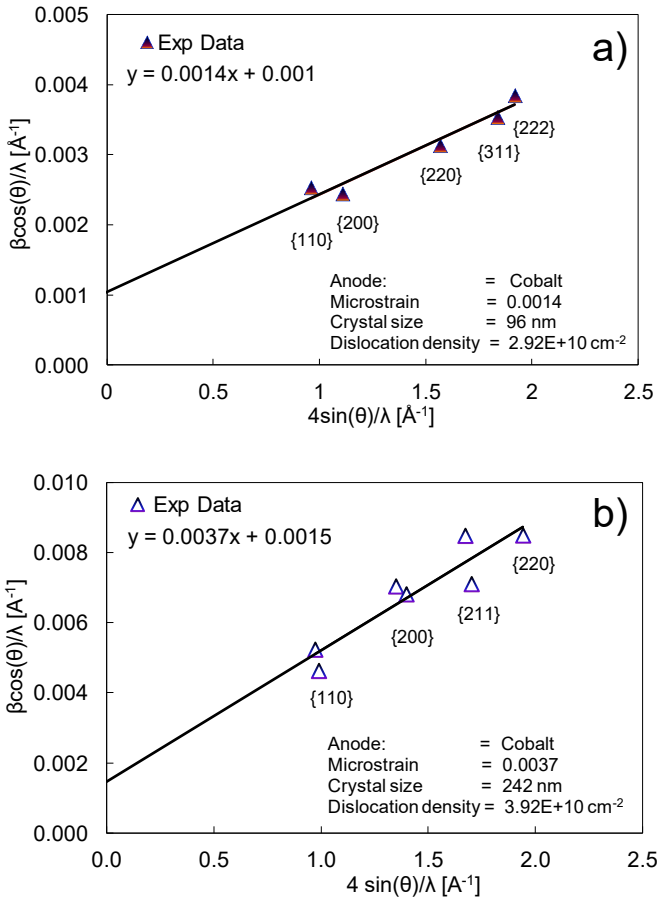


Figure 3.12 Typical example of W-H plot of the X-ray diffraction line profiles measured at a depth of 50  $\mu\text{m}$  of carbonitrided samples: a) retained austenite, b) martensite phase

## **3.8 Complementary investigations**

### **3.8.1 Chemical composition analysis**

The initial chemical composition of the as-received ingot and the carbon and nitrogen profiles after carbonitriding were determined using a Spark Optical Emission Spectroscopy (SOES) which utilizes a slitting destructive method to expose a fresh surface for analysis. At each surface, three points are analyzed and the mean value is determined to represent the local depth composition. For carbonitrided samples, the analysis was carried out at different depths until the core composition of 0.15/0.16 mass.-percent for 18CrNiMo7-6 was attained.

In the first 50  $\mu\text{m}$ , chemical composition analysis was carried out using a Glow Discharge Optical Emission Spectrometry (GDOES or GDOS). This is an appropriate technique for investigation of chemical compositions from the surface down to about 100 $\mu\text{m}$ . It enables identifying the depletion of alloying that might have occurred during carbonitriding treatment.

### **3.8.2 Metallography and microhardness analysis**

Metallographic characterization was carried out using Optical Microscopy (OM). The OM allows examination of microstructures of different shapes and sizes. Before conducting the examination, samples were mechanically polished to obtain a smooth flat mirror surface. After preparation of the surface, samples were chemically etched in 3 % alc.  $\text{HNO}_3$  for 40 sec.

The micro-hardness of the carbonitrided samples were measured using a hardness tester HMV2MCL2 according to DIN50190/1 (German Standard). The measurement was carried out in a Vickers press mode with a press force 1000 p applied for 15 second (HV100). Figure 3.13 presents the section and the case and core structure during metallographic examination.

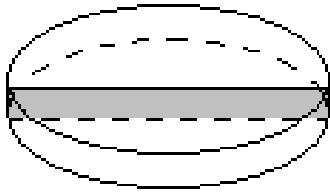


Figure 3.13 Sample sectioning for metallographic examination and hardness testing



## 4 Results

This chapter contains five sections. The first section presents the state after carbonitriding of the samples. In this case, analysis was carried out on untempered (as-quenched state) samples. The second section considers the state during and after tempering of carbonitrided samples. The state after cryogenic treatment of samples with prior tempering treatments forms the third section of this chapter. The fourth and fifth sections of the chapter provide investigations of thermal and mechanical stability respectively. In all cases the main analysis was carried to quantify the retained austenite content and the magnitudes of residual stresses and their distribution with depth. Moreover, chemical composition, metallography and hardness evolutions were considered.

### 4.1 State after carbonitriding

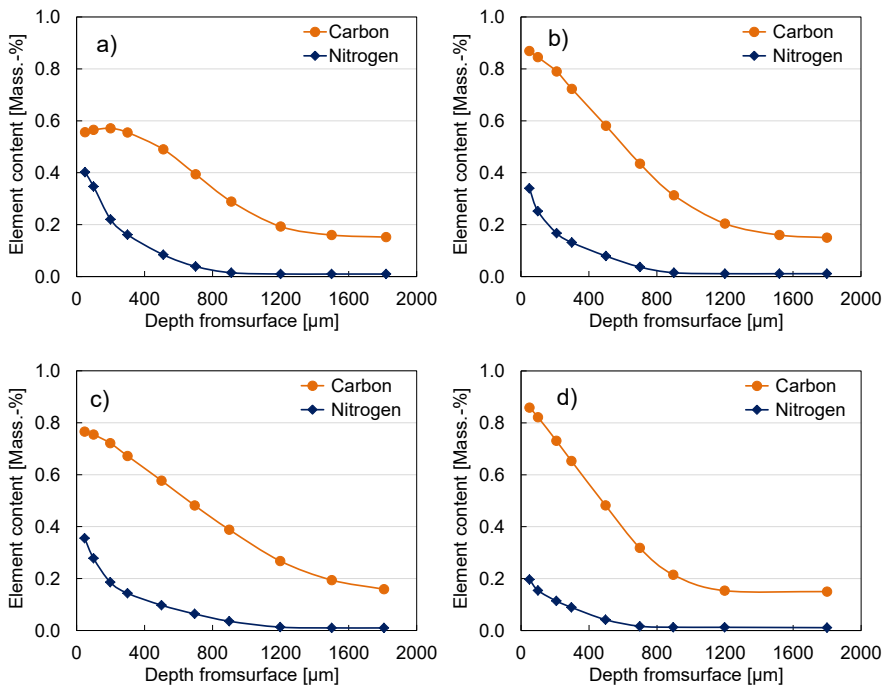
#### 4.1.1 Carbon and nitrogen depth profiles

Figure 4.1 presents the carbon and nitrogen profiles of the as-quenched samples for the various carbonitriding treatments (CN1 to CN5) conducted. The maximum concentration of carbon and nitrogen which occurred at a depth of 50  $\mu\text{m}$  for each treatment is presented in Table 4.1. It is common that the maximum concentration of carbon and nitrogen content occurs beneath the surface as a result of the two stage carbonitriding treatment which is mainly due to the low carbon potential and nitrogen enrichment rate used during the second stage (*the diffusion stage*). Further, the occurrence of maximum concentration at about a depth of 50  $\mu\text{m}$  may be due the fact that nitrogen raises the carbon activity as a result carbon atoms diffuse to high depth from the surface. The observed differences in carbon and nitrogen content among the carbonitriding treatments are mainly due to the different carbonitriding conditions. Such differences in carbon and nitrogen contents after carbonitriding have significant effect on mechanical properties. The differences in mechanical properties arise due to the difference in microstructure fractions.

Although the total case depth target was about 1.2 mm, a variation in this value can be observed with the highest value of about 1.6 mm for CN3 (Figure 4.1c) and the lowest value of

about 0.9 mm for CN4 (Figure 4.1d). The difference in case hardness depth is essential to observing their influence on the location of peak compressive residual stresses.

Elemental analysis in the first 50  $\mu\text{m}$  from the surface observed using GDOES revealed depletion of alloying elements. Figure 4.2 shows a typical depletion of alloying elements for 18CrNiMo7-6 after carbonitriding treatment CN2. Such depletion of alloying elements was observed in the rest of carbonitriding treatments. The depletion of alloying elements, which is linked to oxides and precipitates formation, is more vivid in the first 30  $\mu\text{m}$  from the surface. Chromium and manganese appear to be more sensitive to oxidation whereas nickel is the least oxidized. Furthermore, the intergranular oxidation which is common under endothermic condition and depends on temperature, time, and the carburizing/carbonitriding atmosphere, which contains CO and (CO<sub>2</sub>), extends to a depth of 7.5  $\mu\text{m}$  (Figure 4.2).



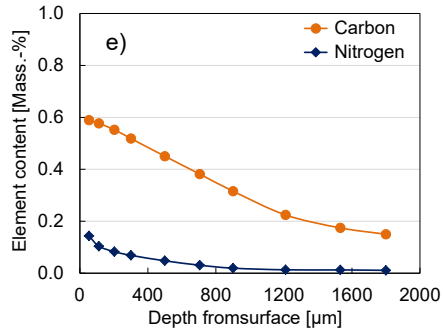


Figure 4.1 Carbon and nitrogen depth profiles after carbonitriding treatment: a) CN1; b) CN2; c) CN3; d) CN4; and e) CN5

Table 4.1 Carbon and nitrogen contents at a depth of 50 µm

S/No.	Carbon [Mass.-percent]	Nitrogen [Mass.-percent]
CN1	0.56	0.40
CN2	0.87	0.34
CN3	0.77	0.36
CN4	0.86	0.20
CN5	0.59	0.18

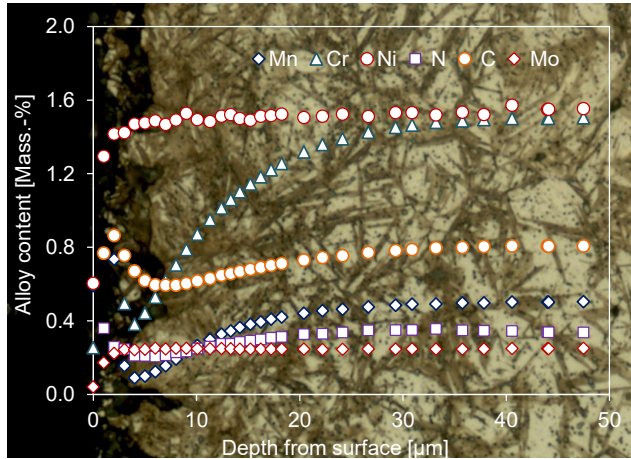


Figure 4.2 Depletion of alloying elements after carbonitriding treatment for CN2 determined using GDOES

#### 4.1.2 Retained austenite distributions

Figure 4.3 presents the variation of X-ray diffraction patterns at different depths for carbonitriding treatment CN1 and CN2 in their as-quenched state. The X-ray diffraction patterns consist of retained austenite reflections ( $\{200\}$ ,  $\{220\}$ ,  $\{311\}$ , and  $\{222\}$ ) whose intensity decreases with depth reflecting the decrease of amount of retained austenite with depth. In contrast, martensite reflections ( $\{200\}$ ,  $\{211\}$ , and  $\{220\}$ ) increase in intensity.

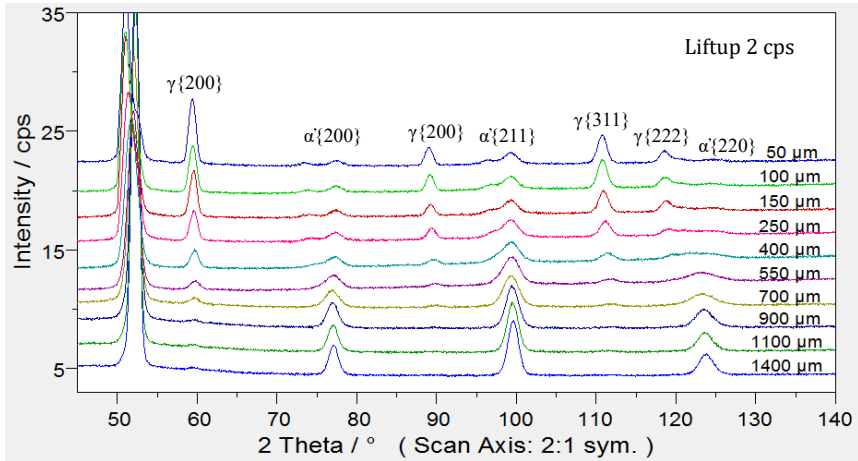


Figure 4.3 Variation of X-ray diffraction patterns as function of depth for an untempered CN2 sample. The X-ray patterns were collected using Co-K $\alpha$  radiations

Analysis of the X-ray diffraction pattern using the Rietveld Method in section 3.7.1 gives the variation of amount of retained austenite with depth. Figure 4.4 presents the retained austenite depth profiles for the five-carbonitriding treatments (CN1 to CN5). The maximum amount of RA is about 50 mass.-percent for CN2, whereas the minimum amount of RA at the surface is about 18 mass.-percent for CN5. The maximum amount of RA occurs in the first 200  $\mu\text{m}$  particularly at 50  $\mu\text{m}$  from the surface. The maximum amount of retained austenite occurs at the depth with the maximum carbon+nitrogen content. Beyond 50  $\mu\text{m}$ , the decrease in retained austenite content correlates well with the decrease in carbon and nitrogen content with depth. The low amount of retained austenite in the first 50  $\mu\text{m}$  from the surface is attributed to depletion of alloying elements.

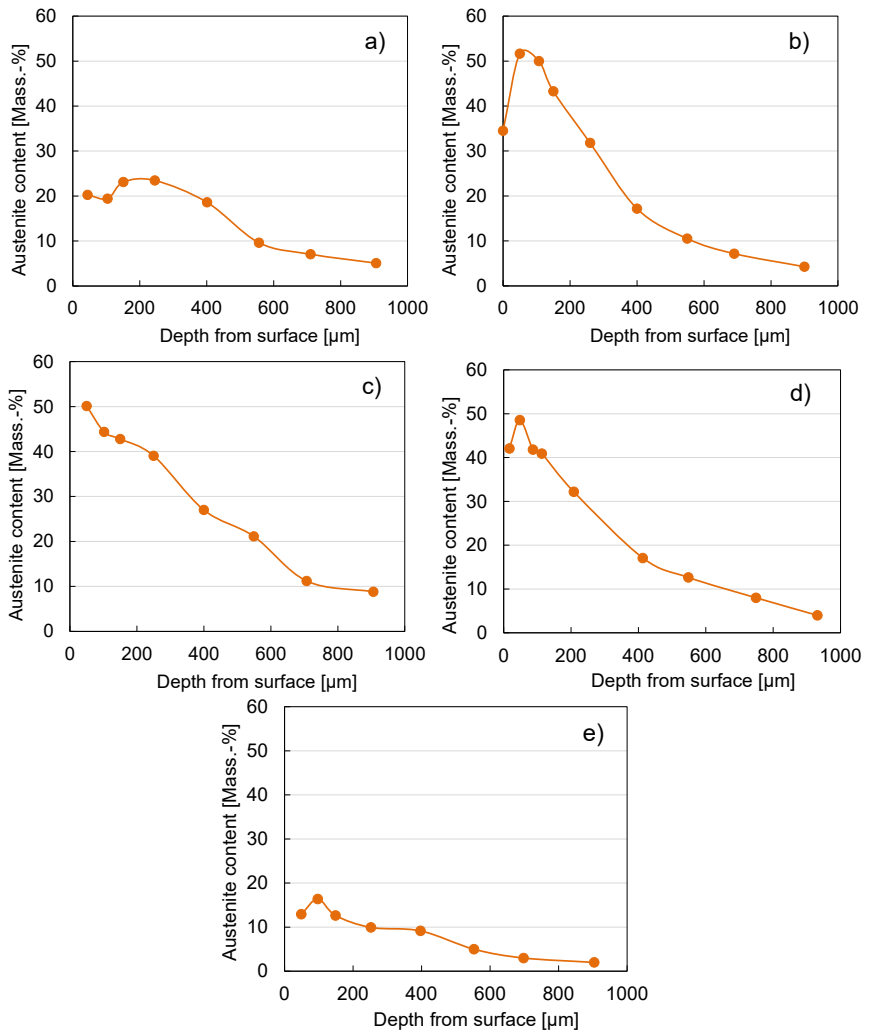


Figure 4.4 Retained austenite depth profiles a) CN1; b) CN2; c) CN3; d) CN4; e) CN5

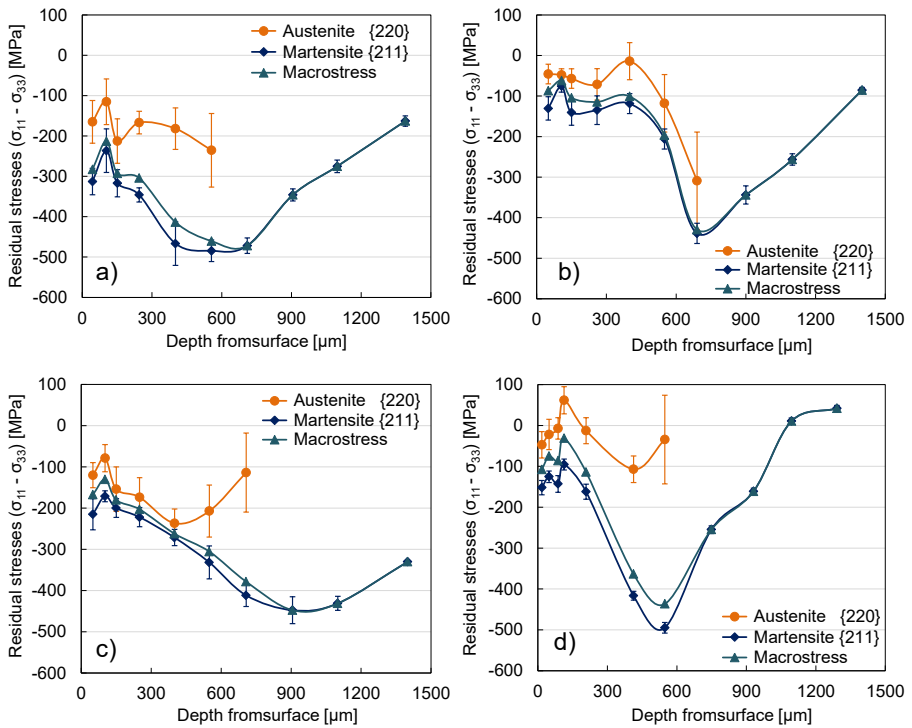
### 4.1.3 Residual Stress Distributions

The analysis of residual stresses in both phases, austenite and martensite, was determined using X-ray diffraction considering the  $\text{Sin}^2\psi$  method. In this case the analysis was conducted on untempered carbonitrided samples. Due to low intensity of retained austenite reflection {220} when its volume fraction falls below 15 mass.-percent, residual stress measurement in retained austenite was limited to certain depths from the surface. Estimation of macrostresses was determined considering the residual stress and volume fraction of each phase.

Figure 4.5 shows residual stress depth distributions in both retained austenite and martensite for the five carbonitriding conditions. It can be seen from this figure that, at all points martensite phase is in higher compressive state in comparison to retained austenite. This is attributed to the high volumetric expansion as result of martensitic transformation. From this figure, residual stress distributions in martensite phase can be divided into two ranges. The first range lies from the surface to about 200  $\mu\text{m}$ , which extends to 400  $\mu\text{m}$  for carbonitriding treatment CN2 (Figure 4.5b). In this range, martensite phase consists of less compressive residual stresses. The average magnitude of compressive residual stresses in this range is between -120 and -300 MPa. It can be noted that the magnitude of residual stresses increases with increasing fraction of martensite phase. Moreover, a shift of up to 60 MPa in macrostresses compared to the residual stresses in martensite are reached. This confirms that when the fraction of retained austenite is greater than 15 %, it is important to measure the RS in both phases in order to determine the macroscopic RS by considering the proportion of each phase. However, when the amount of RA falls below 15%, the macroscopic stresses are close to the RS measured in martensite phase in this range. Residual stress in martensite phase at the depth of maximum retained austenite occurs, varies linearly with RA and can be estimated according to expression in Figure 4.6.

The second range lies between 200  $\mu\text{m}$  and the case/core interface. In this range, the martensite phase is characterized by peak compressive residual stresses followed by continuous decrease in the depth. The magnitudes of peak compressive RS obtained in this work are in the same range as the peak compressive RS observed by Davis [DAV 02] on a survey of a number of carburized parts. The magnitude of peak compressive RS and its location for each carbonitriding treatment are given in Table 4.2. Despite high differences in

RA among the carbonitriding treatments, the magnitude of peak compressive RS is less affected and varies in the range between -400 and -500 MPa. In all cases, the location of peak compressive residual stress lies in the range of 40 to 60 % of the total case depth ( $\approx 1500 \mu\text{m}$ ) where the proportion of martensite to austenite is about 80 %. The location of peak compressive RS observed in this work is in good agreement with the one reported by Ericsson [ERI 85]. Figure 4.7 gives the variation of residual stresses in martensite as a function of C+N content. It can be seen from this figure that the peak compressive RS occurs at a depth where the C+N content is in a range around 0.5 mass.-percent.



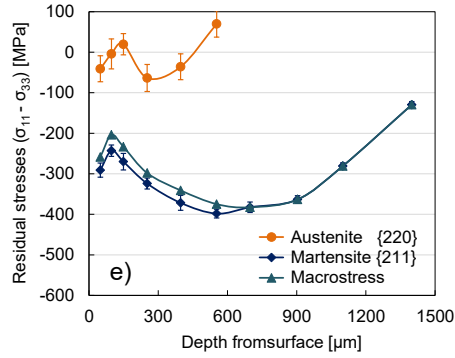


Figure 4.5 Residual stress distributions for untempered carbonitrided samples (as-quenched state): a) CN1; b) CN2; c) CN3; d) CN4; e) CN5

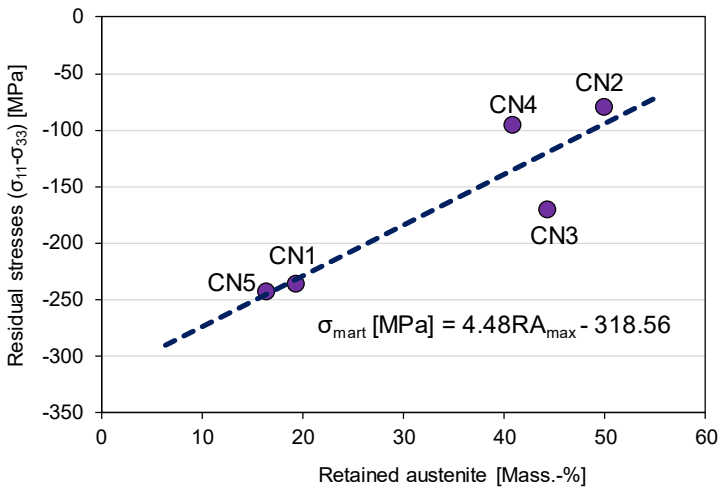


Figure 4.6 Residual stresses in martensite as function of maximum retained austenite content

Table 4.2 Peak compressive residual stresses for untempered carbonitrided samples

S/No.	Peak compressive residual stress [MPa]	Depth from the surface [ $\mu\text{m}$ ]
CN1	-480	550
CN2	-440	690
CN3	-450	960
CN4	-500	540
CN5	-400	550

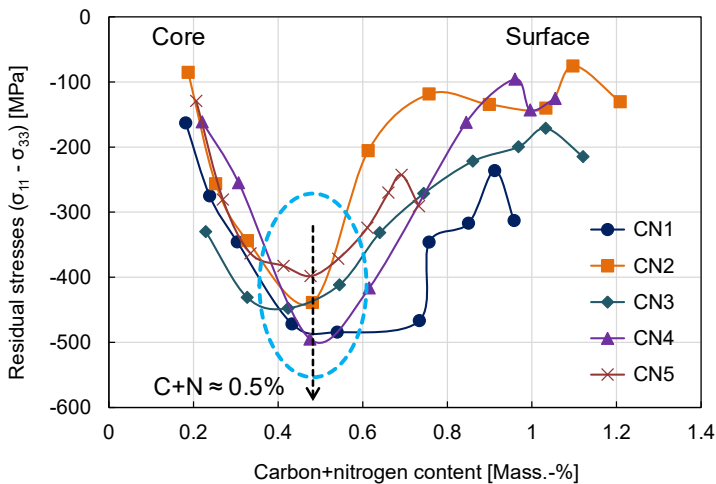


Figure 4.7 Residual stresses in martensite as a function of C+N content for untempered samples

#### 4.1.4 Line broadening analysis

In addition to the phase composition information contained in the X-ray diffraction patterns, it was possible to extract quantitative information regarding the metallurgical defects. The metallurgical defects analyzed include crystallite size of coherently diffracting domain, microstrain and dislocation density. The analysis was based on W-H method [WIL 53] considering the integral breadths and  $2\theta$  position for the different reflections.

Figure 4.8 provides the variation of crystallite size in both retained austenite and martensite phase as a function of retained austenite content for CN1 and CN2. In general, at all point

crystallite-size for retained austenite is considerably greater than those in martensite except at very low amount of RA. For CN1 and CN2, the martensite crystallite size remains relatively constant over the depth. However, larger diffracting crystallite sizes in martensite phase can be expected in regions with lower carbon + nitrogen content [MAK 91]. On the other hand, retained austenite crystallite increases with increasing volume fraction of RA until 20 mass.-percent (in *other terms retained austenite crystallite size decreases with increasing volume fraction of martensite*). Beyond 20 mass.-percent RA, the crystallite size slightly increases with increasing volume fraction of retained austenite. The decrease of RA crystallite size with increasing volume fraction of martensite is attributed to the increase in plastic deformation as well as cutting of retained austenite as larger amounts of martensite is formed [MAK 00].

The change in root mean square (r.m.s) microstrain as a function of volume fraction of retained austenite is given in Figure 4.9. For CN1 which is characterized by high martensite to retained austenite ratio (about 80%), the microstrain remains nearly constant at about 0.0024 for RA and 0.004 for martensite phase. In contrast, for CN2 the microstrain in both phases is general lower and slightly decreases with increasing volume fraction of retained austenite. The observed differences in r.m.s strain between RA and martensite phase can be attributed to the [HOF 98]:

- Variation of dislocation stress fields (type A) of which the highest level occurs in the range of 40 to 60% of the total case depth. This range is characterized by the peak compressive residual stresses in martensite phase
- Level of carbon + nitrogen content in the octahedral sites of both phases (type B), of which in carbonitrided/carburized component decreases with depth and
- Finely disseminated coherent carbides and nitrides and/ or misfit dislocations (type C).

Figure 4.10 illustrates the variation of dislocation density as a function of volume fraction of retained austenite for both CN1 and CN2. The results suggest that retained austenite (martensite) strongly influences the dislocation density, when its volume fraction in the sample is less than 20% ( $\geq 80\%$  martensite) and beyond this value, the dislocation density in both phases remains nearly constant. As expected, at all depths the dislocation density in martensite phase is greater than in retained austenite. A difference of up to  $2.2 \times 10^{11} \text{ cm}^{-2}$  for CN1 and  $2.9 \times 10^{11} \text{ cm}^{-2}$  for CN2 is reached. For martensite phase, the dislocation density

slightly decreases from about  $1.3 \times 10^{11} \text{ cm}^{-2}$  to about  $1.1 \times 10^{11} \text{ cm}^{-2}$  whereas such decrease for retained austenite is about from  $1.1 \times 10^{11} \text{ cm}^{-2}$  to  $0.11 \times 10^{11} \text{ cm}^{-2}$ . When the volume fraction of retained austenite is more than 20%, the dislocation density in retained austenite is independent of retained austenite remains relatively constant at  $0.3 \times 10^{11} \text{ cm}^{-2}$  for CN1 and  $0.2 \times 10^{11} \text{ cm}^{-2}$  for CN2.

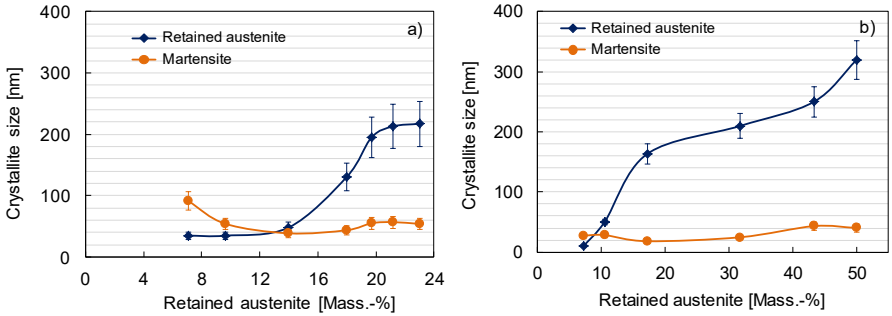


Figure 4.8 Change in crystallite as a function of retained austenite content: a) CN1; b) CN2

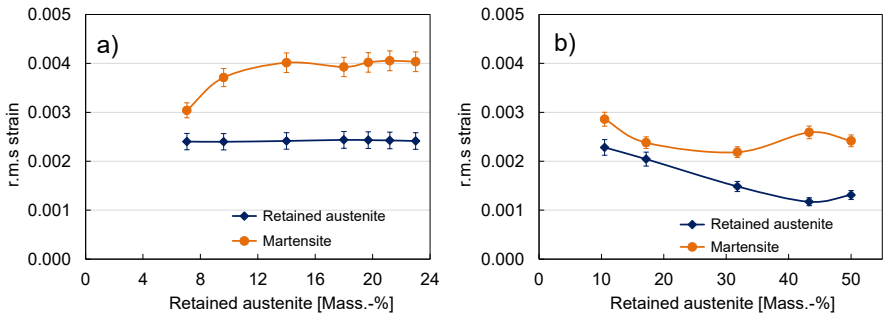


Figure 4.9 Change in r.m.s strain as a function of retained austenite content: a) CN1; b) CN2

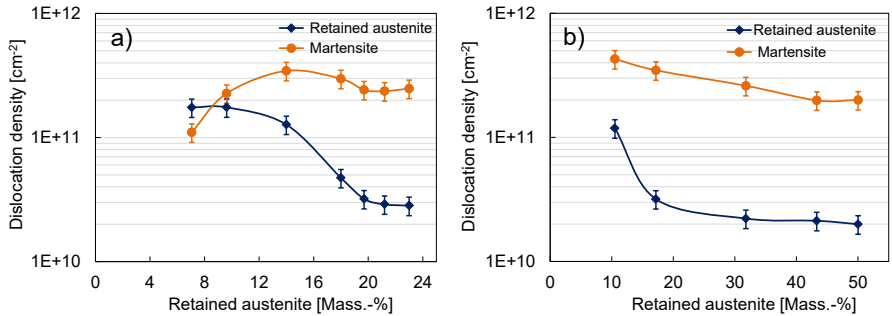


Figure 4.10 Change in dislocation density as a function of retained austenite content: a) CN1; b) CN2

#### 4.1.5 Discussion on state after carbonitriding

This section discusses analysis of the state after carbonitriding of the samples in as-quenched state (untempered). The carbon and nitrogen content reached after carbonitriding depend on the carbon potential, ammonia enrichment rate as illustrated in Figure 4.1. In all cases, the carbonitriding temperature and time were kept constant.

As expected, the volume fraction of retained austenite (Figure 4.4) increases with increasing carbon+nitrogen content in the case. This is because both carbon and nitrogen stabilize austenite and greatly lower the martensite start temperature as indicated in Figure 4.13. As for carbon and nitrogen content, the maximum retained austenite occurs at a depth of 50  $\mu\text{m}$  from the surface. In the first 50  $\mu\text{m}$ , all the carbonitriding treatments retained low amount of austenite. This phenomenon is linked to depletion of alloying elements and subsurface oxidation leading to the increase of martensite start temperature and a lower hardenability. Analysis of the first 50  $\mu\text{m}$  revealed depletion of alloying elements (Figure 4.2), in which chromium is readily depleted mainly due to precipitates and oxides formation. Therefore, this range is likely to favour an increased formation of high temperature transformation products such as lower and/or upper bainite phase during quenching [PAR 99]. The presence of bainite in the subsurface can considerably reduce not only the case hardness but also the level of compressive residual stresses in both martensite and retained austenite phase [ING 83]. Beyond, 50  $\mu\text{m}$  the decrease of retained austenite correlates well with the decrease of carbon and nitrogen content. On the other hand, oxidation is considered normal under endothermic

carbonitriding atmosphere [PAR 99], which is still the most popular method for case hardening. The oxidation occurs as a result of diffusion of oxygen into the steel during carbonitriding.

Figure 4.11 shows the depth of total penetration of oxygen occurred during carbonitriding treatment CN2 with a typical endothermic atmosphere. It can be seen that as high as 58 mass.-percent of oxygen is reached. Beneath the surface there is a rapid fall of oxygen content and reaches about 3.5 mass.-percent at a depth of 2  $\mu\text{m}$  from surface. Beyond 2  $\mu\text{m}$ , the oxygen content decreases continuously to reach zero. The oxygen content in sample depends on the oxygen potential in the carbonitriding atmosphere. In industrial carbonitriding and carburizing practice, however, this oxygen potential is high enough to cause oxidation of metal [KOF 66]. The oxygen diffusing into steel oxidizes chromium, manganese, and silicon while molybdenum and nickel are reduced [KOS 67]. This is most prominent alongside grain boundaries where diffusion is faster [CHA 78]. As an alternative to minimizing or avoiding internal oxidation, low-pressure carbonitriding can be used and a considerable positive results have been achieved.

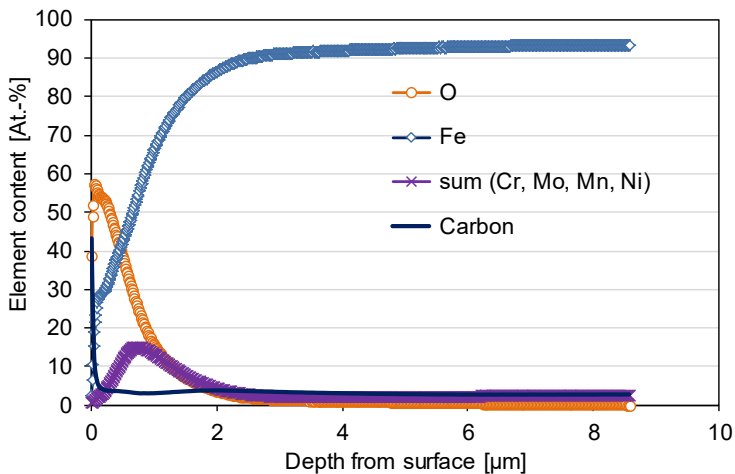


Figure 4.11 Oxygen distribution after carbonitriding under endothermic atmosphere for 18CrNiMo7-6 steel grade

Compressive RS are formed in the case microstructures of carbonitrided samples (components) as a result of transformation and temperature gradient during quenching. The magnitude and distributions of RS, among others, are largely dependent on the case microstructure and the volume fraction. The RS distributions as given in Figure 4.6 can be divided into three ranges. The first ranges from the surface to about 100  $\mu\text{m}$  which is characterized by slightly low compressive RS in martensite. This can be attributed to the presence of high temperature transformation products. The second lies in the range between 50-100  $\mu\text{m}$  to about 400  $\mu\text{m}$  in which the samples are characterized by the lowest compressive RS which is attributed to high volume of retained austenite. Lastly, is the range between 400  $\mu\text{m}$  until the case/core interface, samples are characterized by peak compressive RS, which lies in the range from -400 to -500 MPa. Beyond the location of peak compressive RS, compressive RS decreases progressively until the case/core interface, the point at which a transition of the nature of RS from compressive to tension occurs.

Such variation of residual stresses is given on Figure 4.12 for carbonitriding treatment CN2. Comparing magnitudes of peak compressive RS in all carbonitriding treatments, which is within 40 to 60% of the total case depth ( $\approx 1500 \mu\text{m}$ ), seems that peak compressive RS are less affected by the maximum amount of retained austenite at the near surface. Relating the variation of residual stresses to that of carbon plus nitrogen content indicates that the same peak compressive RS occurs in the range between 0.4 and 0.6 mass.-percent as given in Figure 4.7, in particular at 0.5% C+N. At this concentration, the nitrogen content is almost zero. The range of magnitudes and distributions of residual stresses observed in this work are in good agreement with those found in the work of Parrish and Harper [PAR 85] obtained after a survey of a number of carburize parts.

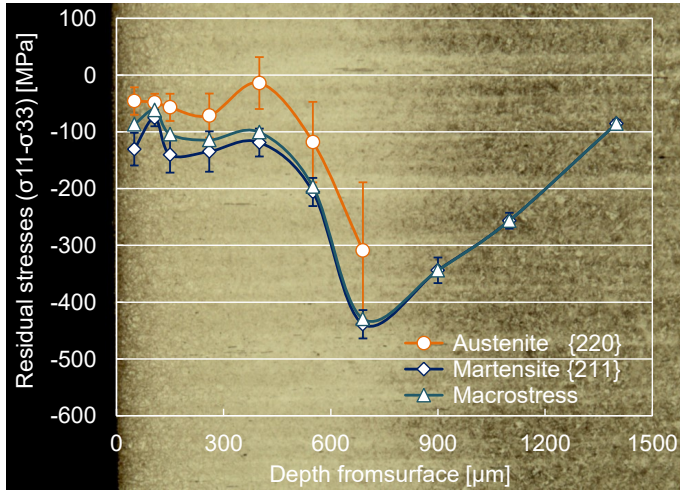


Figure 4.12 Residual stress and microstructure distributions for CN2

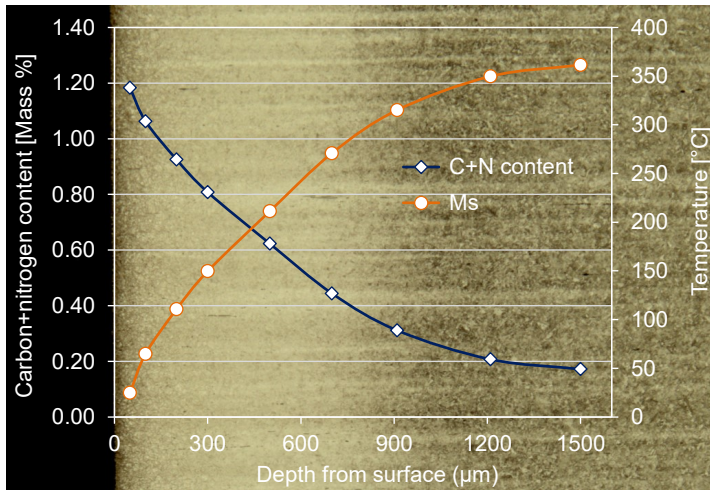


Figure 4.13 Variation of microstructure, carbon+nitrogen content and Ms with depth

## **4.2 State during and after tempering**

This section considers state during and after tempering analysis of carbonitrided samples. The stability of retained austenite and residual stress relaxation are presented. The investigations were carried out considering two-carbonitriding treatments (CN1 and CN2), which contain high difference in initial amount of retained austenite. The maximum amount of retained austenite was 20 mass.-percent for CN1 and 50 mass.-percent for CN2.

### **4.2.1 State during tempering**

In this case, two strategies were considered for analysis during tempering for investigating the stability of retained austenite and residual stress relaxation using in-situ X-ray diffraction. The first strategy involved a continuous heating from room temperature (RT) up to 650 °C at a heating rate of 10 K/min. The second strategy involved a standard tempering treatment cycles of which the isothermal holding was carried at 170 °C, 240 °C, and 300 °C for 2 hours.

#### **4.2.1.1 Carbon and Nitrogen Depth Profiles**

The carbon and nitrogen depth profiles of the as-quenched specimens for both CN1 and CN2 conditions are shown in Figure 4.14. Although similar carbonitriding conditions for both CN1 and CN2 were the same as for results in Figure 4.1a and 4.1b, slight differences on the surface carbon and nitrogen contents occurred. This can be linked to the instability of the gaseous composition in the atmosphere as well as the competing reactions occurring at the surface of the furnace wall and sample fixtures. The maximum carbon and nitrogen content at a depth of 50 μm were 0.58 and 0.28 mass.-percent for CN1 and 0.86 and 0.47 mass.-percent for CN2 respectively. As already stated in section 4.1 (Figure 4.2), the first 50 μm from the surface was characterized by internal oxidation accompanied by depletion of alloying elements and removed before the in situ experiments.

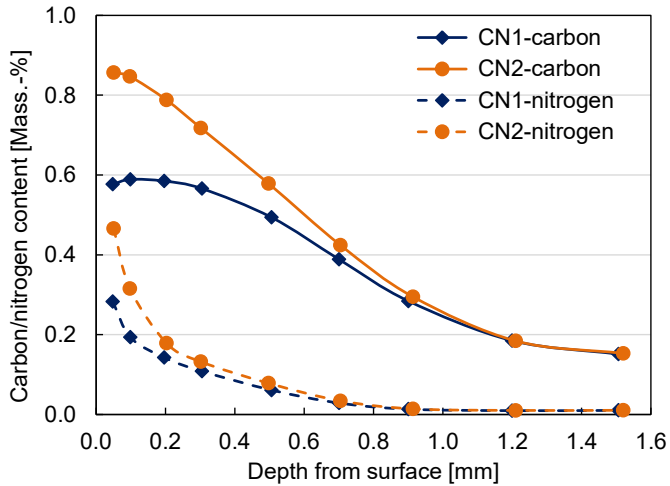
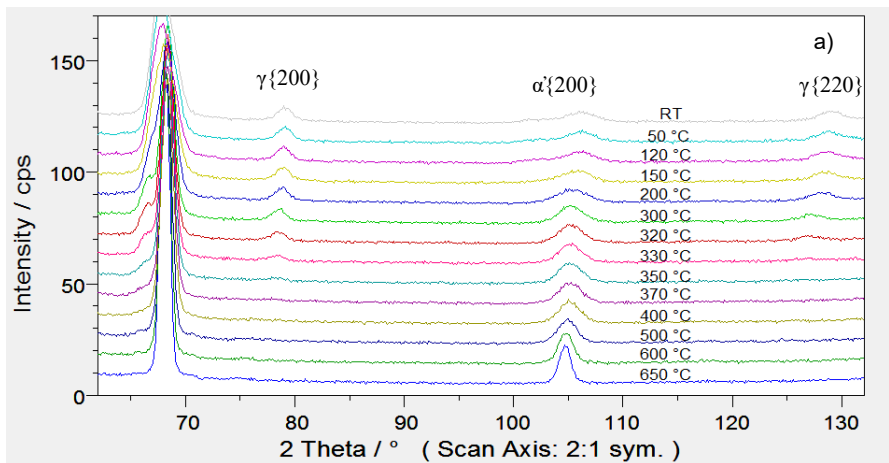


Figure 4.14 Carbon and nitrogen depth profiles for in-situ investigations

#### 4.2.1.2. Evolution of phase fractions during continuous heating

Figure 4.15 shows the X-ray diffraction patterns for CN1 and CN2 collected during heating from RT to 650 °C at 10 K/min. The diffraction patterns consist of austenite ( $\gamma$ ) and martensitic ( $\alpha'$ ) reflections. It can be seen from this figure that the intensity of retained austenite reflections “{200} and {220}” disappear between 320 and 350 °C as a result of transformation of retained austenite into bainite and continue until the reflections have disappeared completely. Figure 4.16 presents the evolution of phase contents as a function of temperature during continuous heating for carbonitriding treatment CN1 and CN2. The initial amount of retained austenite determined from X-ray determined at room temperature is about 18 mass.-percent for CN1 and 50 mass.-percent for CN2. In both CN1 and CN2, RA slightly increases by 2% between 110 °C and 170 °C. The slight increase of RA is attributed to redistribution of carbon and nitrogen through homogenisation and precipitation of  $\epsilon/\eta$ -Fe<sub>2.5</sub>C carbides and  $\alpha'$ -Fe<sub>16</sub>N<sub>2</sub> nitrides leading to the decrease in martensite peak intensity, rather than growth of austenite peaks, which is not expected from thermodynamic point of view. As can be seen in Figure 4.16a and b, the retained austenite present at room temperature remains relatively stable up to about 290 °C. Above

this temperature, retained austenite start to transform and the maximum transformation rate occurs at 340 °C for CN1 and at 350 °C for CN2. At these temperatures nearly 50% of the initial amount of retained austenite had transformed. At 400 °C, the amount of retained austenite present in the sample is about 3.5 and 8 mass.-percent for CN1 and CN2 respectively. On further heating, retained austenite continues to decompose slowly and reaches zero for CN1 and 4 mass.-percent for CN2 at 650 °C. The temperature, at which retained austenite starts to transform (290 °C), is in good agreement with that observed in the work of Amarthalingam [AMA 10].



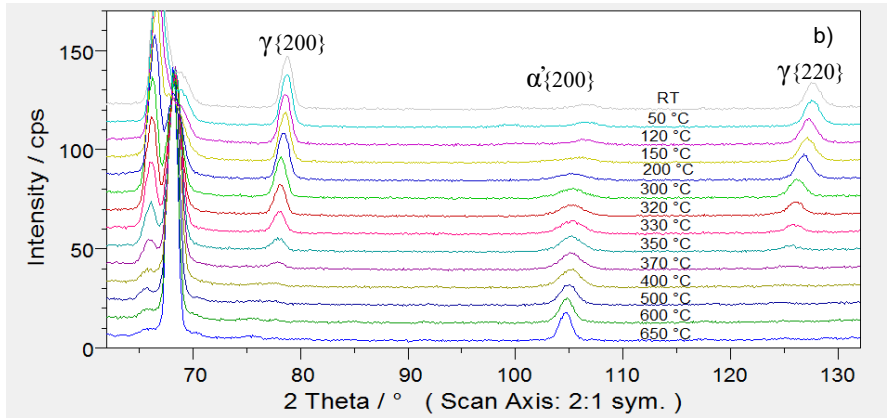


Figure 4.15 Evolution of X-ray diffraction patterns during continuous heating from room temperature to 650 °C: a) CN1; b) CN2

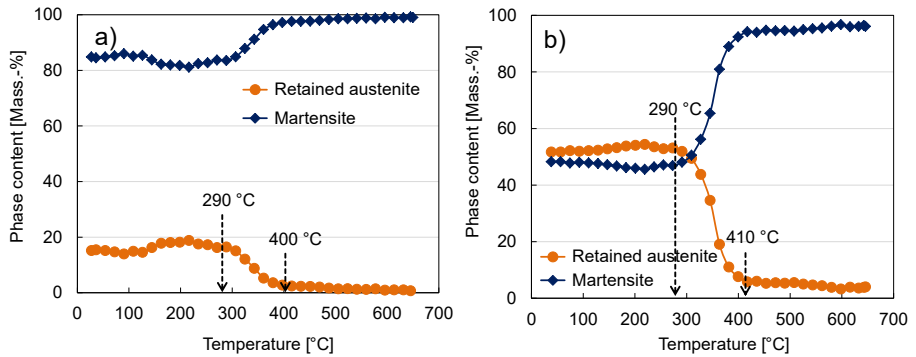


Figure 4.16 Evolution of retained austenite and martensite during continuous heating from RT to 650 °C: a) CN1; b) CN2

#### 4.2.1.3 Evolution of lattice parameters during continuous heating

Figure 4.17 presents the austenite experimental lattice parameters and the resulting calculations of carbon+nitrogen (C+N) content as a function of temperature during continuous heating from 25 °C to 650 °C at a heating rate of 10 K/min. The lattice parameters and C+N content in solution in martensite are illustrated in Figure 4.17c and d. For retained austenite,

the lattice parameter determined from diffraction pattern collected at room temperature is 0.3591 nm for CN1 and 0.3602 nm for CN2. The martensite lattice parameter "a" is 0.2862 nm for CN1 and 0.2852 nm for CN1 whereas the lattice parameter "c" is 0.2947 for CN1 and 0.2988 nm for CN2. The corresponding C+N content estimated at RT for retained austenite are 0.48% for CN1 and 0.83% for CN2. Such concentrations in martensite are 0.67% for CN1 and 1.07% for CN2. However, the C+N content determined using OES were 0.86% for CN1 and 1.07% for CN2. The difference between the estimated and OES value may be due to the maximum solubility of which excess C+N content leads to formation of carbides and nitrides, hydrostatic stresses and tempering effect.

For retained austenite, the change of lattice parameter and C+N content in solution during continuous up to 650 °C can be divided into three ranges. The first is from RT to 190 °C where a slight linear increase in lattice parameter and decrease in calculated C+N content is observed. The decrease in C+N content can be attributed to carbides/carbonitrides formation by diffusion of C and N out of the lattice leading to contraction of austenite lattice parameter. The contraction effect due to changing chemical compositions is outweighed by the increase due to thermal expansion. In the same temperature range, the loss of martensite tetragonality of martensite (Figure 4.17c, d) starts about 110 °C and end at about 200 and 250 °C for CN1 and CN2 respectively. The loss of martensite tetragonality is generally accompanied by carbon/nitrogen segregation, clustering and/or coherent precipitation of  $\eta$ -carbides/nitrides [PAR 99].

The second range is above 190 °C where the change of slope of lattice parameters increase and associated calculated C+N content can be observed. The values obtained on fitting linearly the dependence of lattice parameter and C+N content in solution in retained austenite on temperature are summarized in Table 4.3. Below 190 °C, the thermal coefficient of expansion was  $5.61 \times 10^{-6} \text{ }^\circ\text{C}^{-1}$  for CN1 and  $19.43 \times 10^{-6} \text{ }^\circ\text{C}^{-1}$  for CN2. Above 190 °C, the value of thermal coefficient expansion were  $28 \times 10^{-6} \text{ }^\circ\text{C}^{-1}$  for CN1 and  $27.89 \times 10^{-6} \text{ }^\circ\text{C}^{-1}$  for CN2. This indicates that the influence of temperature on RA lattice expansion below 190 °C is lower particularly for CN1 in comparison to temperatures beyond 190 °C. These values are in good agreement with reported values in the literature [AMA 10]. In this range, the linear increase of coefficient

can result due to thermal expansion, enrichment due to C+N partitioning from martensite [MOO 10] and change in hydrostatic stress.

In the last stage, both lattice parameter and calculated C+N content above 340 °C for CN1 and 500 °C for CN2 deviate from linearity which has been attributed to depletion of carbon and nitrogen content because conversion of  $\epsilon/\eta$ -Fe<sub>2.5</sub>C into cementite.

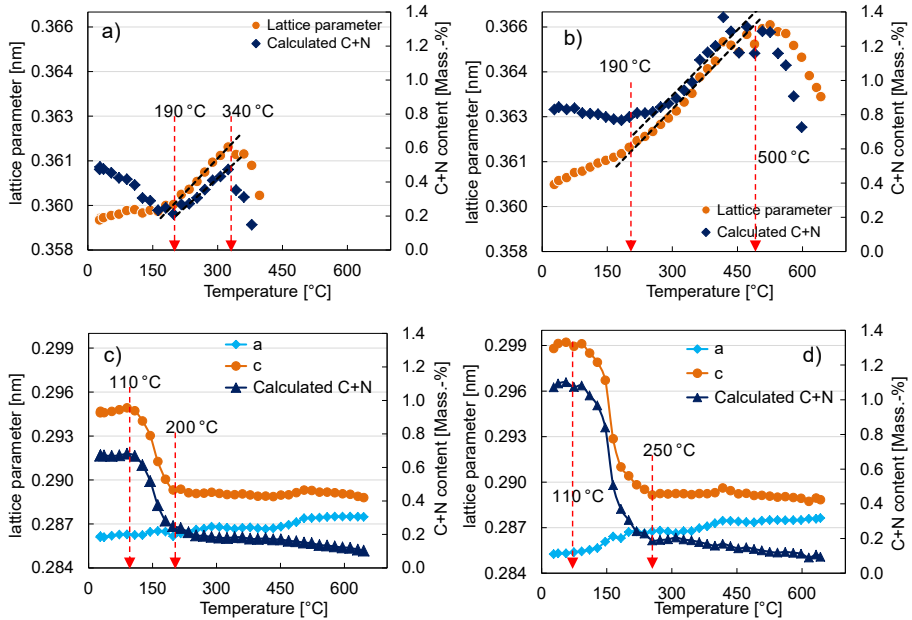


Figure 4.17 Variation of lattice parameters and C+N content during heating from RT up to 650 °C at 10 K/min: a) and b) RA for CN1 and CN2 respectively; c) and d) martensite for CN1 and CN2 respectively

Table 4.3 Lattice parameter coefficients for C+N content and temperature dependence

	Below 190 °C				Above 190 °C			
	Lattice parameter		C+N content		Lattice parameter		C+N content	
	A [nm]	Bx10 <sup>-6</sup> [nm/°C]	A [wt.-%]	B [wt.-%/°C]	A [nm]	Bx10 <sup>-6</sup> [nm/°C]	A [wt.-%]	B [wt.-%/°C]
CN1	0.357	2	0.543	-0.0017	0.357	10	0.113	0.0023
CN2	0.360	7	0.866	-0.0005	0.358	10	-0.260	0.0026

#### **4.2.1.4 Evolution of phase fractions during tempering cycle**

Figure 4.18 presents the evolution of retained austenite content as a function of time during complete tempering cycles. In all cases, the heating and cooling rates were 10 K/min whereas the holding temperatures were 170, 240 and 300 °C for holding time of 2 hours.

In all cases, the analysis of the X-ray diffraction patterns collected at room temperature yielded initial amount of retained austenite of about 18 mass.-percent for CN1 and 50 mass.-percent for CN2. The similarities of the initial amount of retained austenite at RT among the different sample reflect that carbon and nitrogen contents are constant from one sample to another after carbonitriding treatment. On tempering at 170 °C for 2 hours (Figure 4.23a), retained austenite remains relatively thermally stable for both CN1 and CN2. Tempering at 240 °C for 2 hours, retained austenite slightly transforms and as high as 70% of the initial RA remains. It is expected that prolonged tempering at this temperature can lead to further transformation of retained austenite. At 300°C (Figure 4.18c), retained austenite rapidly transforms leading to less than 5 mass.-percent austenite after tempering. In addition, during cooling to RT the austenite remaining at isothermal temperature remains relatively stable.

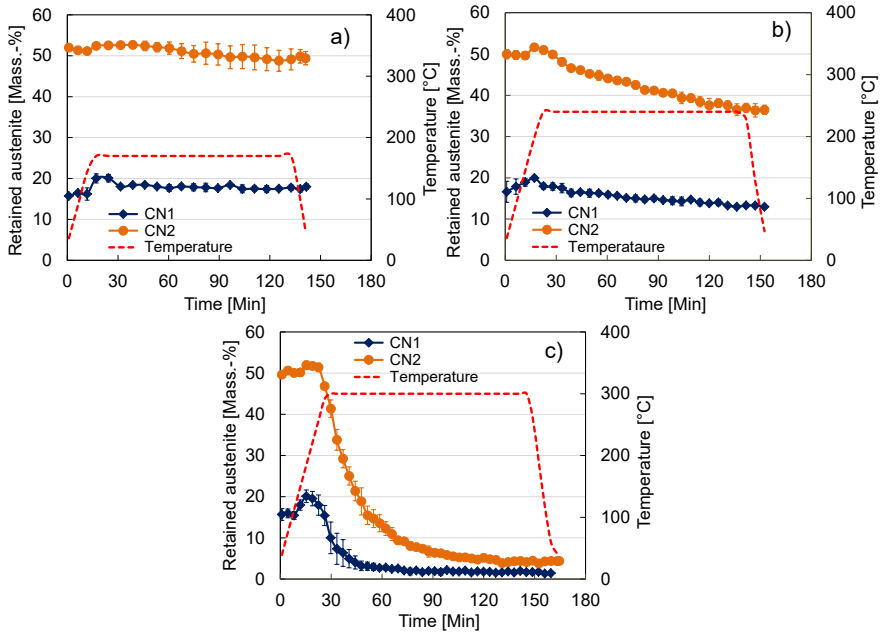


Figure 4.18 Evolution of retained austenite during tempering cycles : a) samples tempered at 170 °C ; b) samples tempered at 240 °C ; c) samples tempered at 300 °C

#### 4.2.1.5 Evolution of lattice parameters during tempering cycles.

Figure 4.19 provides in-situ observation of evolution of austenite lattice parameter during different complete tempering cycles. The isothermal holding was carried out at 170 °C, 240 °C, and 300 °C for 2 hours. It can be seen from this figure that, at each point the lattice parameter for CN2 is significantly greater than that of CN1. This reflects the differences in C+N concentration at a depth of 50 μm after carbonitriding treatment of which was 0.86% for CN1 and 1.33% for CN2. During heating at 10 K/min to the holding temperature, austenite lattice parameter increases almost linearly in two stages, which can be clearly differentiated in Figure 4.19c. The first stage is from RT to about 190 °C with estimated thermal coefficient of expansion of  $5.61 \times 10^{-6} \text{ } ^\circ\text{C}^{-1}$  for CN1 and  $19.43 \times 10^{-6} \text{ } ^\circ\text{C}^{-1}$  for CN2. The second is above 190 °C with estimated value of thermal coefficient of expansion about  $28 \times 10^{-6} \text{ } ^\circ\text{C}^{-1}$  for CN1 and  $27.89 \times 10^{-6} \text{ } ^\circ\text{C}^{-1}$  for CN2.

On holding isothermally at 170 and 240 °C for 2 hours, the austenite lattice parameter remains relatively constant (Figure 4.19a, b). A slight increase in lattice parameter during the initial stages of holding at 300 °C can be observed, which can be attributed to continuation of C+N enrichment. On further holding at 300 °C, austenite lattice decreases rapidly as a result of decomposition of retained austenite and depletion of carbon and nitrogen content due to the formation of  $\gamma'$ -Fe<sub>4</sub>N<sub>1-x</sub> nitrides and conversion of  $\epsilon/\eta$ -Fe<sub>2.5</sub>C into cementite [YOU 93]. In addition, during cooling to RT, the lattice parameter decreases continuously. This is mainly due to thermal contraction.

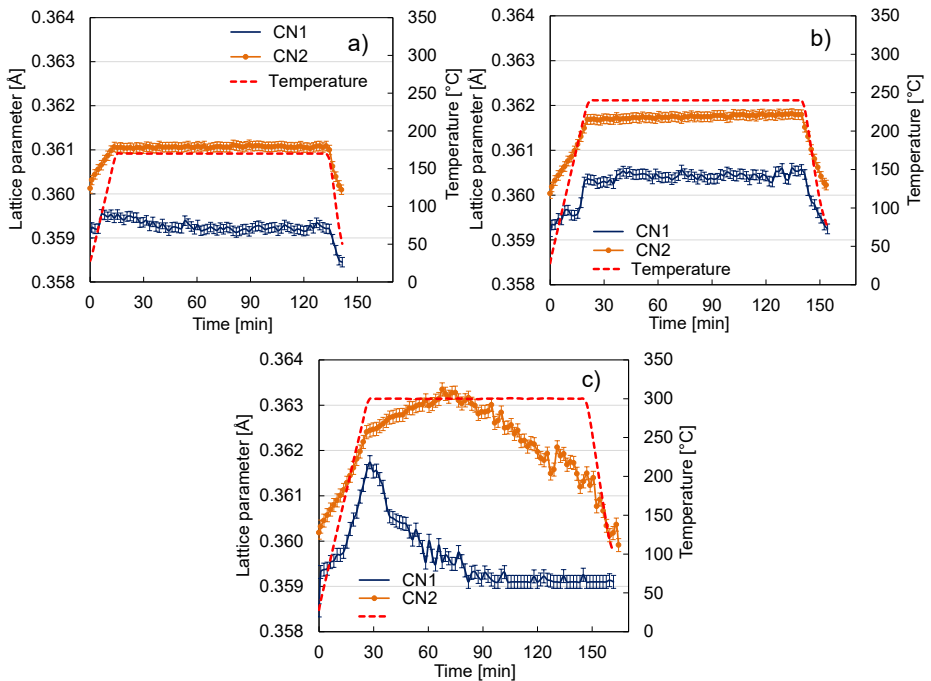


Figure 4.19 Evolution of lattice parameter of austenite during tempering cycles for 2 hours at a) 170 °C; b) 240 °C; c) 300 °C

#### 4.2.1.6 Evolution of residual stresses during continuous heating

The evolution of residual stresses in retained austenite and martensite phase for both CN1 and CN2 treatments during continuous heating is shown in Figure 4.20. It has to be noted that in all cases, the measurements were done at a depth of about 50  $\mu\text{m}$  from the surface. At this depth the samples contain the highest volume fraction of retained austenite, which enables following evolution of RS in both retained austenite and martensite phase.

Analysis of the diffraction patterns collected at room temperature reveals initial values of residual stresses in retained austenite to be fully relaxed (0 MPa) for CN1 and 33 MPa for CN2 whereas in martensite phase stresses were -65 and -233 MPa for CN1 and CN2 respectively. The different values of initial residual stresses can mainly be due to the differences in martensite and retained austenite proportions, which is about 18 and 50 mass.-percent retained austenite for CN1 and CN2 respectively. Furthermore, the magnitude and location of the maximum compressive RS as well as the slight differences on depth of layer removed during etching play an important role on determining RS at a point. It can be seen from this figure that for both specimens CN1 and CN2, the compressive RS in martensite phase relax continuously with temperature and reaches full relaxation ( $\sigma \approx 0$  MPa) at about 400  $^{\circ}\text{C}$ .

Beyond 400  $^{\circ}\text{C}$ , the temperature at which the amount of retained austenite is about 3.5 and 8 mass.-percent for CN1 and CN2 respectively, residual stress state remain relatively constant and about zero. In this range, the influence of such low amount of retained austenite on residual stress in tempered martensite is neglected.

In contrast, the evolution of RS in retained austenite during continuous heating is cyclic, which may be associated to the changes in chemical composition occurring in retained austenite as indicated in Figure 4.17 or to the phase transformation as indicated in Figure 4.16. Below 190  $^{\circ}\text{C}$ , the decrease in tensile stresses in retained austenite may be associated to the decrease in C+N content (Figure 4.20a and b), which is mainly linked to formation of carbides/nitrides leading to overlapped effect of hydrostatic stresses. Above 190  $^{\circ}\text{C}$ , retained austenite is enriched with C+N partitioning from martensite leading to enhanced tensile stresses. It is observed in Figure 4.20 that during heating retained austenite decomposes and it becomes considerably difficult measuring residual stresses when the amount of retained austenite is below 15 mass.-percent.

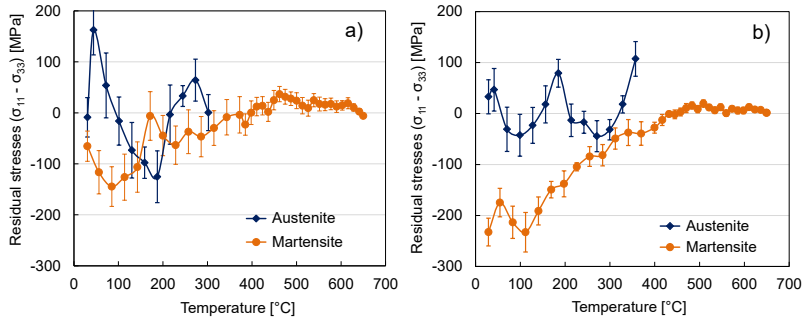


Figure 4.20 Evolution of residual stresses during heating from RT to 650 °C at 10 K/min: a) CN1; b) CN2

#### 4.2.1.7 Evolution of residual stresses during tempering cycles.

Figure 4.21 presents the evolution of residual stresses during different tempering cycles of CN1 and CN2 samples. Due to weak intensity of retained austenite reflections, residual stress analysis in retained austenite was only possible for diffraction patterns having retained austenite more than 18%.

For both CN1 and CN2 treatments, the initial residual stresses in martensite phase range from -100 to -250 MPa. These values are in the same range of magnitudes as the ones observed during continuous heating in Figure 4.20. The difference in initial magnitudes of residual stresses can be attributed to differences in martensite to retained austenite ratio, the depth at which the measurements were conducted ( $50 \pm 10 \mu\text{m}$ ) as well as chemical compositions. It is obvious from these figures that the residual stress relaxation in martensite phase occurs mainly during heating to the isothermal holding temperature. During isothermal holding, the residual stress remains mostly constant. However, the magnitude of compressive residual stresses for CN1 decreases with increasing holding temperature and is about -75, -65, and -30 MPa for isothermal holding temperature of 170 °C, 240 °C, and 300 °C respectively. Similarly, for CN2 residual stresses during isothermal holding remain relatively constant and about -100, -120, and -80 MPa in martensite phase. For CN2, the magnitude of compressive RS during isothermal holding in martensite phase seems to be mostly unaffected with holding temperature. This effect may be attributed to the high volume fraction of retained austenite of about 50%.

During the cooling stage, two trends of residue stresses evolution in both phases are observed. Residual stresses in martensite phase for samples with more than 5 mass.-% of RA remaining after isothermal holding (Figure 4.21a, b, c and d) decreases during cooling stage, which is linked thermal contraction.

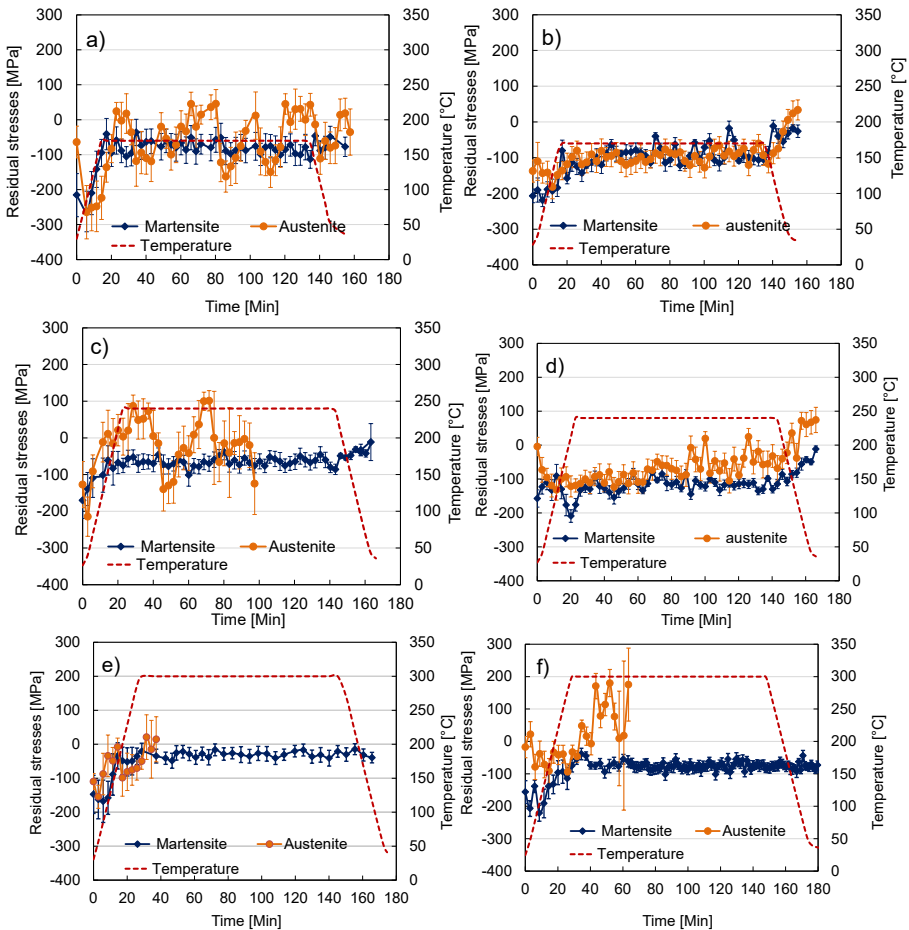


Figure 4.21 Effect of tempering cycles on the evolution of residual stresses in carbonitrided specimens for different isothermal holding temperatures: a), c) and e) at 170/240/300 °C for CN1; b), d) and f) at 170/240/300 °C for CN2, respectively.

## 4.2.2 State after tempering

### 4.2.2.1. Carbon and nitrogen depth profiles

Figure 4.22 shows the carbon and nitrogen profiles for carbonitriding treatment CN2 in as-quenched (*untempered*) state and after tempering at 170 °C for 2 hours. In the first 50  $\mu\text{m}$  the samples were characterized by slight depletion of alloying elements. In this range, the depletion of alloying elements occurs mainly due to oxidation and precipitate formation. Figure 4.23 compares the X-ray diffraction patterns collected using cobalt anode at a depth of 50  $\mu\text{m}$  from the surface. It can be seen that after tempering at 170 °C for 2 hour, martensite reflections (002) and (112) disappear due to loss of tetragonality accompanied by clustering of carbon and nitrogen atoms and formation of transition carbides, nitrides and carbonitrides.

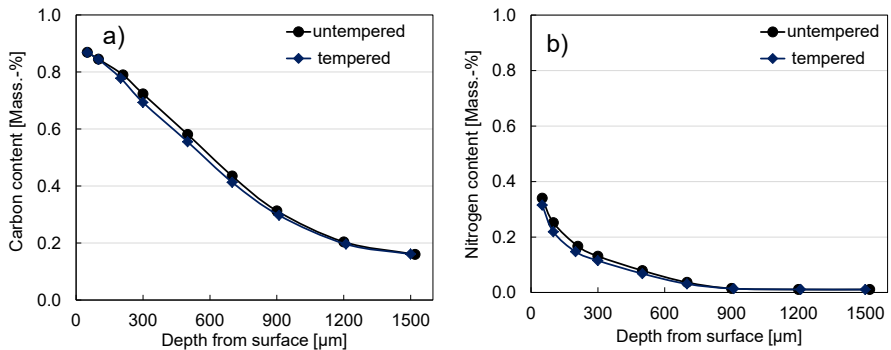


Figure 4.22 Comparison CN2 carbon and nitrogen profiles before and after tempering determined using OES: a) carbon; b) nitrogen

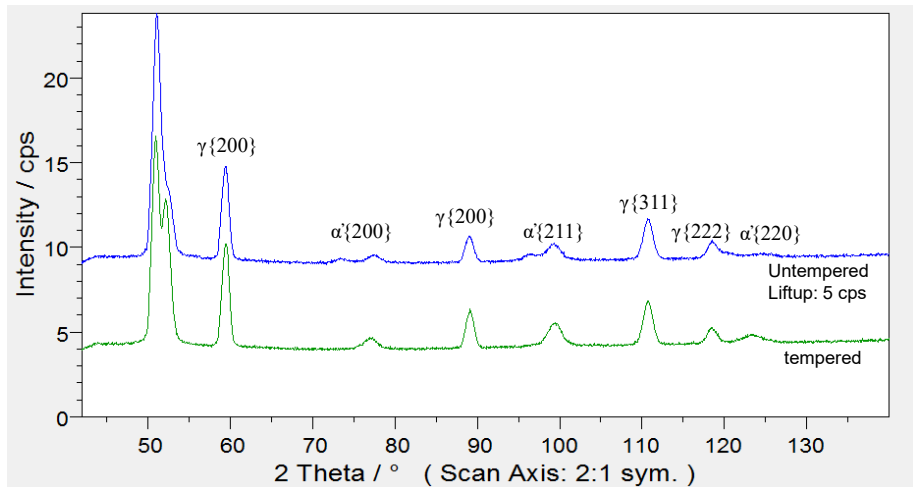


Figure 4.23 X-ray diffraction patterns before and after tempering at 170 °C for 2 hours (Co-K $\alpha$ )

#### 4.2.2.2. Microstructures and microhardness distributions.

Figure 4.24 presents the typical microstructures of the case-hardened layer for 18CrNiMo7-6 carbonitrided specimens after tempering at 170 °C for 2 hours before and after etching with 3 % alc. HNO<sub>3</sub> for 30 seconds. The microstructures consist of tempered plate martensite/ferrite (*dark*) surrounded by retained austenite (*white*), dispersed carbides/nitrides and subsurface grain boundary oxidation of about 10  $\mu$ m. The tempering of carbonitrided samples causes precipitations of coherent  $\epsilon$ -carbides, nitrides and carbonitrides which lead to darkening of martensite plates [PAR 99]. Moreover, precipitation formation is accompanied by a decrease in volume leading to relaxation of compressive residual stresses in martensite phase. According to Zabil'ski et al. [ZAB 79], the volume change occurring during tempering process cannot be accounted for by the precipitation process and transformation of retained austenite (*if there is any*) rather they suggest is due to healing effects of the microstructural defects in the martensite phase.

Figure 4.25 shows the micro-hardness depth profiles of the carbonitrided specimens measured after tempering at 170 °C for 2 hours. In general, the micro-hardness distributions

correlate well with the variation of microstructure from the surface to the core. Despite the difference in carbon and nitrogen content after carbonitriding, the maximum hardness for both samples is about 700 HV. In contrast, the location of the maximum hardness is dependent on phase composition distribution and it occurs at a depth where the proportion of martensite phase is about 80%. For CN1, the maximum hardness occurs in the range of 100 to 200  $\mu\text{m}$  whereas for CN2 it occurs at about 400  $\mu\text{m}$ . In the first 400  $\mu\text{m}$  (Figure 4.25b), a low value of hardness which is mainly linked to high amount of the softer retained austenite phase can be observed. Tempering at 170  $^{\circ}\text{C}$  for 2 hours have little effect on the core hardness remains constant at about 450 HV. In addition, the core is essentially bainitic and its hardness is hardly affected by tempering at a temperature below 300  $^{\circ}\text{C}$  [PAR 99].

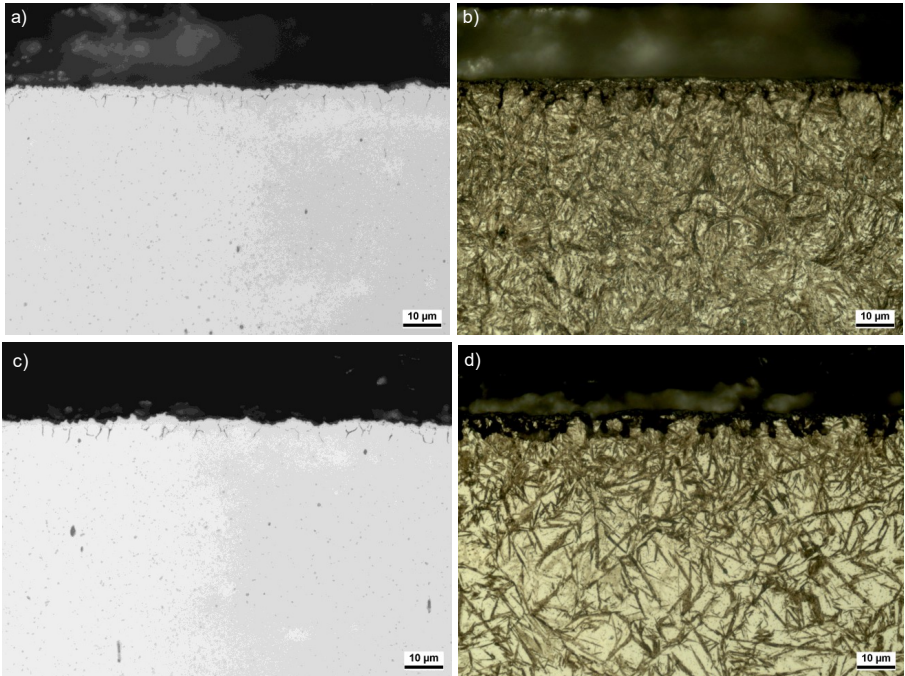


Figure 4.24 Typical example of case microstructures for carbonitrided samples after tempering at 170  $^{\circ}\text{C}$  2 hours: a) CN1 (unetched); b) CN1 (etched); c) CN2 (unetched); d) CN2 (etched).

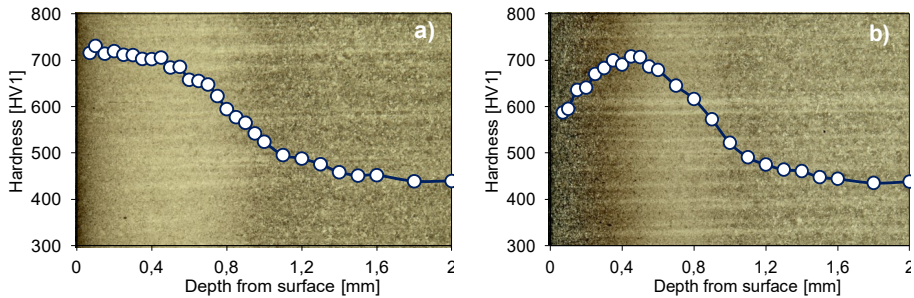


Figure 4.25 Microhardness depth profiles after tempering at 170 °C/2 h: a) CN1; b) CN2

#### 4.2.2.3 Residual stress relaxation

Figure 4.27 compares the residual stress distributions in retained austenite phase before and after tempering at 170 °C for 2 hours for CN1 and CN2 samples. Such comparison in martensite phase is given in Figure 4.27. The tempering process considerably relaxes residual stresses in both phases.

For RA phase, a relaxation CN1 reaches up to 230 MPa at a depth of 150  $\mu\text{m}$  and up to 279 MPa at a depth of 700  $\mu\text{m}$  for CN2. Further, after tempering RA phase is less stressed and is characterized by tension/compression stresses of low magnitudes.

In martensite phase (Figure 4.27), the peak compressive RS is -480 MPa at a depth of 550  $\mu\text{m}$  and -160 MPa at a depth of 550  $\mu\text{m}$  for untempered and tempered specimens (Figure 4.27a) respectively. Such stresses for CN2 are -440 MPa at a depth of 690  $\mu\text{m}$  and -240 MPa at a depth of 880  $\mu\text{m}$  for untempered and tempered specimens (Figure 4.27b) respectively. For CN1 specimen, as high as 320 MPa relaxes whereas for CN2 only up to 200 MPa relaxes. The low relaxation effect for CN2 can be attributed to the high amount of thermally stabilized retained austenite ( $\approx 50$  mass.-percent) in comparison to that in CN1 (20 mass.-percent). The RS relaxation is attributed to re-organization of thermally activated dislocations as well as movement of interstitial carbon and nitrogen atoms toward the area of high dislocation density and grain boundaries [MIT 86]. Moreover, the tempering process shifts the location of peak compressive RS toward the case/core interface.

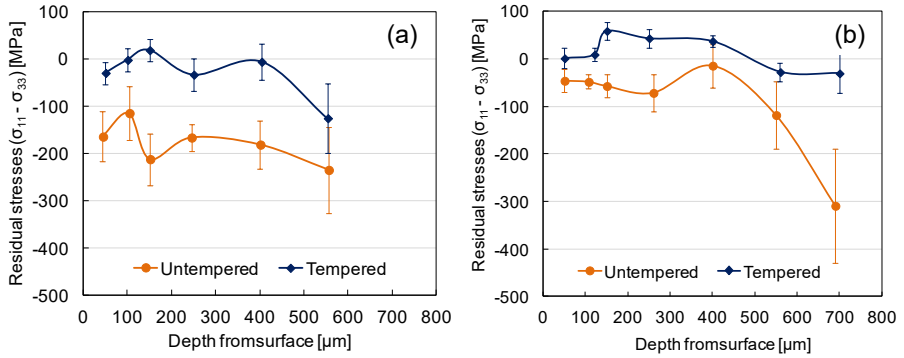


Figure 4.26 Residual stresses before and after tempering in RA phase: a) CN1; b) CN2

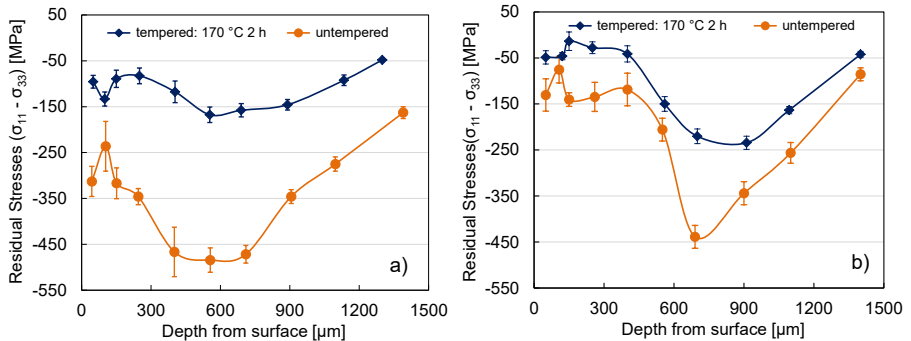


Figure 4.27 Residual stresses before and after tempering in martensite phase: a) CN1; b) CN2

### 4.2.3 Line broadening during tempering

The effect of temperature on crystallite size, root mean microstrain and resulting dislocation density in both phases, retained austenite and martensite, are reported in Figure 4.28 to 4.30. It has to be noted here that the investigation was carried out at a depth of 50  $\mu\text{m}$ , the depth at which the samples contain the maximum amount of retained austenite of about 20% for CN1 and 50% for CN2. It appears from the figures that the variation of these parameters with temperature can be divided into two stages; below and above 150  $^{\circ}\text{C}$  for retained austenite and 200  $^{\circ}\text{C}$  for martensite phase.

Figure 4.28 gives the variation of crystallite size with temperature. It can be seen from this figure that at all depths the crystallite size for CN2 remains considerably greater in comparison to CN1 (Figure 4.28a). On heating from RT to 150 °C, the crystallite size in retained austenite increases with increasing temperature and varies from 40 nm to 200 nm for CN1 and from 350 nm to about 600 nm for CN2. The increase in crystallite size can be linked to recovery effect. Above 150 °C, the crystallite size of retained austenite continuously decreases to reach below 20 nm at about 420 °C for both CN1 and CN2. Such a decrease can be ascribed to decomposition of retained austenite into bainite as well as the formation of carbides and nitrides. In contrast, the martensite crystallite size in both CN1 and CN2 increases and reaches the upper set boundary condition of 1000 nm at 200 °C. It is reasonable to assume that for crystallite size larger than 1000 nm, the line broadening is mainly dependent on microstrain. The increase in martensite crystallite size can be attributed to changing morphology (*diffusionless plate martensite to BCC ferrite/tempered martensite*).

Figure 4.29 reports the variation of root mean square (*r.m.s*) microstrain with temperature. For both CN1 and CN2, the mean microstrain in martensite phase is considerably higher than in comparison to that in retained austenite. In both cases the mean microstrain lies in the range between 0.001 and 0.004. It is thought that microstrain in carbonitrided parts can result from the dislocation stress fields (*strain type A*), and coherent carbides and nitrides precipitates and/or misfit dislocations (*strain type B*) [HOF 01], which are considerably significant in martensite phase. In addition, carbon and nitrogen dissolved in the octahedral interstitial sites play a significant role in enhancing the microstrain (*strain type C*). The variation of the mean microstrain with either the amount of retained austenite or temperature depend will virtually depend on the variation of these parameters. For example, annihilation of thermally activated dislocations during continuous heating or tempering results in a decrease of mean strain.

The effect of temperature on dislocation density in both retained austenite and martensite is reported in Figure 4.30. As expected, dislocation density for CN1 which contain less volume fraction of retained austenite remains relatively higher as compared to that in CN2. On heating to 250 °C, the dislocation density in martensite/ferrite decreases from about  $2.5 \times 10^{11} \text{ cm}^{-2}$  to

$10^{10} \text{ cm}^{-2}$ , which is equivalent to a decrease of about 96% of the initial dislocation density. Above  $250 \text{ }^{\circ}\text{C}$ , the dislocation density gradually decreases to reach  $5 \times 10^9 \text{ cm}^{-2}$  at  $550 \text{ }^{\circ}\text{C}$ . For retained austenite, on heating to  $150 \text{ }^{\circ}\text{C}$  the dislocation density in retained austenite slightly decreases from  $10^{11} \text{ cm}^{-2}$  to  $3 \times 10^{10} \text{ cm}^{-2}$  for CN1 and from  $10^{10} \text{ cm}^{-2}$  to  $7 \times 10^9 \text{ cm}^{-2}$  for CN2, which is equivalent to the decrease of 70% and 40% respectively, of the initial dislocation density. The decrease of dislocation density with increasing temperature can be ascribed to annihilation of thermally activated dislocations as well as coarsening of crystallite size. It can be seen from Figure 4.30a that beyond  $150 \text{ }^{\circ}\text{C}$ , the dislocation density in both treatments increase considerably as temperature increases. The dislocation density increases to  $5 \times 10^{11} \text{ cm}^{-2}$  for CN1 and  $2 \times 10^{11} \text{ cm}^{-2}$  for CN2. The increase in dislocation density on heating beyond  $150 \text{ }^{\circ}\text{C}$  can be attributed to the transformation of retained austenite into bainite/martensite. Due to this transformation, the remaining retained austenite is further plastically deformed due to volume increase. Moreover, it is reasonably believed that plenty of dislocations in martensite can move into the neighbouring retained austenite across their interface. In other words, the dislocations can be absorbed by nearby retained austenite [RON 14]. Wang reported that a dislocation can transmit across the BCC/FCC interface with K-S orientation relationship, showing the complex mechanism of dislocation across the interface [WAN 11]. The dislocations in martensite can move into nearby retained austenite by several slip systems, such as plane normal to the interface or slip plane parallel to the interface, giving rise to the rapid decrease of the average dislocation density in martensite during heating.

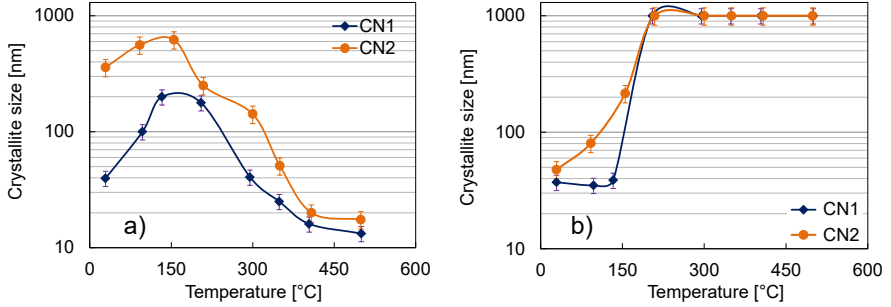


Figure 4.28 Evolution of crystallite size during heating from RT to 650 °C at 10 K/min: a) retained austenite; b) martensite

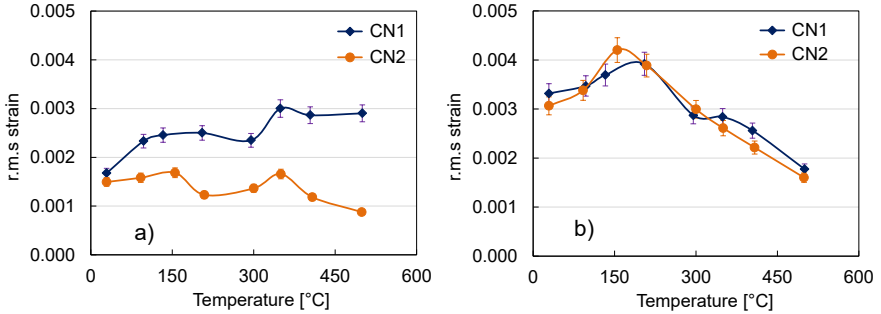


Figure 4.29 Evolution of r.m.s strain during heating from RT to 650 °C at 10 K/min: a) retained austenite; b) martensite

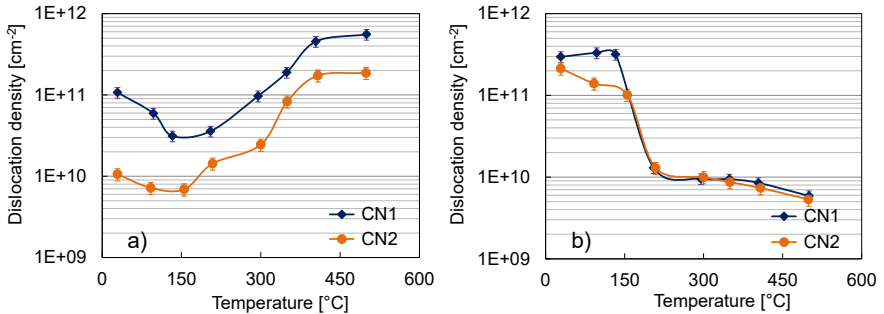


Figure 4.30 Evolution of dislocation density during heating from RT to 650 °C at 10 K/min: a) retained austenite; b) martensite

#### 4.2.4 Discussion on state during and after tempering

Carbonitrided components are always tempered to transform the unstable and brittle as-quenched martensite into more stable tempered martensite. This leads to an increase in ductility and thus minimizes occurrence of delayed fracture [JAT 78, WIS 91]. In this investigation, conventional tempering was carried out at 170 °C for 2 hours. This insures that the minimum surface hardness of more than 60 HRC is maintained.

Figure 4.27 illustrates the effect of tempering on the magnitudes and distribution of residual stresses in martensite phase. It is evident from this figure that tempering relaxes significantly the magnitudes of residual stresses. For CN1 samples, a relaxation of up to 320 MPa is observed while CN2 samples relax only up to 200 MPa. The tendency of CN2 to resist tempering effect is ascribed to its high carbon and nitrogen content in the case. The RS relaxation is attributed to re-organization of thermally activated dislocations as well as movement of interstitial carbon and nitrogen atoms toward the area of high dislocation density and grain boundaries [MIT 86]. In view of this, Parrish [PAR 99] reports two stages of residual stress relaxation. The first stage results from carbides and nitrides segregation and precipitation clustering, which coincide with the initial minor relaxation of residual stresses. The second stage is characterized by precipitation of transition carbides/nitrides and loss of martensite tetragonality, which coincide with the major reduction of residual stresses.

The in-situ X-ray diffraction investigation (Figure 4.16) revealed that during continuous heating at 10 K/min retained austenite starts to decompose at about 290 °C for both CN1 and CN2 treatments. This seems that the difference in the total carbon and nitrogen content (*difference in initial retained austenite*) has little influence on the temperature at which retained austenite starts to decompose. The temperature observed in this work is in good agreement with that observed in the work of Amarthalingam [AMA 10]. In contrast, on continuous heating to 650 °C the end of rapid decomposition is 335 °C for CN1 and 355 °C for CN2. It appears that besides high initial amount of 50 mass.-percent for CN2, retained austenite in CN2 becomes more stabilized than that in CN1. The stabilization of RA may be thought to arise from carbon and nitrogen enrichment. The estimation of C+N content in solid solution illustrated in Figure 4.17 indicates that enrichment of retained austenite with C+N diffusing from martensite structure is prominent above 190 °C.

The evolution of retained austenite during complete tempering cycles with isothermal holding temperature at 170, 240, and 300 °C for 2 hours is given in Figure 4.18. On isothermal holding at 170 °C, retained austenite in both CN1 and CN2 remain relatively thermally stable. This is mainly due to carbon/nitrogen enrichment. Such thermal stability of retained austenite finds support from the work of Neu [NEU 93]. Holding isothermally at 240 and 300°C for 2 h a considerable amount of retained austenite decomposes as result less than 5 mass.-percent of austenite is retained after tempering at 300 °C for 2 hours. Figure 4.31 provides the summary of transformed volume fraction of the initial amount of retained austenite decomposed as a function of tempering temperature. The two carbonitriding treatments show similar decomposition rate reflecting that no difference in thermal stability. At 170 °C almost no transformation of RA while after tempering at 300 °C nearly 100% of RA transformed.

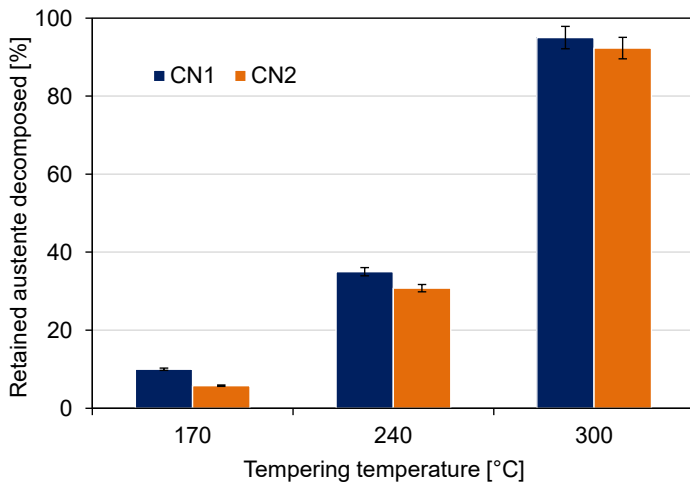


Figure 4.31 Percentage of retained austenite transformed during tempering at different tempering temperatures

The evolution of residual stresses in martensite and retained austenite phase during continuous heating from RT to 650 °C for both CN1 and CN2 is given in Figure 4.20. As can be seen from this figure, the compressive residual stresses in martensite phase for both treatments CN1 and CN2 relax continuously with temperature. The full residual stress

relaxation ( $\sigma \approx 0$  MPa) is reached at about 400 °C, which is attributed to re-organization of thermally activated dislocations as well as movement of interstitial carbon and nitrogen atoms toward the area of high dislocation density and grain boundaries [MIT 86] as well as the transformation of austenite to alpha. Moreover, beyond 400 °C, the temperature at which the amount of retained austenite is about 3.5 and 8 mass.-percent for CN1 and CN2 respectively, residual stress state remain relatively constant and about zero. In this range, the influence of retained austenite on residual stress in tempered martensite is negligible. On the other hand, the evolution of residual stresses in retained austenite during continuous heating is cyclic which may be associated to the changes in chemical composition occurring in retained austenite as shown in Figure 4.20 and the involved volume change due to gamma to alpha transformation. Below 190 °C, the decrease in tensile stresses in retained austenite can be linked to depletion of carbon + nitrogen content as a result of cluster segregation and formation transition of carbides/nitrides formation. Above 190 °C, retained austenite is enriched with carbon + nitrogen segregating from martensite leading to enhanced tensile stresses.

Residual stress evolutions during complete tempering cycles are given in Figure 4.21. This figure indicates that the residual stress relaxation in martensite invariably occurs during the heating phase, re-organization of thermally activated dislocations as well as movement of interstitial carbon and nitrogen atoms toward the area of high dislocation density and grain boundaries [MIT 86]. During isothermal holding, at low temperature, residual stresses remain relatively constant. For CN1, the magnitude of residual stress markedly depends on temperature and decreases with increasing holding temperature (i.e. -75 MPa at 170 °C, -65 MPa at 240 °C, and -30 MPa at 300 °C). In this case, the effect of retained austenite (*which is below 20%*) on residual stresses in martensite phase is negligibly small. On contrary, CN2 has no specific dependence of residual stresses on holding temperature and remains relatively at -100 MPa. During cooling from the holding, further relaxation of residual stresses in occurs, which is mainly linked to the difference in temperature between the surface and the core.

### **4.3 State after cryogenic treatment**

This section presents investigations of the state after cryogenic treatment of carbonitrided samples in CN2 conditions. Prior to cryogenic treatment, the carbonitrided samples were thermally stabilized at different temperatures and times. The cryogenic treatment was carried out at -120 °C for 2 hours. The microstructure and microhardness distributions after cryogenic treatment are considered. Analysis of retained austenite and residual stresses in martensite phase was conducted using X-ray diffraction. Residual stress measurements in retained austenite were not conducted due to low amount of retained austenite.

#### **4.3.1 Carbon and nitrogen depth profiles**

For this investigation, the carbon and nitrogen depth profiles in the sample are the same as the ones given in Figure 4.1b (CN2). For carbonitriding treatment CN2 the maximum concentration at a depth of 50  $\mu\text{m}$  is 0.87 %C and 0.34 %N with an effective case depth of 1 mm.

Similarly, in the first 50  $\mu\text{m}$  the samples were characterized by depletion of alloying elements mainly due to internal oxidation, which is considered normal carbonitriding treatment carried out under endothermic carbonitriding atmosphere [DAV 02].

#### **4.3.2 Metallography and microhardness distributions**

Typical microstructures of the case-hardened layer for carbonitrided 18CrNiMo7-6 samples in their as-quenched state and after cryogenic treatment at different conditions are presented in Figure 4.32. The case microstructures are characterized by plate martensite (dark), retained austenite (white) and finely dispersed precipitates of carbides and/ or nitrides. The martensite in Figure 4.32a, c to e consists of plates with large sizes while such plates could not be resolved with optical microscope for the sample directly cold treated (Figure 4.32b). Darkening of martensite plates, which can be attributed to precipitation of transition carbides/carbonitrides, increases with increasing temperature. A considerable difference in volume fraction of retained austenite can be observed between the sample tempered at 240 °C for 2 and 14 hours respectively (Figure 4.32e and f). In Figure 4.32f, the low amount of retained austenite is associated to decomposition of retained austenite to bainite during

holding at 240 °C. This prompted to in-situ investigation to establish the range of thermal stability of retained austenite and establish its kinetics of decomposition as presented in section 4.2.1. Moreover, the microstructures are characterized by subsurface inter- and/ or intra-granular oxidation as expected for carbonitriding/carburizing treatments carried out in endothermic atmospheres [SAS 82].

Figure 4.33 illustrates the microhardness distributions for as-quenched sample and after different tempering and cryogenic treatments. The variation of microhardness from the surface to the core corresponds well to that of microstructure. The lowest surface hardness value of 600 HV is observed in the as-quenched specimen with its maximum hardness of about 780 HV occurring at a depth of 400  $\mu\text{m}$  from the surface (Figure 4.33a). The low hardness in the surface is due to the presence of soft retained austenite phase of about 50 mass.-percent. Obviously, cryogenic treatment enhances further the case hardness. The direct cryogenically treated specimen (Figure 4.33b) experienced the highest hardness value of about 900 HV because of highest additional transformation of retained austenite to martensite phase. This in turn enhances dimensional stability because less austenite is available to transform to martensite by stress or strain controlled mechanisms [DAV 02]. Comparing Figure 4.33c, d, and e in which the specimens were tempered for 2 hours at 120, 170, and 240 °C, respectively, the maximum hardness value as a result of newly stable martensite decreases with increasing tempering. This is due to the fact that, besides stabilization of retained austenite which increases with tempering temperature, a significant fraction of retained austenite transforms on holding at 240 °C for 2 hours ; consequently fraction of retained austenite transformed during cryogenic treatment decreases with increasing tempering temperature. In other term, the stable and newly formed martensite during cryogenic treatment increases with decreasing stabilization temperature. Moreover, martensite tempering also leads to a decrease in hardness. The low hardness value observed in Figure 4.33f is mainly due to decomposition of retained austenite to bainite occurred during isothermal holding at 240 °C for 14 hours. In addition, the core hardness seems to be less affected by the tempering conditions as well as the cryogenic treatment and remains relatively constant at about 450 HV.

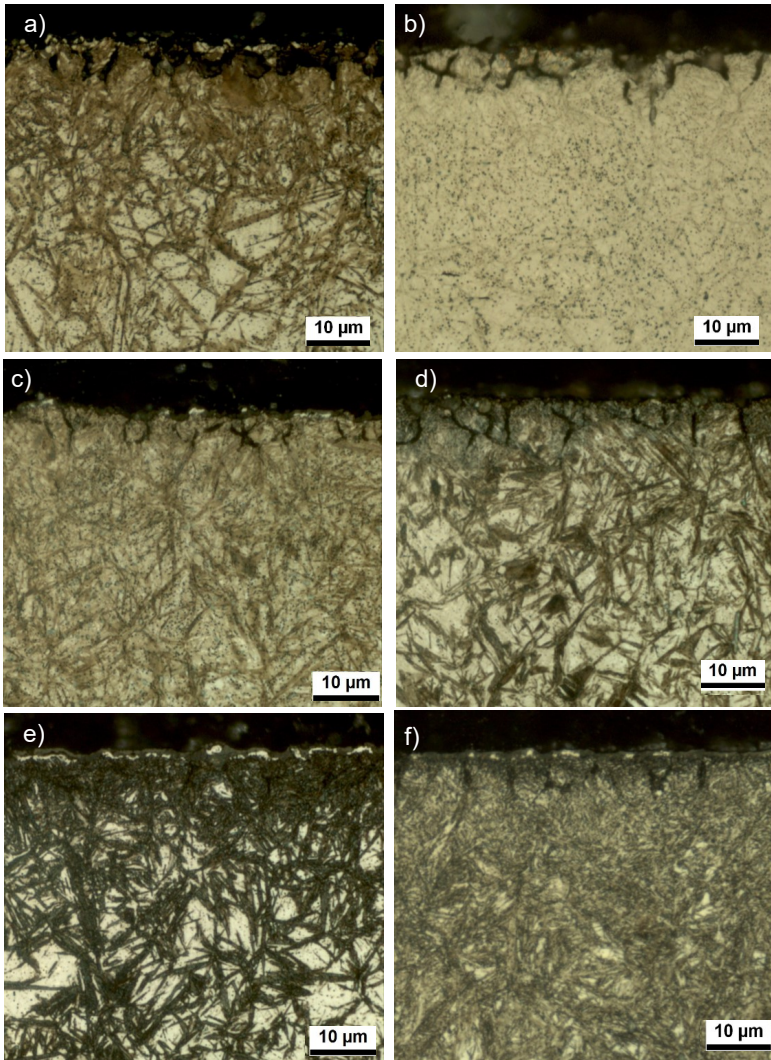


Figure 4.32 Typical case microstructures after cold treatment with prior tempering treatment a) As-quenched, b) directly CT after quenching, c) tempered at 120 °C for 2 hours + CT, d) tempered at 170 °C for 2 hours + CT, e) tempered at 240 °C for 2 hours +CT, f) tempered at 240 °C for 14 hours +CT

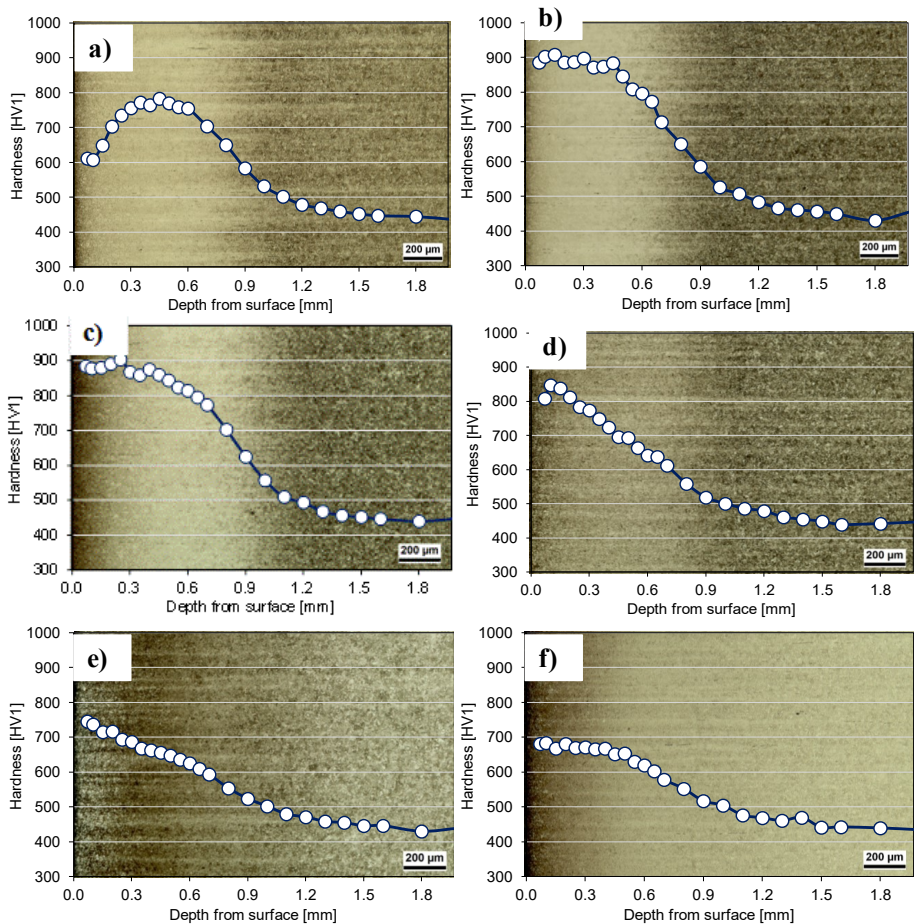


Figure 4.33 Variation of microhardness and case microstructures: a) As-quenched, b) Direct CT, c) tempered at 120 °C for 2 hours + CT, d) tempered at 170 °C for 2 hours + CT, e) tempered at 240 °C for 2 hours + CT, f) tempered at 240 °C for 14 hours + CT

#### 4.3.3 Retained austenite distribution

Figure 4.33 compares the retained austenite distributions for the as-quenched sample and for a sample which was immediately subjected to cryogenic treatment at -120 °C for 2 hours after quenching. In its as-quenched state, the sample retained as high as 50 mass.-percent austenite

whereas the directly cryogenic treated sample retained only 20 mass.-percent austenite. This implies that if the samples are immediately subjected to cryogenic treatment after carbonitriding treatment, as high as 60 Mass.-percent of the initially retained austenite would transform to martensite. These values set a basis for determining the effect of tempering temperature and time on the thermal stabilization of austenite.

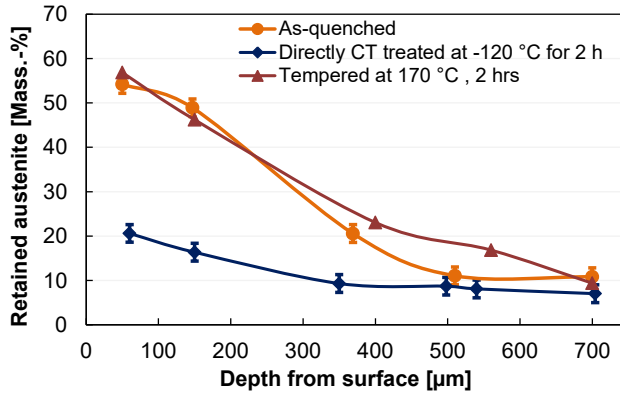


Figure 4.34 Retained austenite profiles for as-quenched and cold treated samples

Figure 4.35 shows the retained austenite depth profiles after cryogenic treatment at -120 °C for 2 hours. Prior to cryogenic treatment, samples were subjected to different tempering conditions. In general, the amount of retained austenite after cryogenic treatment increases with increasing tempering temperature. It can be seen from Figure 4.34a that after tempering the sample at 120 °C for 1 hour only 26% austenite is retained at a depth of 50 µm from surface after cryogenic treatment. On tempering at 170 °C and 240 °C for 1 hour such the corresponding retained austenite were 30% and 33% respectively. This signifies that if after quenching, the samples are held at 120 °C, 170 °C, and 240 °C for 1 hour, only 48%, 40%, and 34% respectively of austenite initially retained (50 mass.-percent) can be transformed to martensite as compared to over 60% for the sample which was immediately subjected to cryogenic treatment after quenching. This implies that after tempering for 1 hour prior to cryogenic treatment, the amount of remaining retained austenite increases with increasing tempering temperature. In other terms, it can be inferred that the stability of retained

austenite increases with increasing tempering temperature prior to cryogenic temperature. Similar trend can be observed in Figure 4.35b in which the samples were tempered for 2 hours at 120, 170, and 240 °C. Comparing Figure 4.35a and b indicates that the amounts of retained austenite after cryogenic treatment are practically the same for samples with prior tempering time of 1 and 2 hours. Their differences observed are within marginal error of 5%. Furthermore, a stage tempering (Figure 4.35d) yields similar results. However, a different tendency is observed on tempering the samples at 120 °C, 170 °C, and 240 °C for 14 hours. In this case, after cryogenic treatment as high as 27% and 30% austenite is retained for samples tempered at 120 °C and 170 °C respectively. On the other, only about 15% austenite is retained for the sample with prior tempering at 240 °C for 14 hours.

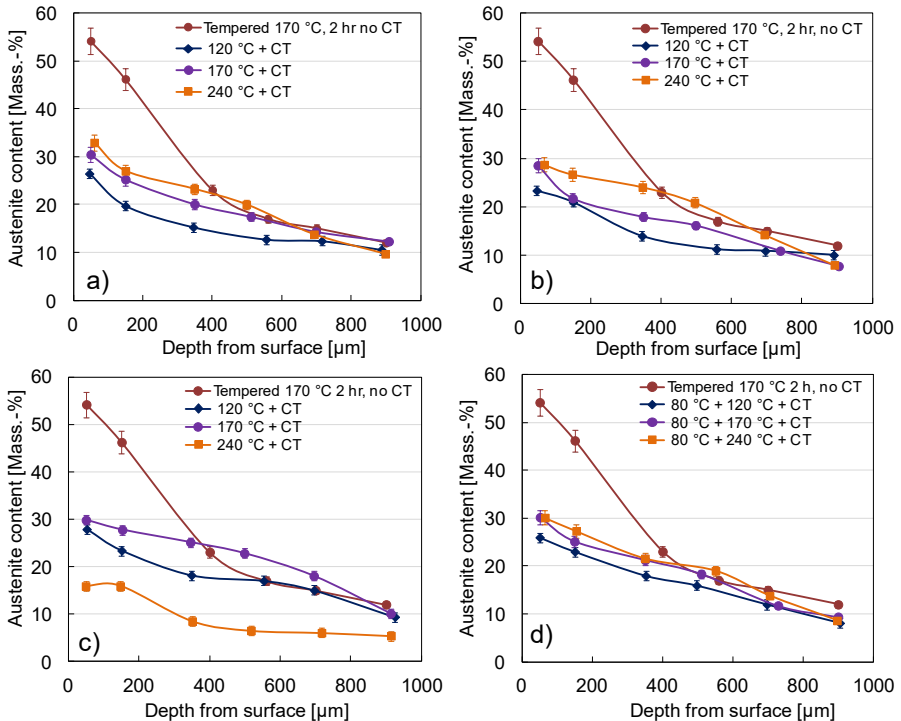


Figure 4.35 Retained austenite distributions after cold treatment for samples tempered at 120, 170, and 240 °C for: a) 1 hrs; b) 2 hrs; c) 14 hrs; and d) stage tempering at 80 °C/14 h then at 120, 170, and 240 for 2 h

#### 4.3.4 Martensite tetragonality ratio

Figure 4.36 and Figure 4.37 illustrate the martensite tetragonality ratio ( $c/a$ ) depth profiles after different tempering conditions followed by cryogenic treatment. The tetragonality ratios for as-quenched, direct cryogenically, and tempered samples are given in Figure 4.36. As it can be observed in this figure, no significant difference in the tetragonality ratio between the as-quenched and the direct cryogenically treated sample. In both cases, the maximum martensite tetragonality ratio at a depth of 50  $\mu\text{m}$  is 1.044. The decrease of tetragonality with depth correlates well with the C+N depth profiles after carbonitriding treatment. On the other hand, tempering at 170  $^{\circ}\text{C}$  for 2 hours decreases the martensite tetragonality and remains constant with depth at about 1.01.

As can be observed in Figure 4.37a to d, tempering prior to cryogenic treatment affects significantly the martensite tetragonality ratio. In all cases, the tetragonality ratio decreases with increasing tempering temperature. A comparison between Figure 4.37b and c present no significant difference in tetragonality ratio on tempering for 1 or 2 hours at different temperatures. However, tempering for 14 hours at 120  $^{\circ}\text{C}$ , 170  $^{\circ}\text{C}$ , 240  $^{\circ}\text{C}$  (Figure 4.37c) and stage tempering (Figure 4.37d), the martensite ratio ( $c/a$ ) decreases significantly. This decrease of  $c/a$  ratio can be attributed to the decrease of C+N content in martensite due to precipitates formation and tempering effect. Beyond 500  $\mu\text{m}$ , however, the tetragonality ratio remains constant and slightly below 1.01.

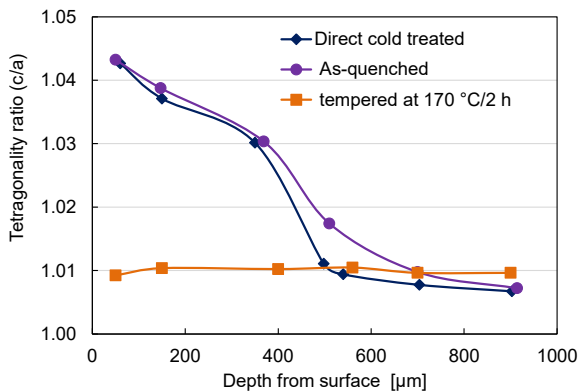


Figure 4.36 Martensite tetragonality ratio for initial conditions

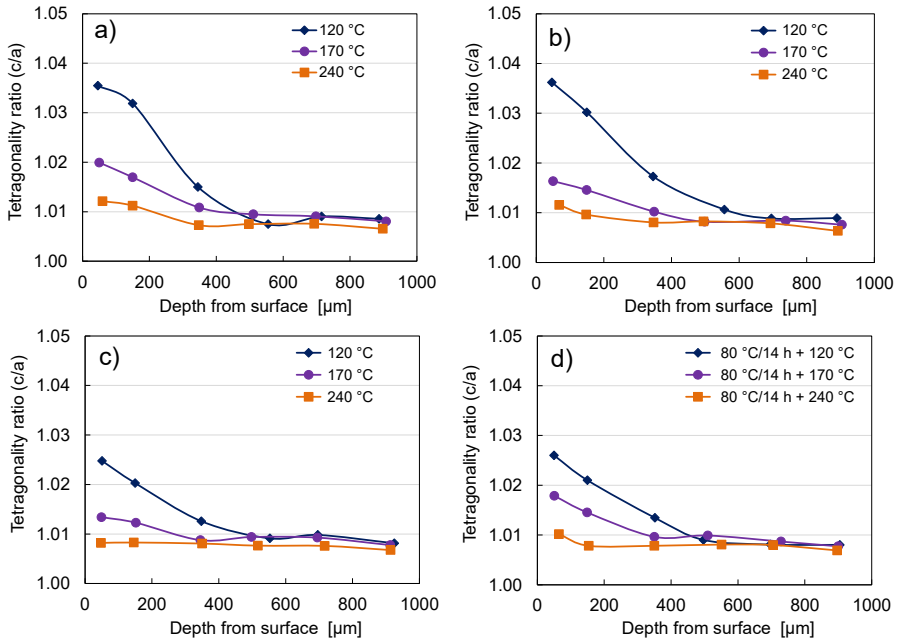


Figure 4.37 Martensite tetragonality ratio (c/a) depth profiles after cold treatment with prior tempering at 120, 170, and 240 °C for a) 1 h, b) 2 h, c) 14 h, d) stage tempering: 80 °C/14 h then at 120, 170, and 240 for 2 h

#### 4.3.5 Residual stress distributions in martensite

The residual stress distributions for as-quenched, tempered, and direct cryogenically treated specimens are given in Figure 4.38. It can be seen from this figure that although in all samples the residual stresses exhibit similar distributions, their magnitudes of RS are greatly different. The similarity arises from the fact that, all specimens are characterized by less compressive in the first 200 μm from the surface, peak compressive RS in the case, and a decrease in compressive RS toward the case/core interface. The peak compressive RS are -470 MPa at a depth of 700 μm for as-quenched sample, -240 MPa at a depth of 850 μm for the sample tempered at 170 °C for 2 hours, and -530 MPa at a depth of 560 μm for the sample which was

immediately subjected to cryogenic treatment after quenching. Considering the compressive RS values in the as-quenched specimen as the basis for comparison, tempering at 170 °C for 2 hours relaxes considerably the compressive RS at each point and shifts the location of compressive RS peak toward the case/core interface. A relaxation of up to about 240 MPa is reached. On the other hand, the immediate cryogenic treatment enhances the magnitudes of compressive RS and slightly shifts the location of compressive RS peak toward the surface. An increase of up to -200 MPa occurred. The increased magnitude of compressive RS is attributed to continued transformation of retained austenite to martensite during cryogenic treatment at -120 °C for 2 hours leading to additional volume expansion in the case.

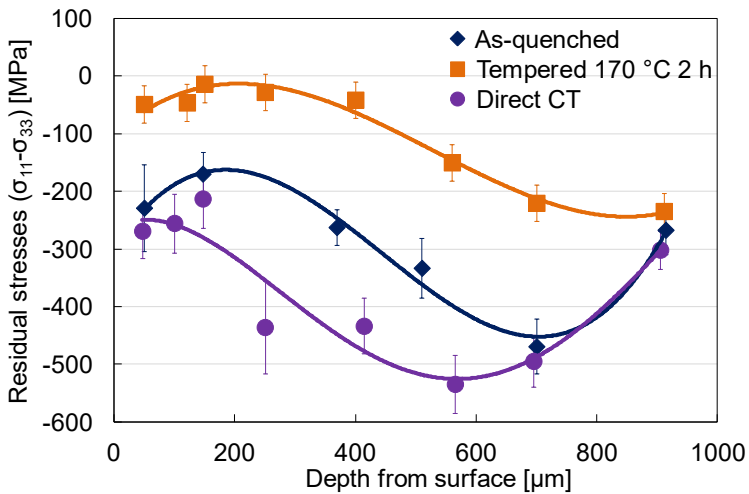


Figure 4.38 Residual stress distributions for initial conditions

Figure 4.39 corresponds to the RS distributions after tempering at different temperatures followed by cryogenic treatment at -120 °C for 2 hours. It can be observed from this figure that tempering prior to cryogenic treatment enhances significantly the compressive RS in the first 300 μm. Moreover, it alters the RS distribution as compared to that observed in Figure 4.38. Compressive RS of up to -500 MPa are reached at a depth of 50 μm. This is an improvement of about -450 MPa as compared to the RS at the same depth in the sample which were tempered at 170 °C for 2 hours in Figure 4.38. Such improvement in compressive RS at a depth of 400

$\mu\text{m}$  for samples tempered at 120 °C, 170 °C and 240 °C for 1 hour is -340 MPa, -250 MPa and -90 MPa respectively. Similar trends are observed for samples tempered for 2 hours at different temperatures. From these results it can be concluded that for short tempering time of 1 hour or 2 hours the enhancement of compressive RS in martensite decreases with increasing tempering temperatures. On the contrary, the sample tempered at 240 °C for 14 hours experienced less compressive RS of about -200 MPa at a depth of 50  $\mu\text{m}$ . Tempering at 240 °C for 14 hours leads to transformation of RA to bainite; as a result less amount of RA is available during cryogenic treatment. Such decomposition of RA is clearly shown in Figure 4.18b, in which a decomposition of about 25% of the initial amount of RA is observed on holding a sample at 240 °C for 2 hours.

Beyond 500  $\mu\text{m}$  the samples experienced less compressive RS in comparison to the as-quenched sample in Figure 4.38. For example, for the samples tempered for 2 hours (Figure 4.39b), the RS at a depth of 900  $\mu\text{m}$  are about -250 MPa for 170°C and -130 MPa for 240 °C. It can be seen in Figure 4.35 that beyond 500  $\mu\text{m}$  less than 20 mass.-% of austenite is retained and a small proportion of which would be expected to transform to martensite during cryogenic treatment, which could further enhance compressive RS. Therefore, in this case, the decrease in compressive RS is largely attributed to thermal relaxation.

In this case, the residual stresses in retained austenite after cryogenic treatment were not considered due to low intensity of retained austenite reflection {220} as the amount is about 20%. However, high tensile residual stresses have been reported in austenite surviving subzero treatment of the carbonitrided EX55 near the surface [KIM 83].

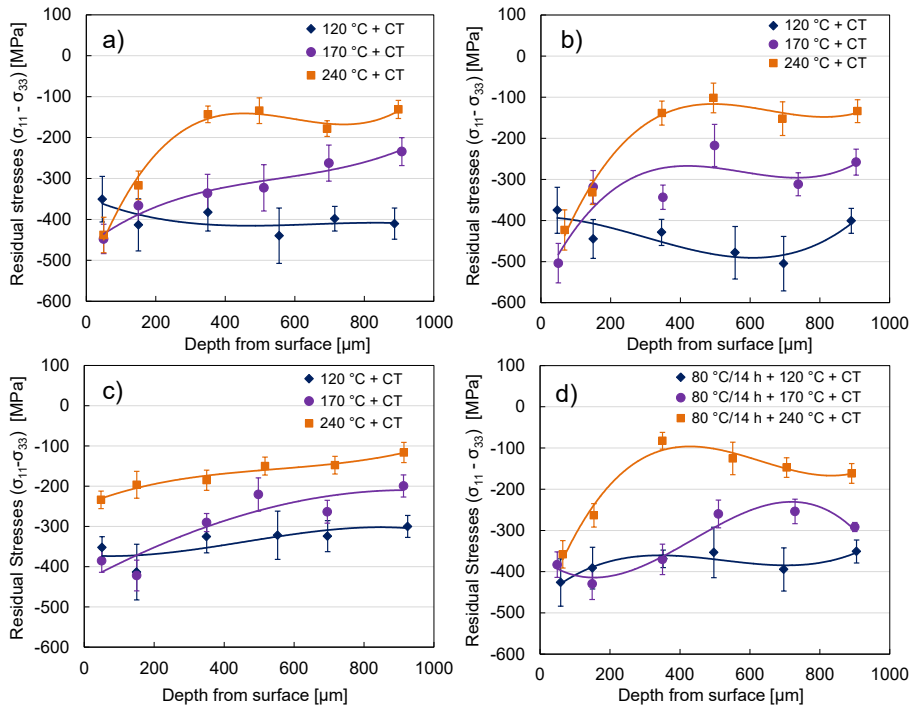


Figure 4.39 Residual stress distributions after cryogenic treatment for samples with prior tempering at different temperatures for: a) 1 h; b) 2 h; c) 14 h; d) 14 h at 80 °C then for 2 h at 120, 170, 240 °C

#### 4.3.6 Discussion on state after cryogenic treatment

In this section, the objective was to investigate the thermal stability of retained austenite during cryogenic treatment. Prior cryogenic treatment, samples were subjected at different tempering temperatures and times to induce different various degree of retained austenite stabilization. The initial amount of retained austenite of the sample after quenching into oil held at 60 °C was about 50% resulting from maximum carbon and nitrogen content of 0.87 %C and 0.34 %N after carbonitriding process.

It is obvious that cryogenic treatment at  $-120\text{ }^{\circ}\text{C}$  for 2 hours continues further the austenite to martensite transformation. For the samples immediately cryogenically treated more than 60% of the initial retained austenite transforms to martensite. Under this condition, martensite formed during quenching and cryogenic treatment and the retained austenite surviving the cryogenic treatment are supersaturated with carbon and nitrogen in solid solution. This implies that no autotempering effect occurred during quenching and cooling to  $-120\text{ }^{\circ}\text{C}$  [STR 09]. Tempering at  $120\text{ }^{\circ}\text{C}$ ,  $170\text{ }^{\circ}\text{C}$ , and  $240\text{ }^{\circ}\text{C}$  for 1 hour followed by cryogenic treatment, showed only 48%, 40%, and 34% of the initial retained austenite (*i.e.*  $\approx 50$  mass.-percent) transforms to martensite respectively. This signifies that tempering prior to cryogenic treatment stabilizes retained austenite and becomes difficult to transform to martensite during cryogenic treatment. The stabilizing effect increases as temperature and time increase. It is apparent that in order to transform the greatest possible amount of retained austenite, the subzero cryogenic treatment should be performed immediately after quenching before tempering.

The thermal stabilization of retained austenite is considered to occur by pinning mechanism [STR 09] rendering more difficult to martensitic transformation during cryogenic treatment. Mohanty [MOH 95] reports that stabilization occurs because of segregation of interstitial atoms (*carbon and nitrogen*) toward the areas of high dislocation density and grain boundaries. The segregated carbon and nitrogen atoms impede further nucleation of martensite phase and hinder the growth of martensite nuclei through: i) the loss of mobility of austenite-martensite interface and ii) the strengthening of retained austenite. Moreover, during tempering, retained austenite is enriched by carbon/nitrogen diffusing from martensite phase leading to enhanced stabilization. Such enrichment of carbon and nitrogen during tempering is given in Figure 4.19. In addition, the presence of nickel in 18CrNiMo7-6 steel enhances the tendency of retained stabilization. Furthermore, there could be other processes occurring during stabilization treatment, as pointed out by Mohanty [MOH 95]. However, it seems reasonable to conclude that multiple processes operate during stabilization. Tempering at  $240\text{ }^{\circ}\text{C}$  for 14 hours followed by cryogenic treatment exhibits a different tendency in which much less austenite is retained in comparison to specimens tempered  $120$  and  $170\text{ }^{\circ}\text{C}$  for 14 hours. It is thought that besides other micro-structural changes such as

coarsening of the  $\epsilon/\eta$  transition carbides ( $\text{Fe}_{2.4}\text{C}$ ) and conversion of  $\alpha'$ -nitride ( $\text{Fe}_{16}\text{N}_2$ ) into  $\gamma'$ -nitride ( $\text{Fe}_4\text{N}$ ) [CHE 92] that may take place in carbonitrided specimens during tempering at 240 °C, retained austenite transforms into bainite particularly on prolonged tempering time leading to reduced initial retained austenite before cryogenic treatment. The in-situ experiment (Figure 4.18) reveals such transformations in which austenite decreases from 50% to 38% on holding at 240 °C for 2 hours.

Furthermore, cryogenic treatment influences the magnitudes and distribution of residual stresses. Considering the residual stress distribution in as-quenched samples as the basis for comparison, tempering at 170 °C for 2 hours does not only relax compressive RS but also shifts the location of peak compressive residual stresses towards the case/core interface. A relaxation of up to 200 MPa for the peak compressive RS and of up to about 160 MPa at a depth of 50  $\mu\text{m}$  from the surface is reached. On the other hand, direct cryogenic treatment improves the peak compressive RS by 70 MPa and shifts the location of peak compressive RS toward the surface. The improved compressive RS are linked to the additional transformation of retained austenite whereas the shift of location of peak compressive RS toward the surface is ascribed to the shift of the location of maximum volume fraction of martensite toward the surface. Despite the fact that more than 60 % of initial RA at a depth of 50  $\mu\text{m}$  transform during direct cryogenic treatment, the improvement of compressive RS was only 40 MPa. This may be due the fact that residual stress at any point is a resultant of several factors including volume expansion associated with austenite to martensite transformation, misfit between austenite and martensite phase and the misfit between the case and core.

Tempering prior to cryogenic treatment alters significantly both magnitudes and distribution of residual stresses for martensite phase as shown in Figure 4.39. It is evident from this figure that if the samples are subjected to elevated temperature prior cryogenic treatment, compressive RS in the first 500  $\mu\text{m}$  are considerably enhanced. For example, samples tempered for 2 hours at 120 °C, 170 °C, and 240 °C prior to cryogenic treatment (Figure 4.39b), the compressive RS at a depth of 50  $\mu\text{m}$  are enhanced to between -350 to -450 MPa as compared to about only -60 MPa for the sample tempered at 170 °C for 2 hours but not cryogenically treated. A similar trend is observed for samples tempered for 1 hour (Figure 4.39a) and stage tempered at 80 °C for 14 hours prior to cryogenic treatment. The enhanced

compressive RS is mainly due to retained austenite to martensite transformation, which is accompanied by increase in volume. It is highly probable that the macrostresses are greatly affected. This is due to the fact that as the volume of fraction of retained austenite decreases the macrostresses tend to approximate that in martensite phase. In this range, the improved compressive RS decrease with increasing tempering temperature. The enhancement of residual stresses observed in this work is in good agreement with those in the work of Diamant [DIA 74]. In contrast, Sveshnikov [SVE 66] and Dukarevich [DUK 73] report that even though the amount of austenite transformed is appreciable, the macrostresses are not greatly affected during subzero treatment.

Due to low intensity of retained austenite reflection {220}, the residual stress in this phase was not determined. However, Kim et al. [KIM 81] determined the residual stresses within the austenite and martensite phases of a carbonitrided surface layer and showed that cryogenic treatment at -85°C for four hours results in high magnitudes of tensile residual stress in the austenite. Consequently, the fatigue strength would be greatly impaired due to the fact that the resistance of retained austenite to fatigue cracking is determined by the amount of applied energy it absorbs and uses in the formation of martensite. This is because the energy used in the martensite reaction and for heating is not available for crack initiation or propagation (ROM 75). If cryogenic treatment raises the level of tensile stresses within the austenite without triggering the martensite reaction, then the ability of the austenite to absorb energy is reduced.

#### 4.4 Thermal stability investigation

This section presents the thermal stability of retained austenite and residual stresses for carbonitrided samples simulating service conditions at different temperatures. The investigations were conducted using the carbonitriding treatment CN2, which after quenching retained high proportion of austenite of about 50 mass.-percent. Prior to thermal cycles, all samples were conventionally tempered 170 °C for 2 hours. The testing temperatures used were -30 °C, RT, 90 °C, and 150 °C whereas the holding times were 14, 96, and 720 hours. X-ray diffraction was used to analyse both retained austenite and residual stresses. Moreover, chemical composition, microstructures and microhardness distributions were examined.

##### 4.4.1 Carbon and nitrogen depth profiles

Figure 4.39 indicates the carbon and nitrogen depth after the carbonitriding treatment CN2. The maximum concentration at a depth of 50  $\mu\text{m}$  is 0.86 %C and 0.36 %N. Similarly, the first 50  $\mu\text{m}$  of the case-hardened layer experienced a depletion of alloying elements.

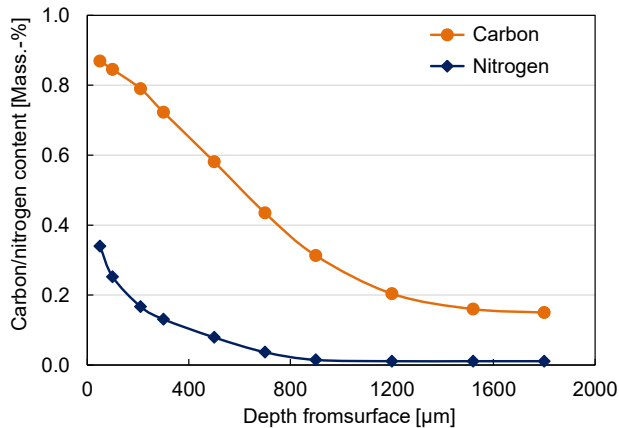


Figure 4.40 Carbon and nitrogen depth profiles in quench + tempered condition

##### 4.4.2 Metallography and microhardness distributions

Typical microstructures of the case-hardened layer for carbonitrided 18CrNiMo7-6 samples after thermal cycles with different conditions are presented in Figure 4.41. As the specimens were subjected to a conventional tempering at 170 °C for 2 hours, loss of martensite

tetragonality and stabilization of retained austenite already occurred. The case microstructures are characterized by plate martensite (dark), retained austenite (white) and finely disseminated carbides and nitrides. On aging at different temperatures for 14 hours reveals no significant difference in the size of martensite plates and fraction of retained austenite. However, darkening of martensite plates on aging at 150 °C for 720 hours is observed, which can mainly be attributed to precipitation in martensite plate. Figure 4.42 shows the unetched case microstructures of the samples aged at different temperatures for 720 hours, in which the grain boundary oxidation and finely disseminated precipitates can clearly be observed at the surface. Comparing precipitates in Figure 4.41a to those in Figure 4.42b to d indicates that the quantity and size of precipitates increase with increasing aging temperature.

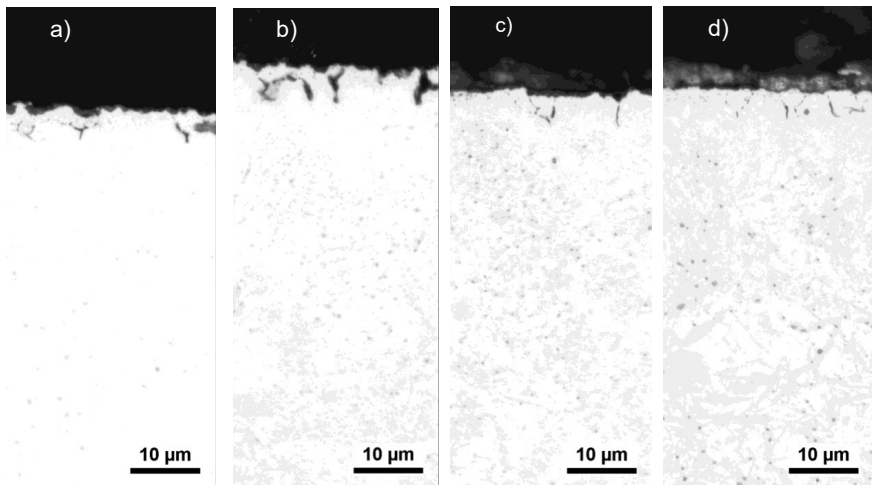


Figure 4.41 Unetched case microstructures after thermal cycles :a) after tempering (Q+T); b) at -30 °C for 720 h after Q+T; c) at 90 °C for 720 h after Q+T; d) at 150 °C for 720 h after Q+T.

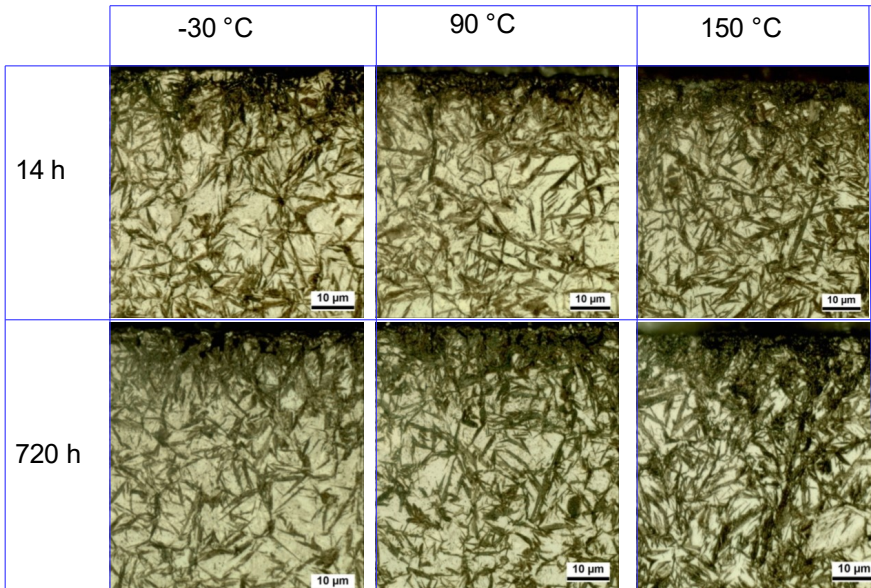


Figure 4.42 Etched case microstructure after thermal cycles

Figure 4.43 illustrates the microhardness distributions for specimens after aging at different conditions. The initial microhardness conditions, which are represented by samples in their as-quenched state and after tempering at 170 °C for 2 hours (Q + T) are given in Figure 4.43a. Tempering at this condition decreases the peak hardness and a drop of up to 70 HV1 can be observed. Comparing the Q+T specimen in Figure 4.43a and specimens in Figure 4.43b indicates that aging at -30 °C enhances significantly the maximum hardness. A shift of up to 50 HV for the peak hardness and of up to 120 HV at a depth of 50 µm from the surface are reached. Moreover, at this temperature holding time seems to have negligible influence on the hardness distribution mainly because martensitic transformation is time independent. On aging at 90 °C (Figure 4.43b), the hardness distribution remains relatively unaffected. In contrast, aging at 150 °C for 720 hours decreases the peak hardness by about 30 HV while improving the hardness at a depth of 50 µm from the surface by about 30 HV. The enhancement of hardness can be connected to decomposition of retained austenite to bainite. In all cases, the location of peak hardness shifts towards the surface. In all cases, the core

hardness seems to be less affected by the tempering conditions as well as the subzero treatment and remains slightly below 450 HV because much carbides/nitrides precipitation may have taken place during tempering.

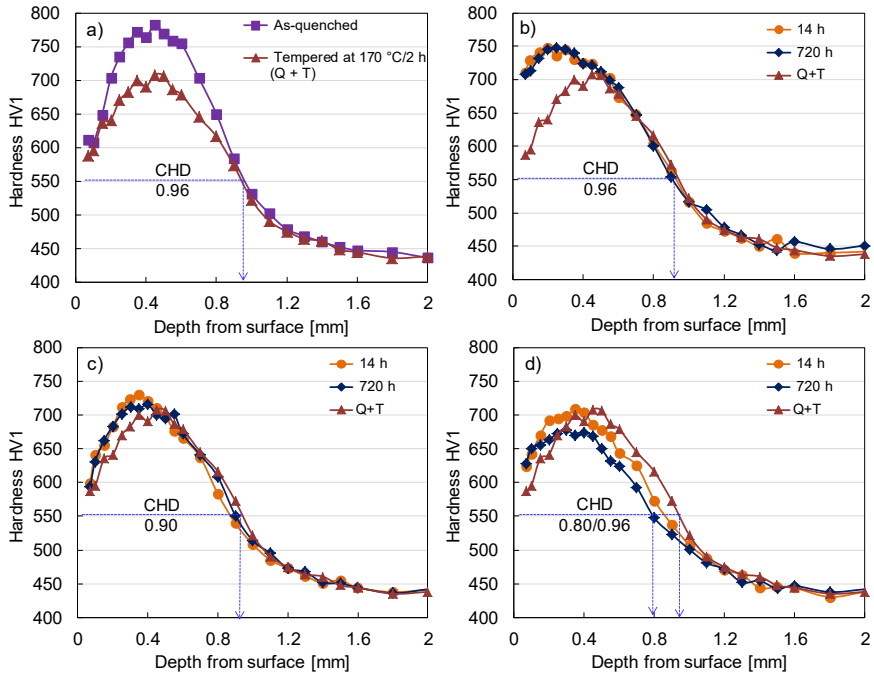


Figure 4.43 Microhardness distributions after thermal treatment for 14 and 720 hours: a) initial conditions; b) -30 °C after Q + T; c) 90 °C after Q + T; d) 150 °C after Q+ T

#### 4.4.3 Retained austenite distributions

Figure 4.44 presents typical examples of variation of X-ray diffraction patterns with depth collected after aging at different conditions. For all aging conditions, the intensity of retained austenite reflections  $\gamma\{200\}$  and  $\gamma\{220\}$  decrease with depth reflecting the decrease of volume fraction of retained austenite with depth. On the other hand, martensite reflections  $\alpha'\{200\}$  and  $\alpha'\{211\}$  intensity increase. Analysis of diffraction patterns collected at a depth of 50  $\mu\text{m}$  after tempering gave 50 mass.-percent as initial volume fraction of retained austenite.

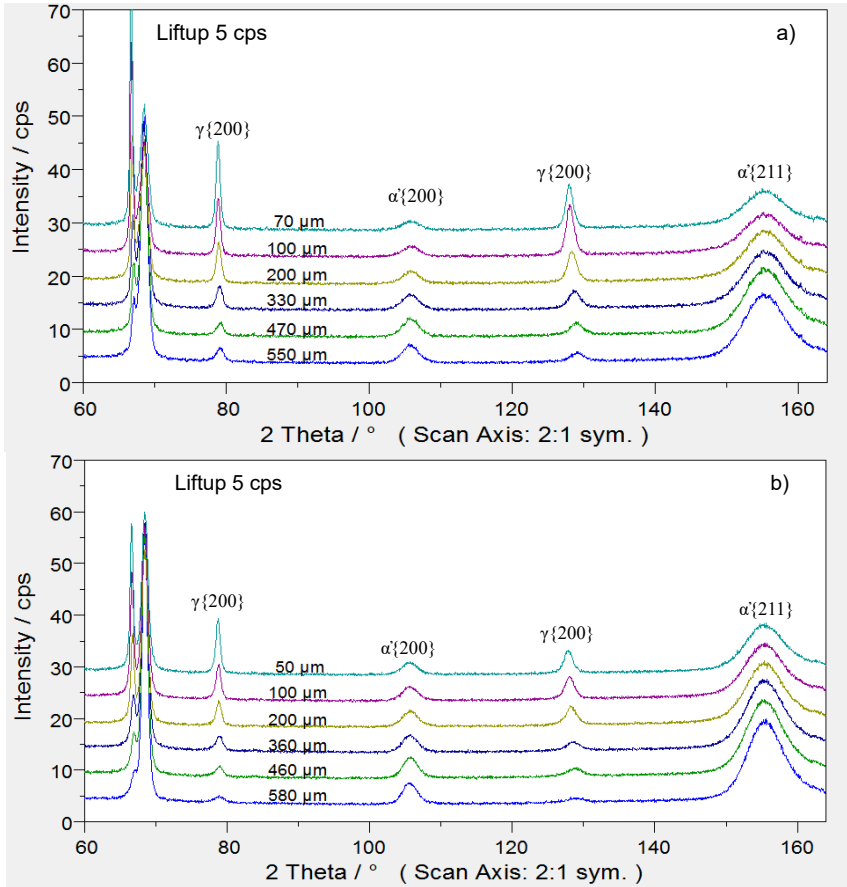


Figure 4.44 X-ray diffraction patterns after thermal cycles for 720 hours: a) 90 °C; b) 150 °C  
 Figure 4.45 gives the retained austenite distributions with depth after aging for 14, 96, and 720 hours at different temperatures. It can be seen from this figure that on aging at RT (Figure 4.45a) and at 90 °C (Figure 4.45c) for 14, 96, and 720 hours, no significant change in fraction of retained austenite at these temperatures occur with time. At these temperatures, the retained austenite remains relatively thermally stable with discrepancies within the marginal scattering band.

On aging at  $-30\text{ }^{\circ}\text{C}$ , the initial fraction of retained austenite is reduced by about 10 mass-percent from about 50% to 40%. This is not only linked to the undercooling by  $-30\text{ }^{\circ}\text{C}$  but also the aging time at  $-30\text{ }^{\circ}\text{C}$ , which is under investigation, influence the transformation of retained austenite to martensite. On aging at  $150\text{ }^{\circ}\text{C}$  for aging time up to 96 h, retained austenite remains relatively thermally stable. On further holding for 720 hours at this temperature, retained austenite is significantly reduced by about 12% from 50 to 38%. The reduction is associated to transformation of retained austenite to bainite (*by interstitial carbon and nitrogen diffusion*) accompanied by increase in volume. The volume change that takes place during aging might influence the magnitude and distribution of residual stress.

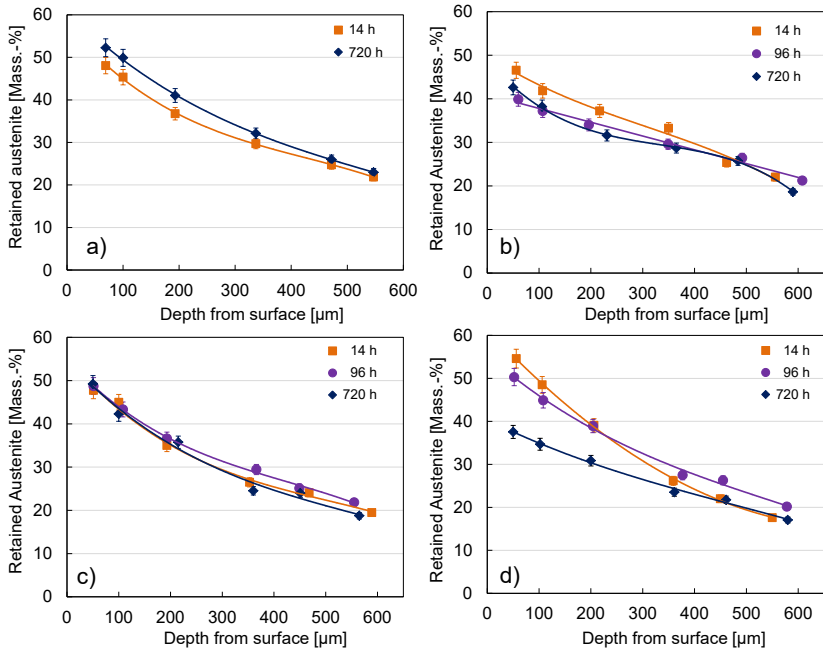


Figure 4.45 Retained austenite distributions after thermal cycles for 14, 96, and 720 hours at different temperatures: a) RT after Q + T; b)  $-30\text{ }^{\circ}\text{C}$  after Q + T; c)  $90\text{ }^{\circ}\text{C}$  after Q + T; d)  $150\text{ }^{\circ}\text{C}$  after Q + T

#### 4.4.4 Residual stress distributions

It has been pointed out in the introduction of this subsection that before thermal cycles, samples were conventionally tempered at 170 °C for 2 hours. Tempering process relaxes compressive RS in the case layer due clustering and such results have been presented in section in section 4.2.

Figure 4.46 to Figure 4.49 give the residual stress distributions in both retained austenite and martensite phase after thermal cycles at -30 °C, RT, 90 °C, and 150 °C for 14 and 720 hours. In addition, the graphs incorporate the macrostresses distributions determined considering the volume fraction and magnitudes of residual stresses of each phase. In general, the temperature and time influence considerably the magnitudes and distribution of residual stresses in the case layer. It can be seen from Figure 4.47a, Figure 4.48a, and Figure 4.49a for which the samples were held for 14 hours, the residual stresses in both retained austenite and martensite at a depth of 50 µm remain relatively thermally stable. At this depth residual stress is 50 MPa for retained austenite and zero (fully relaxed) for martensite. In contrary, isothermal holding at the same temperatures for 720 hours improves slightly the compressive RS in both phases and varies in the range of 0 to -100 MPa (Figure 4.47b, 4-48b, 4-49b). The slight increase in compressive RS can be attributed to thermal-induced volumetric transformation strain. Such thermal induced transformation can be clearly seen in Figure 4.45d during which about 20 mass.-percent of the initial amount of retained austenite (50 mass.-percent) transformed.

On the other hand, thermal cycle at -30 °C for 14 hours considerably enhances the compressive residual stresses in both retained austenite and martensite with the maximum occurring at a depth of 50 µm. Residual stresses up to about -120 MPa in retained austenite and -250 MPa in martensite phase is reached (Figure 4.46a). The increased compressive residual stress is mainly associated to the transformation of retained austenite to martensite resulting in volume increase in the case. Holding isothermally at -30 °C for 720 hours substantially relaxes the compressive RS in the first 100 µm from the surface. Such relaxation might be linked to the migration of supersaturated interstitial carbon and nitrogen atoms to area of high dislocation density. Considering the compressive RS in Figure 4.46b as the basis

for comparison, a relaxation of up to -50 MPa for retained austenite and -75 MPa for martensite is reached.

As indicated in these figures, residual stress analysis was performed in the first 600  $\mu\text{m}$  in which the volume fraction of retained austenite is greater or equal to 20%. In this range, the magnitudes and distributions of macroscopic stresses are strongly influenced by the fraction of RA and residual stresses of the individual phases. Shifts of up to 40 MPa compared to the residual stresses in martensite are reached. Beyond 600  $\mu\text{m}$ , the macroscopic stresses are assumed to correspond to residual stresses in martensite phase.

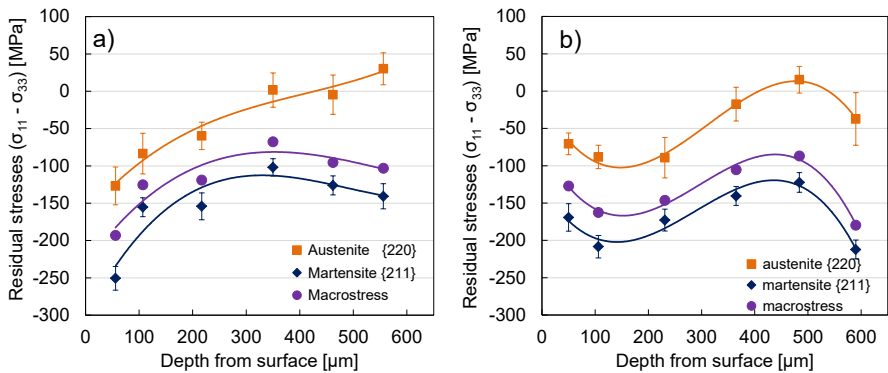


Figure 4.46 Residual stress distributions after thermal cycle treatment at -30 °C : a) 14 h; b) 720 h

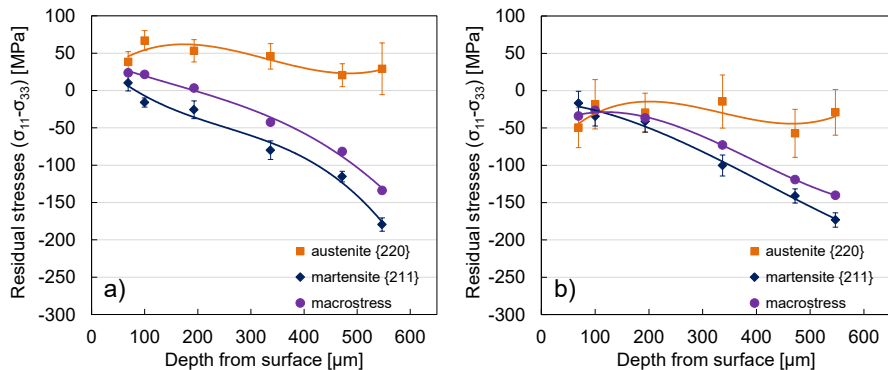


Figure 4.47 Residual stress distributions after thermal cycle at RT after Q + T: a) 14 h; b) 720 h

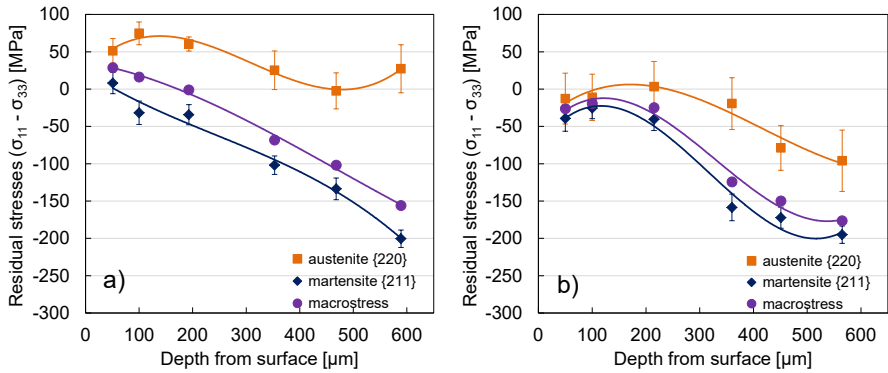


Figure 4.48 Residual stress distributions after thermal cycle at 90 °C after Q + T : a) 14 h; b) 720 h

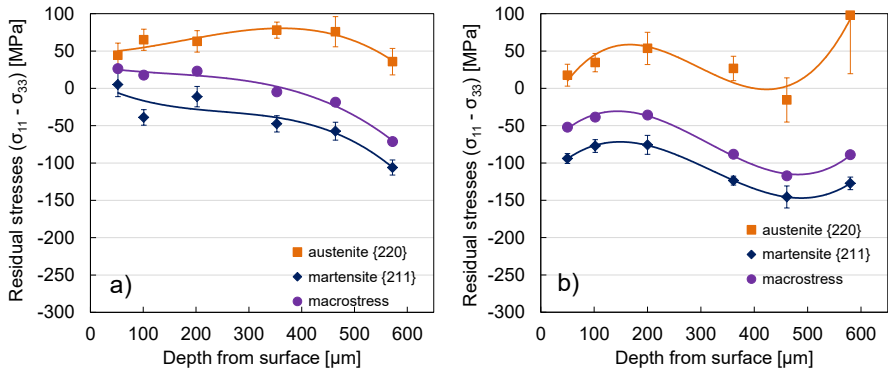


Figure 4.49 Residual stress distributions after thermal cycle at 150 °C after Q + T: a) 14 h; b) 720 h

#### 4.4.5 Discussion on thermal stability of retained austenite

Thermal cycles were used to study the thermal stability of retained austenite and residual stress evolutions by simulating service conditions. Samples used in study retained as high as 50% austenite after carbonitriding and Q + T.

The effect of isothermal holding at different temperatures on retained austenite is given in Figure 4.45. Retained austenite remains thermally stable on isothermal holding at RT, 90 °C

and 150 °C for 14 hours. For example in the work of Neu and Sehitoglu [NEU 93] on carburized 4320 steel, it has been reported that thermally-induced transformation of about 20% of the initially retained would take a year on isothermal holding at 90 °C. Similarly, under these conditions residual stresses in both retained austenite and martensite remain relatively constant and in the range of 0 to 50 MPa. However, it is important to note that stability of retained austenite is both time and temperature dependent. By increasing the time from 14 hours to 720 hours at 150 °C retained austenite decreases from about 52% to 38%. According to Neu and Sehitoglu [NEU 93], such a decrease should take 1 day on isothermal holding at 150 °C. The transformed retained austenite mainly transforms to bainite leading to slight increase of compressive residual stresses in both phases and varies in the range of -25 to -50 MPa. Wang et al. [WAN 86] report that such improvement in compressive residual stresses can be linked to formation of carbides/nitrides.

Regardless of the stabilizing time employed at -30 °C (Figure 4.46b), a reduction of about 20% of the initial retained austenite occurs with the undercooling being the driving force for retained austenite to martensite transformation. The new martensite formed is accompanied by an increase in volume and enhances compressive RS in both retained austenite and martensite. As high as -120 MPa in retained austenite and -250 MPa in martensite phase is reached at a depth of 50 µm from surface for samples with a thermal cycle of 14 hours. Increasing the stabilization time from 14 hours to 720 hours relaxes compressive residual stresses. A relaxation of up to -55 MPA for retained austenite and -90 MPa for martensite (Figure 4.45b) occurred mainly due to clustering and segregation of carbon and nitrogen leading to loss of martensite tetragonality.

## 4.5 Mechanical stability

Shot-peening experiments were performed to investigate mechanical stability of retained austenite and the magnitudes of compressive RS resulting due to transformation-induced plasticity for CN2. In this case, prior to mechanical stability treatment the samples were thermally treated at various conditions. The temperatures used were -30 °C, 90 °C, and 150 °C whereas the time considered was 96 and 720 hours. In this case, a shot peening treatment of StD – G3 -0.6 mm VDFI 8001 with intensity range of 0.25-0.3 mmA and a coverage angle of 1.00-1.25 x t 98% was conducted. Later, X-ray diffraction was employed to analyse both retained austenite content and residual stresses.

### 4.5.1 Retained austenite distribution

Figure 4.50 compares the volume fraction of retained austenite at a depth of 50 µm from the surface before and after shot-peening treatment for CN2 samples. It is obvious that the shot peening treatment induces further transformation of retained austenite to martensite. In both cases, a reduction of up to 20 mass.-percent (i.e. 40 per cent of the initial volume fraction of retained austenite, which was about 50 mass.-percent) is reached. The decrease in retained austenite after shot peening is mainly attributed to deformation induced transformation of case retained austenite to martensite introduced by the impact of shots.

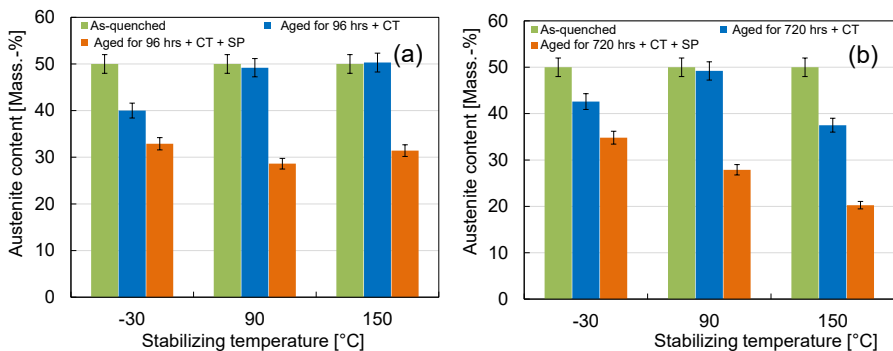


Figure 4.50 CN2 volume fraction of retained austenite for as-quenched, aged + CT, and aged + CT + SP : (a) 96 h; (b) 720 h: CT – cryogenic treatment, SP – shot-peening

#### 4.5.2 Residual stress distributions

Figure 4.51 gives a comparison of residual stresses in retained austenite at a depth of 50  $\mu\text{m}$  from the surface before and after shot-peening (SP). As expected, thermal cycles followed by shot peening treatment induces high compressive residual stresses in retained austenite. The high compressive stress is associated to volume expansion due RA to martensite transformation. The constraint of the associated volume expansion causes the development of additional compressive residual stresses [DAV 02]. As high as -800 MPa compressive RS are induced after shot-peening. Comparing residual stresses in Figure 4.51a and b for shot-peened samples indicates that no significant difference after aging at 90 °C for 96 and 720 hour. The slight less compressive RS the sample aged at -30 °C for 720 °C can be attributed to higher mechanical stabilization than for the sample at the same temperature for 96 hours. Furthermore, the less compressive RS in retained austenite after aging at 150 °C for 720 hours is associated to the transformation of retained austenite to bainite and may be due to less C/N content resulting from further distribution and diffusion into the core; consequently less initial RA present during shot-peening.

Figure 4.52 compares the residual stresses in martensite measured at a depth of 50  $\mu\text{m}$  for thermally stabilized and thermally stabilized coupled with shot-peening treatment. It can be observed from this figure that shot-peening treatment induces high compressive residual stresses in martensite phase. As high as -1200 MPa for samples initially stabilized for 96 and 720 hours are measured. Comparing the RS for shot-peened samples, no significant difference for samples aged for 96 h (Figure 4.52a) and 720 hours (Figure 4.52b) can be observed.

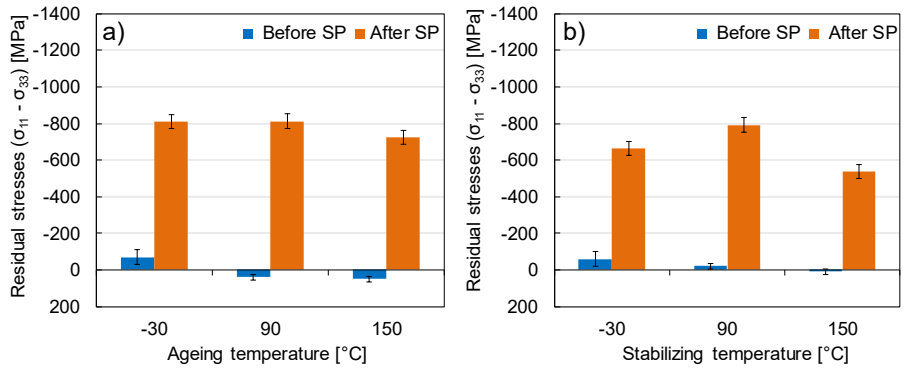


Figure 4.51 Residual stresses in retained austenite after shot peening of samples with prior thermal treatment at different temperatures for: a) 96 h; b) 720 h

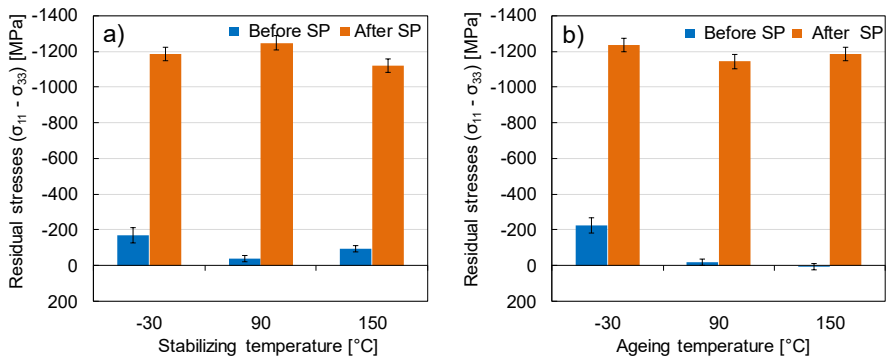


Figure 4.52 Residual stress in martensite after shot peening of samples with prior thermal treatment at different temperatures for: a) 96 h; b) 720 h

### 4.5.3 Discussion on mechanical stability of retained austenite

In this section, the mechanical stability of retained austenite as a function of thermal stabilizing temperature is presented. The percentage of the initially retained austenite transformed during shot-peening process was used to estimate the mechanical stability of retained austenite. In this context, the stability of retained austenite decreases with increasing volume fraction of retained austenite transformed during shot-peening process.

The volume fraction of retained austenite transformed after shot-peening process is given in Figure 4.52. From this figure the amount of retained austenite transformed for samples thermally stabilized for 720 hours is 19% at -30 °C, 42% at 90 °C and 46% at 150 °C which indicates that retained austenite is mechanically unstable. This implies that samples thermally stabilized at -30 °C are more mechanically stable and that the stability decreases with increasing temperature. Increasing the stabilizing temperature raises the dislocations mobility leading to decrease in dislocation density; consequently retained austenite becomes unstable and can readily transform. It is also important to note that there is essentially no difference in mechanical stability of retained austenite for samples thermally stabilized -30 °C for 96 and 720 hours. Similar behaviour is observed for samples thermally stabilized at 90 °C. It is reasonable to assume that stabilizing at -30 °C and 90 °C has little contribution to the mechanical stability of retained austenite because clustering/segregation of carbon and nitrogen atoms and carbide precipitation had taken place during prior conventional tempering at 170 °C for 2 hours. On the contrary, a difference in the amount of transformed RA is observed on stabilizing at 150 °C for 96 and 720 hours. The higher amount of transformed retained austenite observed at 720 hours is attributed to the transformation of RA to bainite during thermal stabilization. In the work of Neu and Sehitoglu [NEU 93], a decrease of about 20% of the initial amount of retained austenite should take a day on isothermal holding at 150 °C. Additionally, such difference in transformed retained austenite may be associated to inhomogeneous deformation since the amount transformed depends on the extent of deformation.

It is obvious that shot peening enhances compressive residual stresses in the case-hardened layer. Such enhancement is given in Figure 4.51 and Figure 4.52 in which as high as -800 MPa in retained austenite and -1200 MPa in martensite are reached. This is mainly attributed to the

deformation-induced transformation of retained austenite to martensite leading to an increase in volume. The constraint of the associated volume expansion causes the development of high magnitude of compressive residual stresses and as a result improves the bending fatigue performance [DAV 02]. The improved bending fatigue results due to the fact that the induced compressive RS within the surface of the treated parts reduces the possibility of crack initiation at the surface.

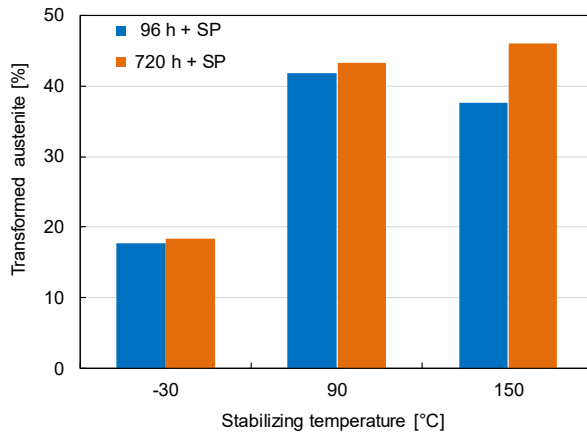


Figure 4.53 Volume of retained austenite transformed after shot peening treatment

## 5 General Discussion of Results

This main objective of this was to investigate the "Influence of Carbonitriding Process on Phase Transformation, Retained Austenite and Residual stresses". The investigation was carried using 18CrNiMo7-6 (DIN 1.6587 German standards) low alloy steel. The specific objectives of this work were to:

- characterize the state after carbonitriding,
- analyse the state during and after tempering,
- investigate the state after tempering coupled with cryogenic treatment,
- investigate the thermal stability of carbonitrided samples,
- investigate the mechanical stability of carbonitrided samples

Five carbonitriding variants with different carbon and nitrogen potentials were carried out. For some of the specific objectives, the carbonitriding condition CN2 was considered. Analysis of the samples in their quenched state and after post-treatments was carried out using X-ray diffraction. In addition, other characteristics such as microhardness, microstructures and chemical composition were also considered.

The state after carbonitriding (as-quenched state) was investigated considering five carbonitriding variants designed as CN1 through CN5. As expected, the maximum fraction of retained austenite increases with the increasing C+N content in the case as shown in Figure 5.1. Under all conditions the total case depth was about 1200  $\mu\text{m}$ . The maximum fraction of retained austenite which occurs at a depth of 50  $\mu\text{m}$  from the surface ranges between 18 mass.-percent for CN5 and 54 mass.-percent for CN2. As expected, the fraction of retained austenite decreases with decreasing C+N content as illustrated in Figure 5.1. In the first 50  $\mu\text{m}$  the carbonitrided samples were characterized by low amount of retained austenite and depletion of alloying elements (Cr, Mn, Mo, and Ni). The depletion of alloying elements is linked to oxidation and formation of precipitates with chromium being more sensitive to oxidation. Analysis indicated that as high as 58 mass.-percent of oxygen diffused into the near surface of the components extending (Figure 4.11). In all carbonitriding conditions the layer affected by oxidation is about 2  $\mu\text{m}$ .

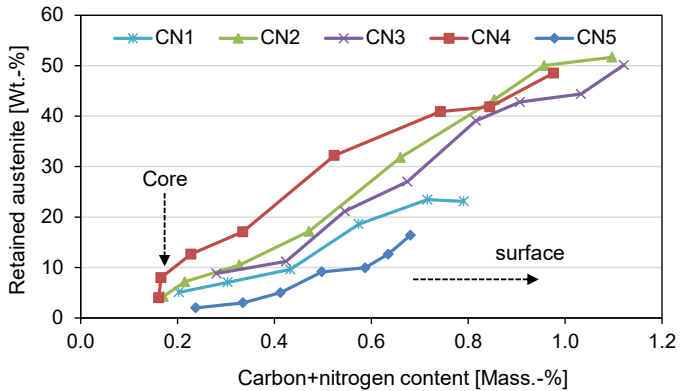


Figure 5.1 Variation of retained austenite as a function of C+N content

In as-quenched states components are characterized by low compressive RS ranging between -50 and -300 MPa. The low compressive RS is mainly due to high fraction of retained austenite, oxidation and depletion of alloying elements. In all cases the peak compressive RS occurs at a depth between 400  $\mu\text{m}$  and the case/core interface. The volume fraction of martensite phase at which the peak compressive RS occurs is about 80 mass.-percent with the carbon content of about 0.5 mass.-percent while the concentration of nitrogen remaining relatively zero. The maximum compressive seems to be less affected by the level of level of retained austenite at the surface.

Analysis of state during and after tempering process revealed significant effect on the fraction of retained austenite, magnitudes and distribution of compressive RS as well as the location of peak compressive RS. During continuous heating from room temperature to 650  $^{\circ}\text{C}$  at the heating rate of 10 K/minutes, retained austenite starts to decompose at 290  $^{\circ}\text{C}$ . This temperature seems to be independent of the level of carbon and nitrogen content attained during carbonitriding treatment. The temperature observed in this work is in good agreement with the one observed in the work of Amarthalingam [AMA 10]. In contrast, the finish

temperature of retained austenite decomposition is highly affected by the level of carbon and nitrogen content attained during carbonitriding. The finish temperature for retained austenite ranges between 335 °C for lower C+N content (CN1) and 355 °C for higher C+N content (CN2). It is thought that the retained austenite (50 mass.-percent) for samples with higher C+N content is highly stabilized than retained austenite (23 mass.-percent) in samples with lower C+N content. The high stabilization is attributed to carbon and nitrogen enrichment in retained austenite. Such carbon + nitrogen enrichment is estimated and provided in Figure 4.17. During continuous heating to 650 °C residual stresses in martensite phase relax continuously with temperature and reach full relaxation at about 400 °C as shown in Figure 20. Such residual stress relaxation is attributed to re-organization of thermally activated dislocations as well as movement of interstitial carbon and nitrogen atoms towards the location of high dislocation density and grain boundaries [MIT 86]. In contrast, evolution of residual stresses in retained austenite is cyclic as observed in Figure 20. Below 190 °C, the relaxation of tensile residual stresses is associated to depression of carbon and nitrogen content as a result of cluster segregation and formation of transition carbides whereas above 190 °C tensile residual stresses are enhanced which is attributed to carbon and nitrogen enrichment in the remaining retained austenite.

During different in-situ tempering cycles, retained austenite remains relatively thermally stable on holding at 170 °C for 2 hours. Such thermal stability of retained austenite finds support from the work of Neu [NEU 93]. However, at higher temperatures retained austenite decomposes rapidly and as a result only less than 5 mass.-percent of austenite is retained on isothermal holding at 300°C for 2 hours as indicated in Figure 4.18. On the other hand, at all isothermal holding temperatures residual stresses in martensite phase remain relatively constant and the relaxation of residual stresses reached increases with increasing isothermal temperature. Similar relaxation of residual stresses is observed during conventional tempering process at 170 °C for 2 hours and as high a 320 MPa of relaxation is reached.

Investigation of the state after tempering coupled with cryogenic treatment showed that prior tempering process of carbonitrided parts lowers the fraction of retained austenite transformed to martensite during cryogenic treatment and that the fraction of transformed

retained austenite decreases with increasing tempering temperature. For example, prior tempering at 120 °C, 170 °C, and 240 °C for 1 hour only 48%, 40%, and 34% of the initial retained austenite were transformed, respectively. The decrease of the fraction of retained austenite transformed into martensite indicates that retained austenite becomes thermally stable and the stability increases with increasing stabilizing temperature. The stabilization occurs by pinning mechanism [MOH 95] rendering the more difficult to martensitic transformation during cryogenic treatment. However, on stabilizing at 240 °C for 14 hours leads to a different tendency as much less austenite is retained after cryogenic treatment at -120 °C for 2 hours. This is thought besides other microstructural changes such as coarsening of the  $\epsilon/\eta$  transition carbides ( $\text{Fe}_{24}\text{C}$ ) and conversion of  $\alpha''$ -nitride ( $\text{Fe}_{16}\text{N}_2$ ) into  $\gamma'$ -nitride ( $\text{Fe}_4\text{N}$ ) [CHE 92] that may take place during tempering of carbonitrided parts at 240 °C, retained austenite transforms into bainite (Figure 4.18); consequently reduces the initial amount of retained austenite before cryogenic treatment.

Furthermore, tempering coupled with cryogenic treatment alters significantly the nature, magnitude and distribution of residual stresses as shown in Figure 4.39. After cryogenic treatment, as high as -450 MPa of enhancement of compressive RS in the first 500  $\mu\text{m}$  from the surface is reached (Figure 4.39b) in comparison to tempered parts but not subjected to cryogenic treatment. The enhancement of compressive RS is mainly attributed to the new martensite formed which is accompanied by volumetric increase. The enhancement of compressive RS observed in this work is in good agreement with the work of Diamant [DIA 74]. Although this work did not analyse the residual stresses in retained austenite surviving after cryogenic treatment due to low intensity of reflection  $\{220\}$ , Kim et al. [KIM 81] report that cryogenic treatment at -85 °C for 4 hours results in high magnitudes of tensile residual stresses in retained austenite.

The thermal stability on retained austenite was carried out at different ageing conditions. The isothermal holding temperatures were -30 °C, 90 °C and 150 °C whereas the ageing times were 14, 96, and 720 hours. In addition, some of the samples thermally stabilized under these conditions were tested for mechanical stability.

Ageing at RT and 90 °C for all ageing times, retained austenite remains thermally stable. However according to Neu and Sehitoglu [NEU 93], on isothermal holding at 90 °C, thermally-

induced transformation of about 20 mass.-percent of retained austenite would a year (3600 hours). Under these conditions, residual stresses in both retained austenite and martensite phase remain relatively in the range between zero and 50 MPa. Isothermal holding at -30 °C for all ageing times between 5 and 10 mass.-percent of the initial retained austenite transforms to martensite. The undercooling by -30 °C provides the driving force for transformation of retained austenite to martensite. The martensitic transformation is accompanied by enhancement in compressive RS as well as altering the residual stress distribution. Up to -250 MPa enhancement of compressive RS (Figure 4.46) is reached. Isothermal holding at 150 °C for 720 hours decreases the initial retained austenite by 10 mass.-percent. In this case, the decrease in retained austenite is attributed to bainitic transformation and is accompanied by improvement of compressive as shown in Figure 4.49b. The mechanical treatment by shot-peening reduces significantly the initial fraction of retained austenite and improves considerably the compressive residual stresses in both retained austenite and martensite phase. The fraction of transformed retained austenite ranges between 19% for samples aged at -30 °C and 46% for samples aged at 150 °C. This signifies that after ageing process at various conditions, the retained austenite is mechanically unstable. Stability decreases with increasing ageing temperature. The transformation of retained austenite to martensite during shot-peening enhances significantly the compressive RS in both phases (Figure 4.51 and Figure 4.52). Enhancement of up to -800 MPa in retained austenite and -1200 MPa in martensite phase is reached. This is mainly linked to deformation-induced transformation of retained austenite leading to an increase in volume. The constraint of the associated volume expansion causes the development of high magnitudes of compressive RS and as a results improves the bending fatigue performance [DAV 02].



## 6 Research Conclusion and Future Perspective

In this work, the influence of carbonitriding process on phase transformation during case-hardening, retained austenite and residual stresses has been investigated. Besides characterization of state after carbonitriding of the samples, state after and during tempering, state after cryogenic treatment, study of thermal and mechanical stability were conducted. In all cases, the main investigated parameters were retained austenite and residual stress distributions. In addition, line broadening analysis for microstructural defects including crystallite size, mean strain and dislocation density was carried out using the Williamson-Hall plot method. The quantification of phase composition and residual stresses was done using X-ray diffraction. Also, chemical compositions, metallography and microhardness distributions were considered.

From the results of this work, the following main conclusions can be summarized as follows:

- 6.1) Analysis of state after carbonitriding of the samples for the different carbonitriding treatments indicated that the maximum amount of retained austenite, which occurs at the depth of 50 to 100  $\mu\text{m}$  from the surface, is highly dependent on the carbon and nitrogen content at the surface. As high as 50 mass.-percent of austenite was retained. The minimum compressive RS in martensite phase occurs in the range characterized by maximum retained austenite. To the contrary, the peak compressive RS occurs where C+N content lies in the range of 0.40 to 0.60% in which martensite fraction is about 80%. In this range the nitrogen content is negligibly small ( $\approx 0.05$ ). The peak compressive RS in as-quenched state appears to be less affected by the maximum amount retained austenite (surface carbon + nitrogen content) and lies in the range of -400 to -500 MPa. In contrast, low content of retained austenite shifts the location of peak compressive RS toward the surface whereas high content of RA shifts the location toward the case/core interface.

Differences were measured between the RS in RA and martensite, so that macroscopic RS values are influenced. From these investigations, it appears that when the fraction of retained austenite is greater than 15%, it is important to measure the RS in both phases

in order to determine the macroscopic residual stress by considering the proportion of each phase.

- 6.2) Analysis of the state during and after tempering process revealed that both in-situ and conventional tempering relaxes significantly residual stresses and shifts the peak compressive RS toward the case/core interface. For conventional tempering at 170 °C for 2 hours, relaxation of up to 320 MPa for the peak compressive RS is reached. Samples containing high carbon and nitrogen experienced less relaxation of compressive residual stress. It is observed that during continuous heating at 10 °K/min, retained austenite remains relatively stable until about 290 °C for both CN1 and CN2. Above this temperature retained austenite decomposes into ferrite and cementite. The end of rapid decomposition of retained austenite is significantly affected by the level of carbon + nitrogen content (retained austenite content) and it occurs at 390 °C for CN1 and 410 °C for CN2.

On isothermal holding 170 °C for 2 hours, retained austenite remains relatively thermally stable and decomposes rapidly on holding at 300 °C, decreasing to less than 5 mass.-percent after tempering. During continuous heating residual stresses in martensite relax continuously and reach full relaxation at about 400 °C for both CN1 and CN2 treatments. Holding the samples isothermally, residual stresses in both retained austenite and martensite remain relatively constant and decrease with increasing holding tempering.

- 6.3) The investigation of tempering couple with cryogenic treatment at -120 °C for 2 hours revealed that this condition is sufficient to induce transformation of retained austenite to martensite after any prior tempering temperature and time. If the sample is immediately subjected to cryogenic treatment at -120 °C for 2 hours after quenching, as high as 60% of the initially retained austenite ( $\approx 50\%$ ) transforms to martensite. However, holding the samples at elevated temperature prior to cryogenic treatment stabilizes retained austenite and it becomes difficult to transform into martensite during cryogenic treatment. For lower stabilizing time of 1 hour or 2 hours, the stabilizing effect increases with temperature. On stabilizing for 1 hour at 120 °C, 170 °C,

and 240 °C, the amount of retained austenite transformed was only 48%, 40%, and 34% respectively, of the initially retained austenite (*i.e.*  $\approx 50\%$  RA). Moreover, stabilizing at 240 °C for 14 hours prior to cryogenic treatment leads to decomposition of retained austenite; consequently less retained austenite is present prior to cryogenic treatment. The constraint of volume expansion associated to the new martensite formed during cryogenic treatment improves compressive RS in martensite phase and shifts the peak compressive RS toward the surface. An improvement of up to 200 MPa of the peak compressive RS in comparison to as-quenched sample is reached. Isothermal holding prior to cryogenic treatment enhances the compressive RS in the first 500  $\mu\text{m}$  as well as altering the residual stress distribution. At a depth of 50  $\mu\text{m}$ , the compressive RS in martensite are enhanced to between -350 to -450 MPa as compared to -60 MPa after conventional tempering at 170 °C for 2 hours. The improved compressive RS decreases with increasing tempering temperature.

- 6.4) Investigation of ageing conditions on the thermal stability of retained austenite indicated that retained austenite remains relatively thermally stable on ageing at RT and 90 °C variant times. Similarly, under these conditions residual stresses in both phases remain relatively constant in the range of 0 to 50 MPa. On isothermal holding at 150 °C for 720 hours, retained austenite becomes unstable and decomposes leading to transformation of about 20 mass.-percent of the initial amount of retained austenite into bainite. Such transformation alters the distribution as well as enhancing the compressive RS in martensite phase. Lastly, undercooling of -30 °C is sufficient to continue the martensitic transformation and as high as 20% of the initial retained austenite is transformed. This in turn improves compressive RS in the first 300  $\mu\text{m}$  in both retained austenite and martensite phase.
- 6.5) Investigation of mechanical stability by shot-peening of carbonitrided samples revealed that retained austenite is mechanically unstable and readily transforms to martensite during mechanical treatment of prior aged samples. During shot-peening, high as 45% of the initial retained austenite is transformed. The fraction of retained austenite increases with increasing prior ageing temperature. For samples aged for 720 hours at -

30 °C, 90 °C, and 150 °C, the amount of retained austenite mechanically transformed was as high as 48%, 40%, and 34% respectively, of the initially retained austenite.

The shot-peening treatment enhances significantly the compressive residual stresses in both phases. The constraint of the volume expansion resulting from deformation-induced transformation of retained austenite to martensite causes the development of high compressive RS in both retained austenite and martensite. As high as -800 MPa and -1200 MPa compressive RS in retained austenite and martensite phase respectively, is induced. Such high compressive RS in both retained austenite and martensite improves the bending fatigue performance because it reduces the possibility of crack initiation at the surface.

The detailed information about carbon and nitrogen, retained austenite, residual stress depth profiles, state after of cryogenic treatment in both retained austenite and residual stresses and thermal and mechanical stability of RA revealed in this work are useful since no information of this kind is available in the context of carbonitrided low alloy steels.

## **Future Perspective**

This work presented detailed information about the influence of carbonitriding process variants on retained austenite distribution, its thermal and mechanical stability. Furthermore, the work provides insight about the magnitudes and distribution of residual stresses produced during case hardening, cryogenic treatment and shot-peening treatment. In addition, the work considers thermal relaxation of residual stresses.

Besides all these insight information, there are still areas for future investigations. Considering the following areas will help address the limitations of the current knowledge and improve understanding the influence on mechanical properties.

- The first area which could be considered is the mechanical testing of the carbonitrided specimens. The varying carbon and nitrogen (retained austenite content) could help identify the carbonitriding variant giving the optimal mechanical properties. In this

case, a four bending test and tensile test can be employed. These tests could give complementary information about stability of retained austenite.

- After quenching, the case microstructures were characterized by high proportion of martensite, retained austenite and finely disseminated precipitates with a size of about 0.5  $\mu\text{m}$ . The content and classification of precipitates could not be quantified using laboratory X-ray diffraction because of low intensity. In this case, high-energy X-rays source such as Synchrotron can be used. Alternatively, Differential Scanning Calorimetry can be used.



## 7 Bibliography

- [ABU 06] F. B. Abudaia, On the Stabilization of Retained Austenite, Journal of Engineering Research, Issue 5, 6, 2006
- [AMA 10] M. Amarthilangam et al, In situ phase transformation studies on transformation induced plasticity steel under simulated weld thermal cycles using synchrotron diffraction. In Kannengiesser T. Babu SS, Komizo Y-I, Ramirez AJ (Eds) in situ studies with photon, neutron and electrons scattering. Springer, Berlin, (2010), p. 133-148
- [BIS 10] S. Bischoff, H. Klümper-Westkamp, F. Hoffmann, H. W. Zoch, Development of a sensor system for gas carbonitriding – Part 1, HTM J. Heat Treatm. Mat. 65 (2010) 3, p. 141-148
- [BIS 88] D. L. Bish, S. A. Howard, Quantitative Phase Analysis using the Rietveld Method, J. Appl. Crystallogr. Vol. 21, (1988), p. 86-91
- [BOY 87] H. E. Boyer (Ed), Case Hardening of Steel, ASM International, Metals Park, Ohio 44073, (1987), p. 22
- [BÖT 99] A. Böttger, P. J. Warren, G. D. W. Smith, M. J. van Genderen, S. J. Sijbrandij and E. J. Mittemeijer, Tempering of Iron-Carbon-Nitrogen Martensite: (Re) Distribution of Interstitial Atoms, Materials Science Forum Vols 318-320, (1999) p. 103-108
- [BRA 83] H. Brandis and W. Schmidt, Contribution to the Influence of Retained Austenite on the Mechanical Properties of the Case-hardened Steel, Proceedings of the Symposium sponsored by the Heat Treatment Committee, 112<sup>th</sup> AIME, Atlanta-Georgia, (1983).
- [BRU 73] H. Brugger, Werkstoff und Wärmebehandlungseinflüsse auf die Zahnstragfähigkeit, VDI-Berichte, No. 195, (1973), p. 135-144
- [BRU 73] F. S. Bufington, K. Hirano and M. Cohen, Acta Met., 9 (1961) 434
- [CAR 16] Carbodur: Case-hardening Steel, extracted from [www.edelstahl-witten-krefeld.de](http://www.edelstahl-witten-krefeld.de), January 2016, 04:00 (*German local time*)
- [CHA 95] H. Chandler (Ed), Heat Treater's Guide: Practices and Procedures for Irons and Steels, 2<sup>nd</sup> Ed, ASM International®, (1995), p. 96-101
- [CHA 78] R. Chatterjee-Fischer, Metall. Trans. 9A:1553 (1978)
- [CHE 92] L. Cheng, A. Böttger, and E.M. Mittemeijer, Metallurgical Transaction A, Vol. 23A, (1992), p. 1129-1145
- [CHE 90] L. Cheng, and E.M. Mittemeijer, Metallurgical Transaction A, Vol. 21A, 1990, p. 13-26
- [CHO 82] K. Chongkim, Advances in X-Ray Analysis, 1982, vol. 25, p. 343-353.
- [COH 70] M. Cohen, Trans. JIM, 11 (1970) 145
- [CON 12] J. R. Connolly, Introduction to X-ray powder Diffraction, Spring 2012

- [DAV 02] J R. Davis and Davis & Associates (Eds), SURFACE HARDENING OF STEEL: Understanding the Basics, ASM International, (2002), p. 64-65, 127-128
- [DAV 78] R. Davies and C. G. Smith, "A Practical Study of the Carbonitriding Process", Metal Progress, (1978), p. 40-53
- [DAW 74] C. Dawes and D.F. Tranter, Application of Gas Carburizing Theory to Practice, Met. Technol., Sept 1974, p 397-405
- [DEB 75] M. Debuyschere, Essai de Fatigue Eprouvettes en Acier 20CN cémentées – Trempées, Traitement Thermique 98, (1975), 59-65.
- [DEL 88] R. Delhez, Th. H. Keisjer, E. J. Mittemeijer, J. I. Langford; Size and strain parameters from peak profiles: Sense and Nonsense.; Aust. J. Phys., Vol. 41, (1988), p. 213-227
- [DIA 74] A. Diament, R. El Haik, R. Lafont, and R. Wyss, "Surface Fatigue Behaviour of Carbonitrided and Case-Hardened Layers in Relation to Distribution of Residual Stresses and the Modifications of the Crystal Lattice Occurring During Fatigue", May 1974 (Caen, France), International Federation for the Heat Treatment of Materials.
- [DUK 73] I. S. Dukarevich, M.A. Balter, Thermomechanical Treatment in Hydrogen-containing Atmospheres Improved Carburised-Steel Qualities, Russ. Eng. J., Vol 53, (1973) 8, p. 62-65
- [EIG 96] B. Eigenmann, E. Macherauch, Mat.-wiss.u. Werkstofftech. 27, (1996), p. 426-437
- [EL-H 01] F. M. El-Hossary, N. Z. Negm, S. M. Khalil, A. M. Abed Elrahman, D. N. McIlroy, RF plasma carbonitriding of AISI 304 austenitic stainless steel, Surface and Coating technology 141 (2001) p. 194-201
- [EPP 12] J. Epp, T. Hirsch, C. Curfs, Metallurgical and Materials Transactions A, Vol. 43A, (2012) p. 2210-2217
- [ERI 85] T. Ericsson, Adv. in surface treatments, Vol. 4, (1985), p. 78-113
- [FER 84] P. Ferguson and K. H. Jack, Scripta Metall., Vol. 18, (1984), p. 1184-1194
- [FRA 60] H. E. Frankel et al, Fatigue Properties of High Strength Steel, Trans. ASM, (1960), p. 257-276.
- [FIT 03] M. E. Fitzpatrick and A. Lodini, Analysis of Residual Stress by Diffraction using Neutron and Synchtron Radiation, Taylor & Francis, London, 2003
- [FIT 05] M. E. Fitzpatrick, A. T. Fry, P. Holdway, F. A. Kandil, J. Shackleton, L. Suominen, Determination of Residual Stresses by X-ray Diffraction – Issue 2: Measurement Good Practice Guide No. 52, Crown, ISSN 1744-3911, 2005
- [GAR 05] C. Garcia-Mateo, F. G. Caballero, Materials Transactions 46, (2005), p. 1839-1846
- [GEN 68] M. J. van Genderen, A. J. Böttger and E. J. Mittemeijer, First Stage of Precipitation in Iron-carbon-Nitrogen Martensite: Diffraction Analysis Using Synchrotron Radiation, Scripta METALLURGIA et MATERIALIA, Vol. 26, (1968), p. 883-888

- [GEN 68] J. Genin and P. A. Flinn, Mössbauer Effect Study of Clustering of Carbon Atoms during Room-Temperature Aging of Iron-Carbon Martensite, *Trans. TMS-AIME*, Vol 242, (1968), p. 1419-1430
- [GEN 85] A. van Gent, F. C. van Doorn, and E. J. Mittemeijer, *Metall. Trans. A*, 1985, Vol. 16A, p 1371-1784
- [GUI 07] R. Guinebretière, *X-ray diffraction by Polycrystalline Materials*, ISBN 13: 978-1-905209-21-7
- [GUL 53] A. P. Gulyaev, *Heat Treatment of Steel*, Mashgiz, 1953
- [HAL 49] W. H. Hall, *Proc. Phys. Soc. London A* 62, (1949), p.741-743
- [HAR 43] F. E. Harris, Case Depth – an Attempt at a Practical Definition, *Metal Progress*, 44 (1943)
- [HAU 97] V. Hauk, *Structural and Residual Stress Analysis by Non-destructive Methods*, Elsevier, Amsterdam, 1997
- [HER 11] D. H. Herring, Carbonitriding of Fasteners, *Fastener Technology International*, June 2011
- [HOF 98] B. Hoffmann, O. Vöhringer, E. Macherauch, 4th European Conf. on Residual Stresses, S. Denis, J.-L. Lebrun, B. Bourniquel, M. Barral (Eds), *Societe Française de Métallurgie et de Matériaux*, Vol. 2, (1998) p. 785-794
- [HOF 01] B. Hoffmann, O. Vöhringer, E. Macherauch, Effect of Compressive Plastic deformation on Mean Lattice Strains, dislocation densities and flow stresses of martensitically hardened steels, *Materials Science and Engineering A*319-321 (2001), p 299-303
- [HON 81] R. W. K. Honeycombe, *STEELS: Microstructure and Properties*, Edward Arnold ltd, 9181, ISBN 0 7131 2793 7
- [HOR 78] R. M. Horn, R. O. Ritchie, Mechanisms of tempered martensite embrittlement in low alloy steel, *Metallurgical Transactions A*, 9A, (1978), p. 1039-1053
- [IMA 71] Y. Imai, T. Oguro, and A. Inoue, Formation of  $\chi$ -Carbide in the Carbon Steel, *J. Iron Steel Inst. Jpn*, Vol. 57 (No.4), (1971), p. 113-114
- [ING 83] D. W. Ingham, and P.C. Clarke, Carburise Case Hardening: Computer Prediction of Structure and Hardness Distribution, *Heat Treat. Met.*, Vol 4, (1983), p. 91-98
- [JAC 51] K. H. Jack, "Structural Transformations in the Tempering High-Carbon Martensitic Steels", *Journal of Iron and Steel Institute*, 169 (1951) 26
- [KAR 07] O. Karabelchtchikova, *Fundamentals of Mass Transfer in Gas Carburizing* (Doctoral Dissertation). Retrieved from <http://www.wpi.edu/Pubs/ETD/Available/etd-121807-234414/>
- [KAT 14] R. J. Katemi, J. Epp, F. Hoffmann, M. Steinbacher, *Advanced Materials Research* Vol. 996, (2014), p. 550-555
- [KIM 81] C. Kim, D.E. Diesburg and R.M. Buck, *J. Heat Treat.* Vol. 2 (No. 1), (1981), p 43-53.

- [KOF 66] P. Kofstad, High Temperature Oxidation of Metals, Wiley, NY, 1966
- [KOG 68] L. I. Kogan, R. I. Entin, X-Ray Diffraction Study of the Lattice Parameter of Austenite at Intermediate Transformation Temperatures, Fiz. Metal. Metalloved. (1968), 25, 383-384
- [KOI 59] D. P. Koistinen, The Distribution of Residual Stresses in Carburized Cases and Their Origin, Trans. ASM, Vol 50, (1958), p. 227-241
- [KOI 59] D. P. Koistinen and R.E. Marburger, A General Equation Prescribing the Extent of the Austenite-Martensite Transformation in Pure Iron-Alloys and Plain Carbon Steels, Acta Metall., Vol 7, (1959), p. 59-60
- [KOK 05] A. Kokosza, J. Pacyna, Journal of Materials Processing Technology, 162-163 (2005) p. 327-331.
- [KOK 10] A. Kokosza, J. Pacyna, Archive of Metallurgy and Materials, Vol 55 (4), (2010), p. 1001-1006
- [KOS 67] I. S. Koslowski Met. Sci. Heat Treat. 25:157 (1967)
- [KRA 89] G. Krauss (Ed), CARBURIZING: Processing and Performance, ASM International, (1989), p. 83-100
- [KRA 15] G. Krauss, STEEL: Processing, Structure, and Performance, 2<sup>nd</sup> ed, ASM International, Materials Park, Ohio 44073-0002, 2015
- [KUB 79] O. Kubaschewski and C.B. Alcock, Metallurgical Thermo-chemistry, 5<sup>th</sup> Ed, Pergamon Press Ltd, Frankfurt, 1979
- [KUN 82] C. Y. Kung and J.J. Rayment, An Examination of the Validity of Existing Empirical Formulae for the Calculation of Ms Temperature, Metall. Trans. A, Vol 13, (1982), p. 328-331
- [LAR 80] J. A. Larson, C. F. Jatczak, S. W. Shin, Retained Austenite and its Measurements by X-ray Diffraction, SP-453, ASE, 1980
- [LIŠ 92] B. Liščić, H. M. Tensi, and W. Luty (eds.), Theory and Technology of Quenching, Spring Science +Business Media, New York, 1992.
- [LEE 11] S. J. Lee, C. J. Van Tyne, Prediction of Martensite Volume Fraction in Fe-Cr-Ni Alloys, ISIJ International, Vol. 51, 2011, p. 169-171
- [LEM 54] B. S. Lement, B. L. Averbach and M. Cohen, "Microstructural Changes on Tempering Iron-Carbon Alloys", Trans. ASM 46 (1954) 851
- [LIE 66] G. Liebmann, what happens to Retained Austenite?, Zeit für wirtschaftliche Fertigung, 61, No. 5, (1966) p 235-238
- [MAC 86] E. Macherauch and K.H. Kloss, Proceedings of the International Conference on Residual Stresses, Garmisch-Partenkirchen, FRG, (1986), p. 167-174

- [MAC 92a] E. Macherauch and O. Vöhringer, Residual Stresses after Quenching, in *Theory and Technology of Quenching*, B. Liščić, H.M. Tensi, and W. Luty, Ed., Springer-Verlag, (1992), p. 117-181
- [MAC 92b] E. Macherauch, H. Wohlfart, and U. Wolfstieg, Zur zweckmässigen Definition von Eigenspannungen, *Härt.-Tech- Mitt.*, Vol 28, (1973), p. 201-211
- [MAK 91] J. D. Makinson, W. N. Weins, T. W. Snyder, and R. J. de Angelis, The Substructure of Austenite and martensite Through a Carburized Surface, *Advances in X-Ray Analysis*, 34, 1991
- [MIT 83] E. J. Mittemeijer, The Relationship between Residual Macro- and Microstresses and Mechanical Properties of Case-Hardened Steels, in *Case-Hardened Steels – Microstructure and Residual Stress*, Diesburg, D.E (Ed), (1983), p. 161-187
- [MIT 86] E. J. Mittemeijer, A. van Gent, P.J. van der Schaaf, *Metall. Trans. A*, vol. 17A, (1986) ,p. 1441-1445
- [MIT 88] E. J. Mittemeijer, L. Cheng, P. J. van der Schaaf, C. M. Brakman, B. M. Korevaar, *Metall. Trans. A*, vol. 19A, (1988), p 925-932
- [MOH 95] O. N. Mohanty, *Material Science and Engineering B32* (1995) p. 267-278
- [MOO 10] E. De Moor, C. Föjer, J. Penning, A. J. Clarke, J. G. Speer, *Phys Rev B*, 2010, 82: 104210
- [MOH 95] P. V. Morra, A. J. Böttger, E.J. Mittemeijer, *Journal of Thermal Analysis and Calorimetry*, Vol. 64 (2001), p 905-914
- [MOR 01] P. V. Morra, A. J. Böttger and E. J. Mittemeijer, *Journal of Thermal Analysis and Calorimetry*, Vol. 64 (2001) 905-914
- [NAG 83] S. Nagakura, Y. Hirotsu, M. Kusunoki, T. Suzuki, and Y. Nakamura, Crystallographic Study of the Tempering of Martensitic Carbon Steel by Electron Microscope and Diffraction, *Metall. Trans. A*, Vol 14, (1983), p. 1025-1031
- [NAZ 59] G. T. Nazarenko, Decomposition Range of Retained Austenite, *Metallov*, May 1959, Vol. 5, p. 28-30
- [NEU 93] R. W. Neu and H. Sehitoglu, Thermal Induced Transformation of Retained Austenite in Simulated Case of a Carburized Steel, *J. Eng. Mater. Technol. (Trans. ASME)*, Vol 115, (1993), p. 83-88
- [NIS 78] Z. Nishiyama, *Martensitic Transformation*, Academic Press Inc., 111 fifth Avenue, New York, New York 10003, 1978
- [NOY 87] I. C. Noyan and J.B. Cohen, *Residual Stress: Measurement by Diffraction and Interpretation*, 1987, Springer-Verlag, New York
- [OKH 06] C. Okhi, Atmospheric Control Method for JIS-SUJ2 Carbonitriding Process, *NTN Technical Review No.74* (2006), p. 44-53
- [ONI 93] M. Onink, C.M. Brakman, F.D. Tichelaar, E.J. Mittemeijer, S. van der Zwaag, J.H. Root, N.B. Konyer, *Scripta Metallurgica and Materialia*, Vol. 29, (1993), pp. 1011-1016,

- [PAR 99] G. Parrish, *Carburizing: Microstructures and Properties*, ASM International, 1999
- [PAR 85] G. Parrish and G.S. Harper, *Production Gas Carburizing*, Pergamon Press Inc., 1985.
- [PRA 88] K. H. Prabhudev, *Handbook of Heat Treatment of Steel*, Tata McGraw-Hall Publishing Limited, New Delhi 1100 08, 1988
- [RAD 04] R. Radoi, M. Danila, P. Fernandez, J. Piqueras, Mean crystallite size, size distribution and root mean square residual microstrain measurement from X-ray line broadening of milled ZnSe nano-powders, DOI: 10.1109/SMICND.2004.1403061
- [PRE 66] B. Prenosil, Eigenschaften von durch Diffusion des Kohlenstoffs und Stickstoffs im Austenit entstehenden Schichten, *Härterei-Tech. Mitt* 21, Heft 2, (1966), p. 124-137
- [RAZ 67] C. Razim, Effects of Residual Austenite and Reticular Carbides on the Tendency to Pinning of Case-hardened Steel, Thesis, Techn. Hochschule Stuttgart, 1967
- [RÉT 02] T. Réti, Residual stresses in Carburized, Carbonitrided, and Case-Hardened Component, in *Handbook of Residual Stress and Deformation of Steel*, G. Totten, M. Howes, T. Inoue, Ed., ASM International, 2002
- [RIE 69] H. M. Rietveld, A profile refinement method for nuclear and magnetic structures, *J. Appl. Crystallogr.* 2, (1969), p. 65-71
- [ROB 53] C. S. Roberts, B. L. Averbach, and M. Cohen, The mechanism and kinetics of first stage tempering, *Transactions ASM*, 45: 576, 1953
- [ROM 75] O. N. Romaniv, YN. Gladkii, and N.A. Deev, Some Special Features of the Effect of Retained Austenite on the Fatigue and Cracking Resistance of Low-Temperature Tempered Steels, *Fiz. Khim. Mekh. Mater.* Vol 11 (No.4), (1975), p. 63-70
- [RON 14] Y. Rong, N. Chen, X. Zuo and J. Dai, The mechanism of Ductility enhancement of retained austenite in High strength Steels, International Conference on Material Science and Material Engineering, (2014), p. 201 -208
- [SAK 91] Y. Sakuma, O. Matsumura, H. Takechi, *Metall. Trans.* 22A, 1991, 489
- [SAS 82] C. N. Sastry, K. H. Khan, W. E. Wood, *Metallurgical Transactions A*, vol. 13A, April 1982, pp. 676-680
- [SKR 72] Y. M. Skrychenko, L. K. Orzhitskaya, V. V. Letivin, and V. N. Chevokin, Decomposition of Retained Austenite in Complex-Alloyed Die Steels during Tempering, Translated from *Metallovedenie i Termi-cheskaya Obrabotka Metallov*, No. 6, (1972), p. 52-54
- [SMI 87] D. K. Smith et. al, Quantitative X-ray powder diffraction using full diffraction pattern. *Powder Diffr.* 2, (1987), p. 73-77
- [SPE 69] G. R. Speich, Tempering of Low-Carbon Martensite, *Trans. TMS-AIME*, Vol. 245, (1969), p. 2553-2564
- [SPE 72] G. R. Speich and W. C. Leslie, Tempering of Steel, *Metall. Trans.* Vol 3, (1972), p 1043-1054
- [STO 44] A. R. Stokes and A. J. C. Wilson, *Proc. Phys. Soc. London* 56, (1944), p 174-181

- [STR 09] P. Stratton and C. H. Surberg, Retained Austenite Stabilization, Heat Treating Progress, (2009), p. 25-27
- [STE 15] M. Steinbacher, F. Hoffmann, H.-W. Zoch, S. Lombardo, T. Tobie, Recent Developments on the Microstructure and the Mechanical Properties of Carbonitrided Parts, J. Heat Treatm. Mat. Vol. 70 (2015) 5 p. 201-2017
- [STE 56] W. Steven and A.G. Haynes, The Temperature of Formation of Martensite and Bainite in Low-alloy Steel, JISI, Vol 183, 1956, p 349-359
- [SVE 66] D. A. Sveshnikov, I. V. Kudryavstev, N. A. Gulyaeva, and L. D. Golubovskaya, Chemicothermal Treatment of Gears, Met. Sci. Heat Treat. (USSR), (No. 7), (1966), p. 527-532
- [SYL 81] J. Slycke, T. Ericsson, J. Heat Treating 2:3 (1981)
- [SCH 18] P. Scherrer, Nachr. Ges. Wiss. Göttingen, (1918), p. 98-100
- [STE 16] M. Steinbacher, F. Hoffmann, H.-W. Zoch, S. Lombardo, T. Tobie, Recent Developments on the Microstructure and the Mechanical Properties of Carbonitrided Parts. Part 1: Investigation on Materials Properties, HTM J. Heat Treatm. Mat. 70 (2015) 5, p. 201 - 207
- [STR 09] P. Stratton, C. H. Surberg, Retained austenite stabilization in carburized SAE 8620, Heat Treating Progress, (2009), p. 25-27
- [SUG 92] K. Sugimoto, M. Kobayashi, S. Hashimoto, Metallurgical Transaction A, 23A, (1992), p. 3085-3091
- [THE 74] K-E. Thelning, Steel and its Heat Treatment: Bofor Handbook, Butterworth & Co (Publishers) Ltd, London: 88 Kingsway, WC2B 6AB, 1974
- [TOT 02] T. Totten, M. Howes, T. Inoue, Handbook of Residual Stress and Deformation of Steel, ASM International, (2002), p. 105-108
- [TOT 06] G. E. Totten, Steel Heat Treatment Handbook, 2<sup>nd</sup> ed, Taylor & Francis Group, 2006
- [WAN 86] J. Wang, Z. Qin, J. Zhou, Formation and Properties of Carburized Case with Spheroidal Carbides, The 5th International Congress on Heat Treatment of Materials (Budapest), International Federation of the Heat Treatment of Materials (Scientific Society of Mechanical Engineers), (1986), p. 1212-1219
- [WAN 11] J. Wang, A. Misra, An Overview of Interface-dominated Deformation Mechanisms in Metallic Multilayers, Curr.Opin. Solid State Material. Sci. 15 (2011) 20
- [WAN 01] J. Wang, S. van der Zwaag, Metallurgical and Materials Transactions A, Vol 32A, (2001), p. 1527-1539
- [WIE 05] M. Wießner, S. Kleber, A. Kulmburg, In-situ Investigation during Tempering of a High Speed Steel with X-ray Diffraction, Part. Part. Syst. Charact. 22 (2005), p. 407-417
- [WEL 70] C. Wells, W. Batz, and R.F. Mehl, Diffusion coefficient of carbon in austenite, Transactions AIME, 188:553-560, 1970

- [WER 57] F. E. Werner, B. L. Averbach and M. Cohen, "The tempering of Iron-Carbon Martensite Crystals", *Trans. ASM* 49 (1957) 823.
- [WIL 53] G. K. Willianson, W.H. Hall, *Acta Metall.* 1, 1953, p 22-31
- [WIL 86] A. Wildau: Ph. D. Dissertation, Technical University of Aachen, Aachen, Germany, 1986
- [WIN 11] K. M. Winter, "Independently controlled Carbon and Nitrogen potential. A New Approach to Carbonitriding Processes. Heat Treat 2011, Proc. 26<sup>th</sup> Heat Treating Society Conf., 31.10.-02.11.11, Detroit, USA, B. L. Ferguson, R. Jones, D. S. M. Mackenzie, D. Weires (Eds), ASM Int., Detroit, USA, (2011), p. 9-16
- [YI 11] H. L. Yi, K. Y. Lee, H. K. D. H. Bhadeshia, *Materials Science and Engineering A* 528 (2011), p. 5900-5903
- [YOU 93] R. A. Young, *The Rietveld Method*, IUCr Book Series, Oxford University Press 1993, p 1-39
- [ZAB 79] V. V. Zabil'ski, V.I. Sarrak, and S.O. Suvorova, *The role of relaxation Process on the Volume Change Occuring in Steels during Tempering*, *Fiz. Met. Metalloved.*, Vol 48 (No. 2), (1979), p. 323-331
- [ZAC 89] M. A. Zaconne, J. B. Kelley, and G. Krauss, *Strain Hardening and Fatigue of Stimulated Case Microstructures in Carburized Steel*, *Conf. Proc. Processing and Performance (Lakewood, CO)*, ASM International, July 1989